AD-A117 981 OFFICE OF NAVAL RESEARCH ARLINGTON VA F/G 17/5
NAVAL RESEARCH REVIEWS. VOLUME XXXIV. NUMBER 1.(U)
1982 W J LESCURE

UNCLASSIFIED NL

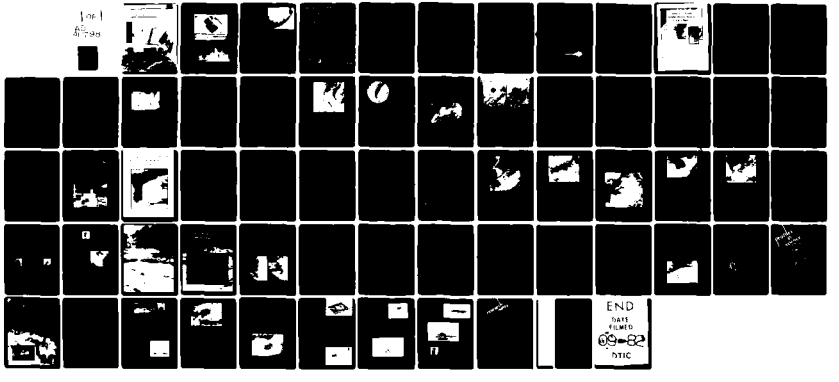

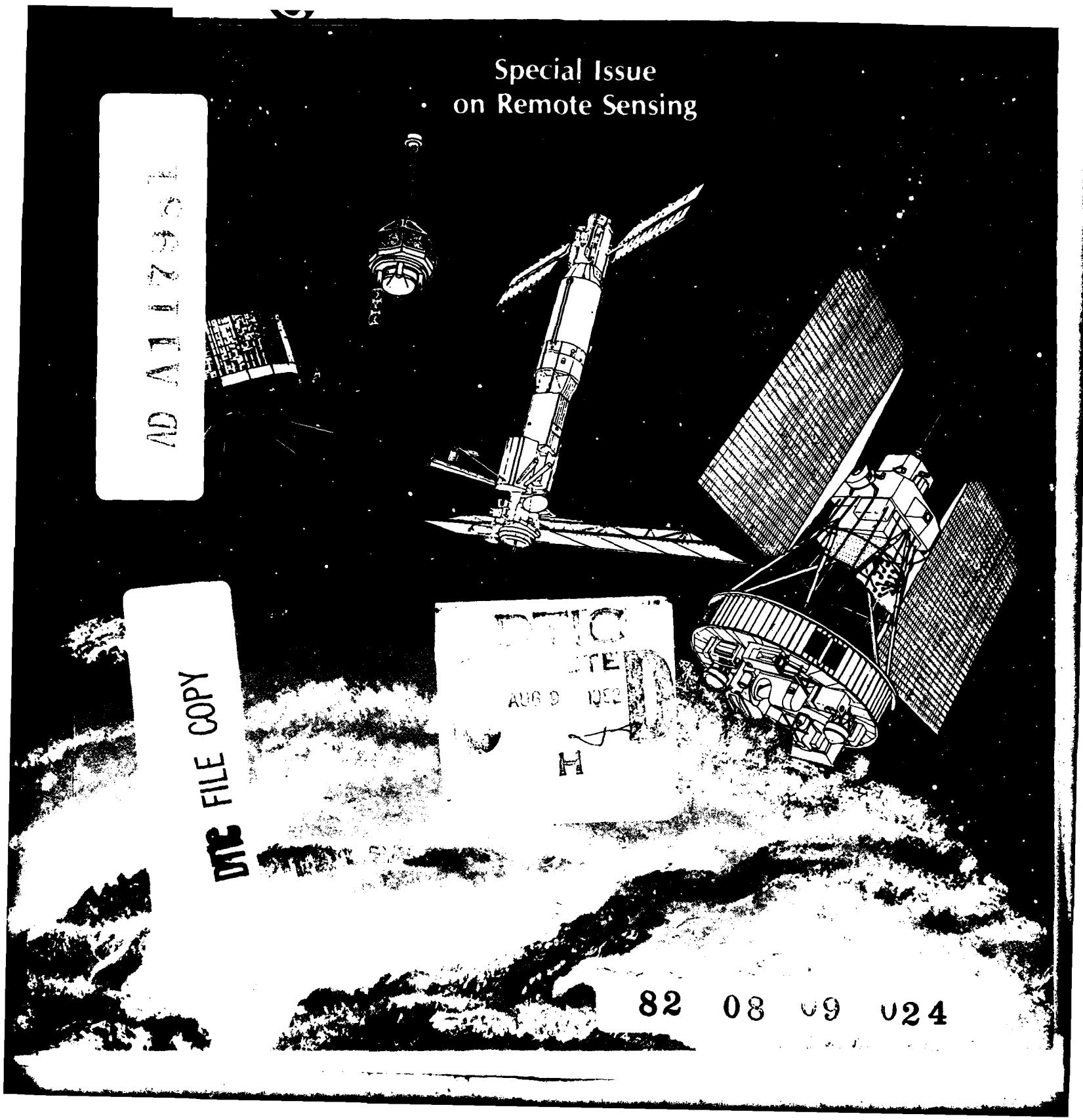

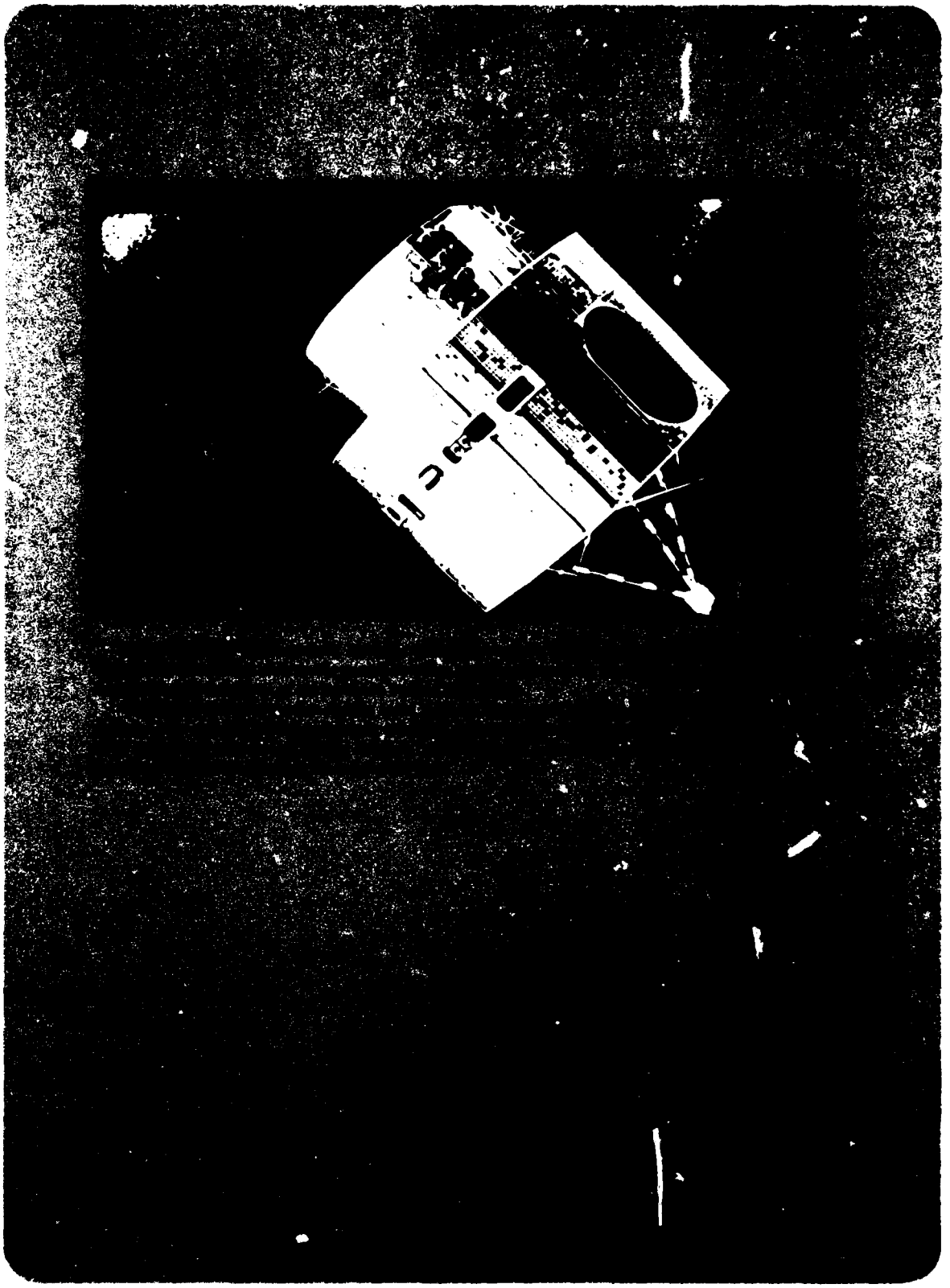

and at depth is important because near surface currents are "contaminated" by local surface winds which make a determination of the mean flow difficult.

The dual-frequency microwave current meter has been successfully tested from towers in the Atlantic Ocean and in the North Sea. System tests using a mobile platform (a research vessel the *AGOR-16 USNS Hayes*) are planned for this July in both the Gulf Stream and in the shoals near Nantucket Island. ■

(Dale L. Schuler, NRL)

Winter-Season Thermal Stress to High-Latitude Reef Systems

The effects of cold-air outbreaks over high-latitude reef systems are being investigated by scientists at the Coastal Studies Institute of Louisiana State University. Nan Walker, funded by a NASA Graduate Student Research Grant, and Drs. H. H. Roberts, L. J. Rouse, Jr., and O.K. Huh, funded by ONR, have found that these outbreaks over the reefs and associated shallow environments can create thermal stress conditions severe enough to kill reef-building corals, thereby affecting long-term reef development. Over the last five years digital thermal infrared data from high-resolution radiometers of the NOAA-5 and NOAA-6 environmental satellites have provided a means for determining regional sea-surface temperature variations during particularly cold outbreaks of polar air. Synoptic satellite data were used in conjunction with a computerized heat flux model to investigate shallow-water chilling processes. The model incorporates hourly meteorological parameters and the bulk aerodynamic equations to hindcast changes in water temperature throughout critical cold-air outbreaks. These results, coupled with in situ temperatures and biological observations (from Florida Bay and the northern Bahama Banks), have provided a data base from which a comprehensive appraisal of thermal stress events on reef communities has been formulated.

During January 1977 and 1981 consecutive cold fronts crossed south Florida and the northern Bahamas, causing abnormal chilling. Field and laboratory experiments identify 16°C as a thermal stress threshold for most reef-building corals, below which they have difficulty maintaining life-supporting processes. Water temperatures below 16°C were experienced in Florida Bay for 8 consecutive days during the 1977 event and for 10 days in

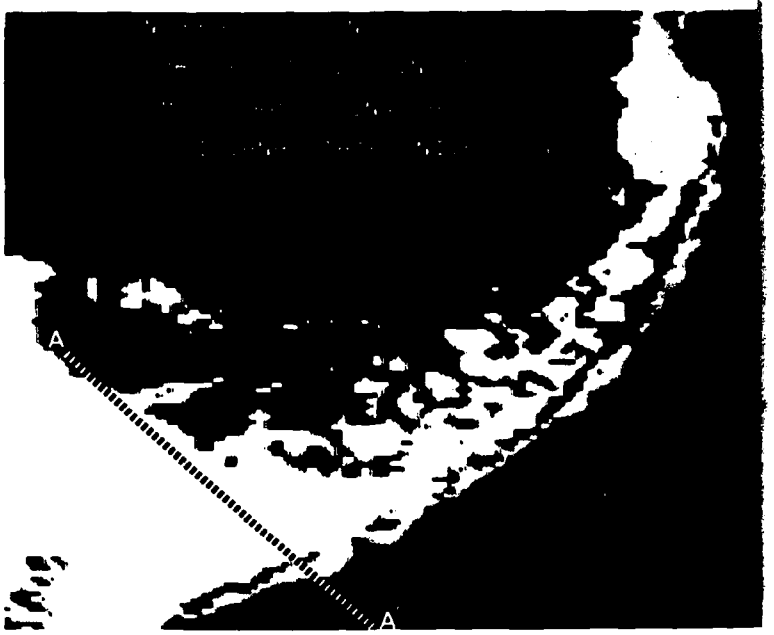

1981. Minimum Florida Bay temperatures obtained from corrected satellite data and confirmed from "surface truth" measurements were 12.9°C and 9.0°C, respectively. The figure above illustrates a profile of radiation temperatures extracted from digital satellite data along the transect A-A'.

Massive fish kills and numerous coral mortalities were observed in the study area during the 1977 and 1981 cold-air outbreaks. Results show that cold-water stress conditions can exist over vast shallow-water areas with residence times of several days. Offbank movement of chilled waters, driven by northerly winds, density gradients, and tidal pumping, can limit coral growth and control the spatial distribution of reef development in high latitudes. ■

(Paul Twitchell, ONR Boston)

Continued from page 5

The CO_2 laser is focused on the water surface causing an explosion called "thermal blow-off." Preliminary studies have indicated that the explosion creates an acoustic field in the water having a pulse width of 20-30 μsecs. and a frequency spectrum peaking between 25-30 kHs. On page 5 is an example of a typical data return from one pulse of the radar. The air blast (surface explosion noise) and the bottom bounce signals are quite evident. The depth is easily calculated because the difference between the speed of sound in water and air is quite exaggerated. The measurement was taken while at sea and underway. ■

(James S. Bailey, ONR)

Naval Research Reviews

Office of Naval Research
One/1982
Vol XXXIV

ARTICLES

DEPARTMENTS

Some illustrations in this issue are black and white reproductions of color photographs obtained from man-computer, interaction display systems which compromise the image quality.

About Our Cover

Orbiting the earth are satellites of the past, present, and some planned for the future. These satellites have and will continue to provide data to oceanographers who interpret it for the eventual use of the operational forces. The sketches are based upon material supplied by the National Oceanic and Atmospheric Administration and the National Aeronautic and Space Administration. Art by Neil Floyd.

Naval Research Reviews publishes articles about research conducted by the laboratories and contractors of the Office of Naval Research and describes important naval experimental activities. Manuscripts submitted for publications, correspondence concerning prospective articles, and changes of address, should be directed to Code 732 Office of Naval Research, Arlington, Va. 22217. Requests for subscriptions should be directed to the Superintendent of Documents, U.S. Government Printing Office, Washington, D.C. 20402. Yearly subscription prices for this quarterly publication are $11.00 in the United States and Canada and $13.75 elsewhere. The issuance of this periodical is approved in accordance with Department of the Navy publications and printing regulations.

Remote Sensing Research

by Paul F. Twitchell
Office of Naval Research, Boston

The U.S. Navy has a long history in remote sensing research and its application to communication, navigation, surveillance, weapons detection and delivery systems. The Geography Division of the Office of Naval Research (ONR) initiated in the 1950's a research program focusing on remotely sensing the environment. ONR was a pioneer in this field and continues today as an important force in many new areas of remote sensing research. In 1962 ONR sponsored the first International Symposium on the Remote Sensing of the Environment. In recent years these meetings have grown into major conferences each resulting in proceedings of several volumes. In 1973 ONR's Remote Sensing Program was reviewed in *Naval Research Reviews*[1]. In this issue are four papers focusing on a few facets of remote sensing of the ocean.

For more than forty years, Navy scientists have been integrating advances in microwave technology into the fleet including shipboard and aircraft fire control radars, weapons guidance, and ocean surveillance from space. In the past twenty years the use of radio waves to measure ocean surface dynamics has contributed greatly to the understanding of wave dynamics. Navy scientists, particularly the late John W. Wright of the Naval Research Laboratory, have played a significant role in studying phenomena at the air-sea interface relating to short-wave modulation by long waves, the spectral development of ocean surface waves, and wave growth predictions. Many of the basic scientific questions, however, have not been answered; for example, phenomena such as nonlinear wave-wave energy transfer and strong nonlinear wave-current interaction require improved theoretical understanding to fully explain radar amplitude modulation and to extract wave spectra information from radar returns. Professor Erik Mollo-Christensen's article in this issue addresses some of these unanswered questions.

Microwave remote sensing of the ocean uses radiometric and altimetry devices. For about a decade scanning microwave radiometers have flown on U.S. satellites. The Navy has and continues to develop techniques for using the "brightness temperature" as measured by the radiometers. One practical application has been the identification and classification of sea ice. Among the information gained from radar altimeters on satellites are the locations of large ocean eddies and the slope of the ocean surface across a major current system. The location and speed of currents can be estimated from space using ocean slope measurements.

The infrared sensors that are common today on aircraft and satellites are traceable to basic research funded in part by the physics and chemistry branches of the Office of Naval Research in the 1950's. Hardware developments and their applications were accelerated through the Infrared Information Symposiums organized and run by ONR. Special credit should be given to two late ONR scientists, T. B. Dowd of the Boston Branch Office and L. B. White of the Chicago Branch Office for directing these symposia which provided a forum for the development of modern electrooptical weapons systems.

H. L. Clark and other scientists at the Naval Research Laboratory developed an early (1942) infrared system for remotely sensing the sea surface from lighter-than-air ships[2]. By the 1960's airborne infrared systems were in common use. Two ONR funded investigators, P. M. Saunders at Woods Hole Oceanographic Institution and E. D. McAllister at Scripps Institute of Oceanography, used airborne infrared systems in their basic investigations of oceanic processes. Contemporary ONR-funded efforts that employ infrared sensors are reported in this issue by Otis B. Brown and Robert Evans of the University of Miami and Oscar Huh and Lawrence Rouse of Louisiana State University.

By using environmental satellites in the early 1960's, the Navy pioneered in research which obtained on a synoptic (1000's km) and meso (100's km) scale environmental characteristics of the ocean and atmosphere. Over the past two decades advances in quantifying satellite data have resulted in cost saving for data acquisition, and a better understanding of the physical processes of the ocean. The Office of

Naval Research has sponsored many scientific meetings and workshops to advance the application of remote sensing tools for the study of oceanic processes. At the meeting on Physical Oceanography and Satellites held at Woodshole in June 1978, Professor Verner Suomi concluded with the following statement[3]:

> Remote sensing and data collection from satellite platforms show considerable promise for improving our understanding of a wide range of scales of ocean flows and their interaction with the atmosphere and underlying surface. The data volume from these new tools will be immense compared to traditional methods of gathering oceanographic data. If the full benefits of these new tools and data sets are to be realized, new methods are required to convert these composite data sets into information. The problem is similar to that experienced by the meteorological satellite operations. We therefore recommend that rapid analysis tools using minicomputers and interactive video displays be made available to oceanographic researchers: further that a modest number of these tools be made available to individual researchers or to small groups rather than through a simple or small number of large institutional data processing facilities. Our present ability to fully utilize these vast data sets is limited. Nevertheless, we recommend that as many, and as complete, data sets as possible be archived, taking into account reasonable cost but at the same time being mindful of the future potential value of the data for studies of the time-history of large scale flows. We stress that any archiving scheme will have value only in direct proportion to provisions for economical and ready access to the data of the research and operational community.

The Navy remote sensing program is addressing the needs suggested by Professor Suomi and Navy environmental support requirements outlined in the following table.

As indicated by Table 1 the Navy environmental support requirements span a broad range of time-and space-scales demanded by each of the several Navy mission areas. Applications of satellite oceanographic data include support of fleet mission operations and support of various research and development programs.

There exists a Navy Operational Requirement

Table 1
Navy Environmental Support Requirements
(ADAPTED FROM Noble and Felt)

MISSION SUPPORT:
STRIKE, ANTISUBMARINE, ANTISURFACE, AMPHIBIOUS, and MINE WARFARE

TIME-SCALES

HOURS	(AIR OPERATIONS)
DAYS	(TYPHOON FORECASTING, ICE OPERATIONS)
WEEKS	(MISSION PLANNING, SHIP ROUTING)

SPACE-SCALES

10m	(COASTAL PROCESSES)
1-50km	(OCEANIC FRONTS, EDDIES, CURRENTS)
50-1000km	(SEVERE STORMS, GLOBAL "WEATHER")

APPLICATIONS
TACTICAL AND STRATEGIC MISSION OPERATIONS
RESEARCH AND DEVELOPMENT PROGRAMS

for Satellite Measurement of Oceanographic Parameters (SMOP OR-WO527-OS). The specifications for horizontal resolution, precision, and accuracy of measurement of identified parameters are shown in Table 2. The dual figures in the statement of resolution, precision, and accuracy represent estimates of minimal acceptable thresholds for operational utility when the document was prepared[4].

To achieve the operational requirements outlined above there is a need for basic and applied research on sensors, image enhancement and display, data interpretation, integration of satellite data into numerical models and other topics. The paper in this issue by Thomas Brubecker of Colorado State University is an example of the efforts to translate in near real time the immense volumes of data streaming down from satellites into a useful presentation for an operational person such as an aircraft pilot. In a later issue of *Naval Research Reviews* there will be additional articles on improving satellite data transmission and processing.

Another area of research is the application of

Table 2
Operational Requirements Satellite Measurements of Oceanographic Parameters
(SMOP OP-WO527-OS)

PARAMETER	HORIZONTAL RESOLUTION*	PRECISION	ACCURACY*
SURFACE WIND			
SPEED	10/ /25 km	5%/ /20%	2m/sec/ /4m/sec
DIRECTION	10/ /50 km	±5°/ /10°	±10°/ /22.5°
SEA SURFACE TEMPERATURE	10/ /25 km	0.25/ /0.8°C	0.5/ /1.0°C
SEA VERTICAL TEMP. STRUCTURE**	10/ /100 km	0.25/ /1.0°C	1.0/ /2.0°C
WAVES			
SIGNIFICANT HEIGHT	10/ /25 km	0.3m/ /10%	0.3 m/ /10%
AMPLITUDE COMPONENTS	1/ /25 km	0.3m/ /0.7m	0.3m/ /0.7m
WAVELENGTH COMPONENTS	1/ /25 km	5%/ /15%	5%/ /15%
DIRECTION	1/ /50 km	10°/ /30°	10/ /45°
ICE			
COVER	0.5/ /25 km	10%/ /25%	12%/ /30%
THICKNESS	2/ /50 km	0.25/ /2m	0.5/ /2m
AGE	10/ /50 km	6/ /12 mos.	6/ /12 mos.
ICEBERGS	0.015/ /0.1 km	N/A	POSITION 0.5/ /2 km

* OPERATIONAL TARGET / / MINIMUM ACCEPTABLE THRESHOLD
** DEPTH 300/ /50m; VERTICAL RESOLUTION ± 2/ /10m

satellite imagery of ocean surface characteristics and atmospheric profiling into numerical models of oceanic and marine boundary layer dynamics. At the present time there is a need to find resources to continue and expand efforts to optimize the ingestion of a satellite data into numerical models used to describe and predict operationally important environmental information.

The remote sensing articles in this issue represent only a small fraction of the ongoing remote sensing programs of the Navy. In-house remote sensing activities of the Navy include research at Naval Environmental Prediction Research Facility (NEPRF) where significant contributions have been made on tactical applications of satellite data and the development of a Satellite Processing and Display System (SPADS). At the Naval Research Laboratory pioneering work on sensor technology is internationally recognized. The Naval Surface Weapon's Center, Dahlgren (NSWC/DL) and the Navy Oceanographic Office (NAVOCEANO) are pursuing research using satellite data. At the Naval Ocean Research and Development Activity (NORDA) scientists are developing techniques for effective operational use of satellite imagery and investigating methods for applying satellite data to numerical models. Other in-house efforts related to systems developments include the multispectral satellite data analysis at Naval Ocean Systems Center (NOSC) and the application of satellite sea surface temperature data at Naval Underwater Systems Center (NUSC). Scientists of the West Coast ONR Office have a long tradition in fostering new remote sensing cooperative efforts with other agencies and various elements of the operational Navy.

Navy scientists and their university colleagues funded by the Office of Naval Research and Naval Air Systems Command (Air 370) Atmospheric/

Oceanographic Program communicate with each other through professional societies. On occasion workshops or meetings are organized by ONR to encourage advances in areas of research of interest to the Navy. The results of ONR-sponsored activities are well promulgated through professional society publications or special volumes; recent examples include a workshop report in the Bulletin of the American Meteorological Society[5] and a book[6], Navy planners and managers draw upon such resources through groups such as the Navy Environmental Remote Sensing Coordinating Advisory Committee (NERSCAC) to introduce research products. For example, a specific research finding could be integrated into the Tactical Environmental Support System (TESS) development. The Navy operational community is presently formulating plans for effective and affordable implementation of satellite products into global and regional environmental prediction systems.

The author wishes to acknowledge contributions from colleagues within the Office of Naval Research, the Naval Research Laboratory, and from other organizations mentioned throughout the text. ■

References

1. Bailey, J. S., 1973. "ONR's Remote Sensing Program," *Naval Research Reviews*, Vol XXIV, No. 10, pp. 1-10.

2. Clark, H. L., 1967. "Some Problems Associated with Airborne Radiometry of the Sea," *Journal Applied Optics*, Vol. 6, No. 12, pp. 2151-2157.

3. Twitchell, P. F., 1979. "Meeting on Physical Oceanography and Satellites," *Bulletin American Meteorological Society*, Vol. 60, No. 3, pp. 225-231.

4. Noble, V. E. and R. Y. Felt, 1981. "U.S. Navy Planning for Satellite Oceanographic Data Exploitation," *Proceedings International Space Technical Applications, 19th Goddard Memorial Symposium*, Vol. 52, Science and Technology, pp. 117-130.

5. Mollo-Christensen, E., 1981. "Oceanographic Satellite Data User's Workshop," *Bulletin American Meteorological Society*, Vol. 62, No. 2, pp. 262-263.

6. Cracknell, A.P., editor, 1981. *Remote Sensing in Meteorology, Oceanography and Hydrology*, 542 pages, John Wiley and Sons, New York.

New Laser Technique for Inshore Bathymetry

Rapid surveillance of inshore water for bathymetry and underwater obstacles is important for a variety of applications. Extensive research has been performed in this area during the past several years using a pulsed blue-green laser to map shallow water depth from aircraft. Limitations to this system such as turbidity have necessitated research on a more versatile or less restricting system.

A new laser technique is being studied for inshore bathymetry and object detection. The system is a hybrid system consisting of an infrared laser (CO^2) transmitter and a highly sensitive microphone receiver that is located in the air.

Continued on page 61

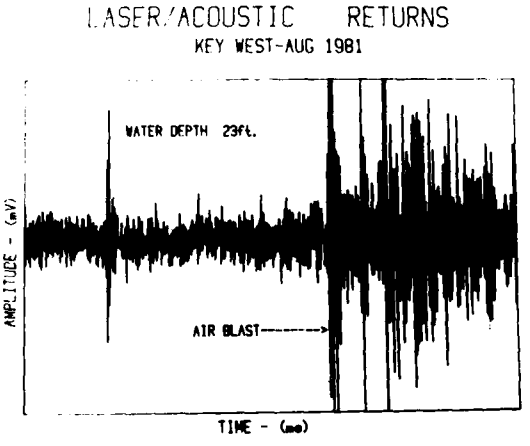

Figure 1.

ACRONYMS
These Acronyms Appear Frequently in This Issue

AVHRR	Advanced Very High Resolution Radiometer
CNOC	Commander Naval Oceanography Command
CZCS	Coastal Zone Color Scanner
CMSP	Defense Meteorological Satellite Program
ERTS	Earth Resources Technology Satellite
FOV	Field of View
GOSSTCOMP	Global Operational Sea Surface Temperature Computation
HIRS	High-Resolution Infrared Sounder
IFOV	Instantaneous Field of View
INDEX	Indian Ocean Experiment
IR	Infrared
IRIS	Infrared Interferometer Spectrometer (also Infrared Information Symposium)
LANDSAT	Land Satellite (Earth Resources Technology Satellite)
McIDAS	Man-computer Interactive Data Access System
NASA	National Aeronautics and Space Administration
NAVAIR	Naval Air Systems
NAVOCEANO	Navy Oceanographic Office
NEPRF	Naval Environmental Prediction Research Facility
NERSCAC	Navy Environmental Remote Sensing Coordinating Advisory Committee
NESS	National Earth Satellite Service
NIMBUS	Polarorbiting Meteorological Satellite
NOAA	National Oceanic and Atmospheric Administration
NOAA-5, NOAA-6, NOAA-7, etc.	Operational Polarorbiting Meteorological Satellites
NOMSS	Naval Oceanographic and Meteorological Support System
NORDA	Naval Oceanographic Research and Development Activity
NOSC	Naval Ocean Systems Center
NRL	Naval Research Laboratory
NSWC	Naval Surface Weapons Center
NVSC	Naval Underwater Systems Center
RSMAS	Rosentiel School of Marine and Atmospheric Science
SAR	Synthetic Aperature Radar
SASS	SEASAT-A Scatterometer System
SCAMS	Scanning Microwave Radiometer
SEASAT	Sea Satellite (a satellite designed to measure oceanic characteristics, it operated for a short time in 1978)
SEBEX	Surface Expression of Bathemetry Experiment
SLAR	Side Looking Airborne Radar
SMMR	Scanning Multifrequency Microwave Radiometer
SST	Sea Surface Temperature
TESS	Tactical Environmental Support System
THIR	Temperature, Humidity, Infrared Radiometer
VAS	Vertical Atmospheric Sounder
VTPR	Vertical Temperature Profile Radiometer

Visible and Infrared Satellite Remote Sensing: A Status Report

Otis B. Brown
and

greater importance to the understanding of oceanic variability than the quasi-quantitative values of the data.

Satellite-based remote sensing of the environment first reached public notice with display of color earth pictures taken from the Mercury manned spacecraft. In fact scientific sounding rockets and military passive sensors were routinely mapping the oceans before this time[1,2]. Multi-spectral color pictures captured public and scientific fancy. However, it was to be some 15 years later with the launch of the NIMBUS-7 Coastal Zone Color Scanner before these promises could start to be realized over oceanic areas; the Earth Resources Technology Satellite, later called LANDSAT, provided quasi-operational land remote sensing in the early 1970s.

Application of infrared remote sensing to the study of meteorological variability was quickly appreciated by analysts and an operational military program was initiated in 1963. This program was managed by the U.S. Air Force and concentrated on determination of world-wide cloudiness, cloud-top temperatures and tactical applications for aircraft logistical use. It was not focussed on the study of oceanic surface thermal variability. The past decade has seen active Navy participation in these efforts, now called Defense Meteorological Satellite Program, with a gradual orientation of the system toward improving ocean thermal-imaging capabilities.

In this report we will discuss the visible/infrared sensing problem, some applications and conclusions. The sensing problem logically splits into two sections: technology to acquire the data, ie., sensors, and algorithms or processing paths for the data once acquired. We will not discuss the sensor problem except as needed for algorithm development.

Sensor Processing

Sensor data processing can be divided into the following 4 categories:

1) ingest, calibration, and remapping
2) navigation
3) calibrated image retrieval, magnification, geometrical correction, and hard copy output
4) interactive analysis with ground truth data, contour plots, etc.

These four classes of activity are necessary for any satellite data analysis procedure; similar systems have been developed for LANDSAT, SMS, DMSP and other geophysical sensing satellite programs. In fact, as will be noted, parts of the procedures to be described are adapted from other efforts. The present system is oriented towards polar-orbiting, rotating scanner, small acceptance-angle sensors. Figure 1 summarizes the overall procedure.

Data Ingest and Calibration

A qualitative appreciation for passive remote sensing measurement techniques is necessary to understand properly the data ingest procedure design. Consequently we will give a brief introduction to visible/infrared remote sensing technique prior to discussion of data ingest procedures.

Remote sensing systems make radiometric measurements in specified electromagnetic frequency bands of energy emitted or reflected by the earth. The absorption spectrum for radiation passing through the atmosphere to space from the sea surface is shown in Figure 2. There are three areas of this spectrum ("windows") in which we have interest: the visible band between 0.3 and 0.7 micrometers, and infrared bands between 3.7 and 4.2 micrometers and 10.0 and 12.0 micrometers. These windows all have the characteristic of having relatively low absorption for radiation; thus they yield relatively clear views of

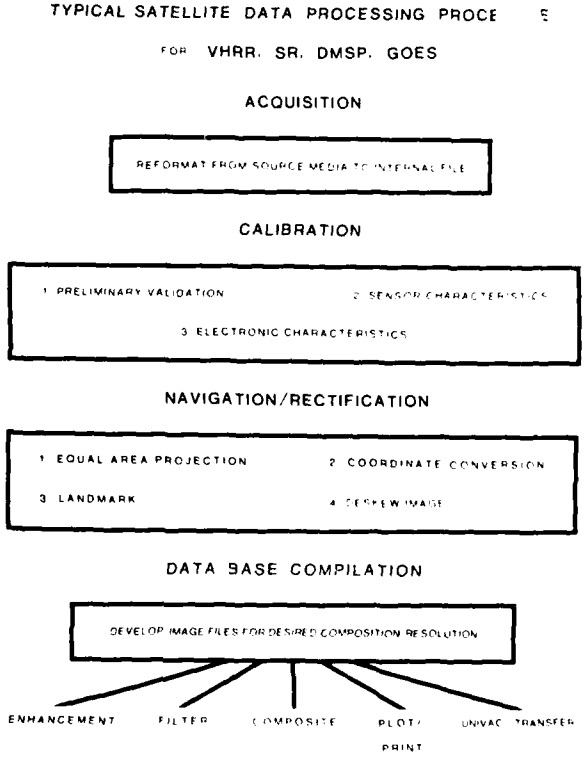

Figure 1. Schematic view of the satellite data processing procedure.

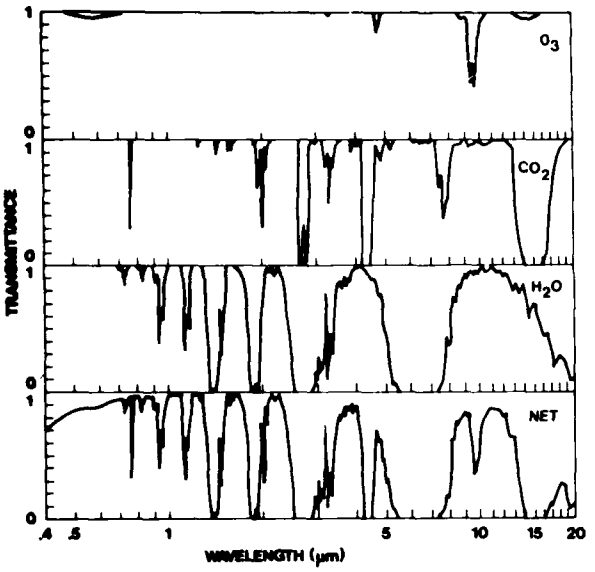

Figure 2. Atmospheric transparency for sea surface light as seen from a satellite. Computed for a U.S. standard atmosphere utilizing the LOWTRAN 4 code (from Selby et al., 1978).

the earth's surface. Scanning radiometers operating in these windows produce two-dimensional images of the sensed outgoing energy. A point value at the spacecraft for a scan-line element pair (pixel) is sensed as either a voltage or current value proportional to the incident energy. This analog value is digitized and telemetered to earth, or telemetered and digitized on earth. TIROS-N is an example of the former[4], and NOAA-5 of the latter[5]. Final digital count values are transcribed into computer-compatible format on earth. Possible error sources in this system occur during the digitization and transmission steps. NASA, NOAA and DMSP spacecraft-data streams contain known references by which telemetry and digitizer errors can be identified and corrected. Sensor calibration is subject to drift as well, due to changes in environmental factors aboard the spacecraft. This three-step process can be described functionally:

$$L = L(C(V(A))) \qquad (1)$$

where L is a radiance, an energy measure, C a drift-voltage transfer function, V a voltage transfer function, and A the telemetered signal level. In the case of infrared radiometers the final temperature is a non-linear function of the radiance L, it is not directly sensed. Seawater can be characterized as a grey body emitter in these two infrared windows with an emissivity, ϵ of .98. To convert the energy value to temperature, a blackbody transform is applied to L, i.e.

$$T = T(L / \epsilon) \qquad 2.$$

where T is an equivalent blackbody temperature (Planck) function. These transforms have been documented by Koffler[6].

T is a radiometrically correct temperature at the top of the atmosphere. Two principal effects must be taken into account: variation in atmospheric absorption as a function of scanner angle (path length) and humidity. Path length absorption is strongly controlled by the atmospheric water vapor since the vertical distribution of water vapor is not constant. Scientists have examined these effects and shown that the sensed temperature can be up to 10C in error for very humid maritime atmospheres at large scan angles.[7,8] Two methods are presently available in our laboratory for calibration. The first is a zero-order method based on climatological mean humidity profiles. This was developed by National Earth Satellite Service and is described by Smith[9]. A temperature correction matrix is derived by regression as a function of scan angle and sensed surface temperature. Sensed surface temperature and total water vapor concentration are found to be highly correlated. Scenes with homogeneous moisture fields are readily analyzed by this technique which produces semi-quantitative two-dimensional surface temperature maps. Functionally,

$$T = H(\alpha, T) \qquad (3)$$

with α the scanner angle and T calculated from equation 2. This correction, though based on climatic mean moisture profiles, is ideal for quick-look and image sorting applications.

The second method which provides a better correction for atmospheric absorption is based on multispectral sensing in the water vapor bands. The new AVHRR radiometers have two or three channels in the infrared: 3.7μ-4.2μ, 10μ-11μ and 11μ-12μ, which are channels 3, 4 and 5 respectively. The integrated atmospheric transmissivity over each of these three channels differs, and consequently algorithms can be constructed which depend on the difference of the perceived surface temperature in these channels. The simplest algorithm assumes that the atmosphere is optically thin enough that the perceived surface temperature difference between any of the channels can be parameterized as a simple function of the bulk atmospheric water vapor seen by the satellite sensor. Functionally a formula of the following form is applied:

$$T_s = a_0 + a_1 T_3 + a_2 (T_3 - T_4) \qquad (3a)$$

where the T_i's are temperature retrievals in various channels for a given location and the a_i's give the parameterized correction. The a_i's can be derived from first principles theoretically[10] or can be derived empirically from good composite sets of surface and satellite observations.[11] Both of these methods give better control on the temperature accuracy at a sacrifice in processing throughput.

Visible measurements suffer from similar problems although they arise from different sources. An analyst rarely desires a radiance measurement at the top of the atmosphere, but rather wishes to know the upwelled radiance at the sea surface or the mean chlorophyll concentration or sediment load in surface waters. Whereas emitted thermal radiation is an intrinsic property of the medium, upwelled visible light arises from back-scattered solar radiation. Consequently, one must calculate the amounts of solar radiation reaching the surface directly and scattered from the atmosphere, the resultant that is transmitted into the sea, that which is back-scattered by the sea and suspended materials and is transmitted through the surface and back through the atmosphere to the satellite. The atmosphere, ocean and suspended material selectively affect the down and upwelled radiances as they propagate from the sources to the satellite sensor. It is a problem which has recently been straightforwardly parameterized. Atmospheric correction algorithms have been proposed.[12,13,14,15] The method of correcting for these effects[12] and with the clear water modifications[16] is summarized in the following.

Radiance which reaches the sensor $L_t(\lambda)$ is composed of contributions from atmospheric Rayleigh scattering $L_r(\lambda)$, aerosol scattering $L_a(\lambda)$ and finally the desired contribution $L_w(\lambda)$ from the water. These terms combine as:

$$L_t(\lambda) = L_r(\lambda) + L_a(\lambda) + t(\lambda) L_w(\lambda) \qquad (4)$$

where $t(\lambda)$ is the diffuse transmittance of the atmosphere. This formulation assumes that the sensor is not viewing specularly reflected sunlight (glitter) and that the fresnel reflection from the sea surface is included in the Rayleigh/aerosol terms. The Rayleigh-scattered light is directly calculable from theory. Hence, if $L_w(\lambda)$ is known, then $L_a(\lambda)$ is derivable. The initial formulation of the correction process uses this approach.[17] If it is known that the aerosol size-refractive index distribution is horizontally homogeneous over the region of interest, then this algorithm quickly generalizes.

This implies that the aerosol selectivity:

$$S(\lambda_2, \lambda_1) = L_a(\lambda_2) / L_a(\lambda_1) \qquad (5)$$

is constant over the region of interest.

In offshore areas, such as the Sargasso Sea or the Gulf Stream, it is well known that there is very little terrageneous material in surface waters; Figure 3 shows that upwelled visible radiance in the red (670 nanometer channel for NIMBUS-7) is quite small as a consequence. One thus can assert that whatever is seen in this part of the spectrum must arise from the atmosphere. That is, we assume

$$t(\lambda_0) L_w(\lambda_0) \cong 0 \qquad (6)$$

Then in a straightforward way one finds that

$$L_w(\lambda) = [t - 1(\lambda)]^{-1} \{L_t(\lambda) - L_r(\lambda) - S(\lambda, \lambda_0) [L_t(\lambda_0) - L_r(\lambda_0)]\} \qquad (7)$$

Alternatively, $S(\lambda, \lambda_0)$ can be computed with high accuracy if $L_w(\lambda)$ is known for some area in the scene. Gordon and Clark[16] show that $L_w(\lambda)$ for Case 1 waters can be calculated with just a knowledge of the solar zenith angle and that operationally these waters are easily identified.[18] Thus, in this method, the procedure is to find a "clear water" area, compute $L_w(\lambda)$, derive $S(\lambda, \lambda_0)$, and proceed to correct the image. A case study is presented later in this report.

Geometrical Correction

Equally as important as radiometric correction to the final data product is conversion of scanner elements to some easily manipulated aspect ratio (metric). Some satellite systems, e.g. DMSP, ac-

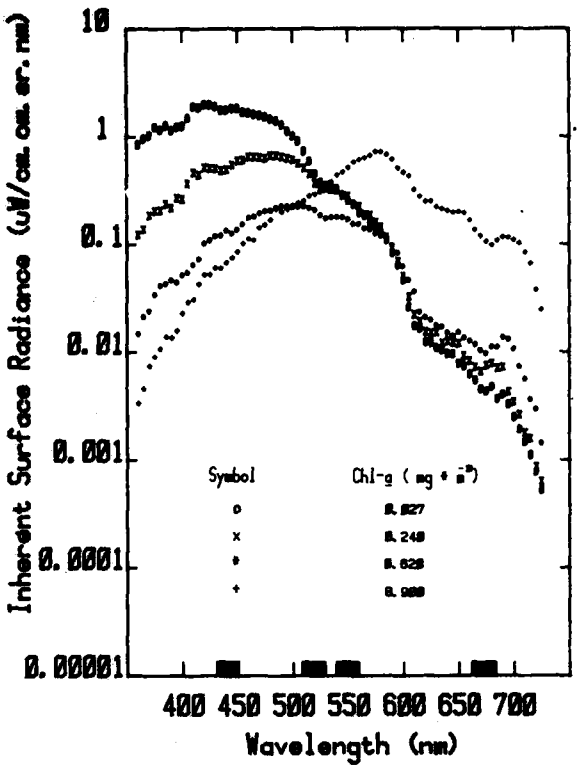

Figure 3. Upwelled light spectral sensitivity to suspended materials (from Gordon and Clark, 1980).[47]

complish a portion of this in hardware by control of scanner or display write-rate[19]. NOAA and most other polar orbiting satellites have fixed-rate scanners and are operated with orbits that have inclinations differing from 90 degrees[4]. Thus, these instruments geometrically distort the pixel aspect ratio at larger scanner angles. Other distortions due to satellite vehicle pitch, roll and yaw may also be present. Pitch, roll and yaw have much more complicated interactions with the scan-line aspect ratio. Variations in these parameters are deduced by study of the differences in high precision navigation generated and observed landmark positions.

Legeckis and Pritchard[20] describe an algorithm for geometrical correction of scan line data. Although similar methodology is used, latitude, time and height-dependent functionals are not based on mean estimates, but carry the full dependence of each parameter. Estimates of these parameters are available from an ephemeris-driven, high precision navigation algorithm that will be described in a latter section. The geometrical correction produces scan lines containing pixels with a prescribed aspect ratio. Functionally a unidirectional mapping from scan-element to new constant aspect ratio scan-element pixels is defined:

$$F = F(s, e, \phi, h) \qquad (8)$$

where s is scan line, e element, ϕ latitude and h satellite height. Figure 4 sketches the algorithm. To first order, there are two effects to be corrected: pixel distortion along a scan line and relative scan line motion. The pixel distortion is taken to be discrete, i.e., old samples are mapped to the nearest whole new sample. As shown in Figure 5, the vector contains varying repetition factors "n", which increase as a function of distance from the nadir point. A given old sample is mapped into "n" new samples. A single run-length encoded transform vector is constructed based at the nadir point, since, to first order, the correction is symmetric about the nadir track. This transform is quite fast due to run-length encoding of the mapping. The second distorting factor, earth rotation, to first order, manifests itself as a line-shift correction. These are either line slips or advances relative to the previous line dependent on satellite nadir track sense, scanner mode and hemisphere.

Data sets that result from transforms 1-8 comprise remapped scan-line sets which are stored on disk and/or tape. These fixed-format, calibrated,

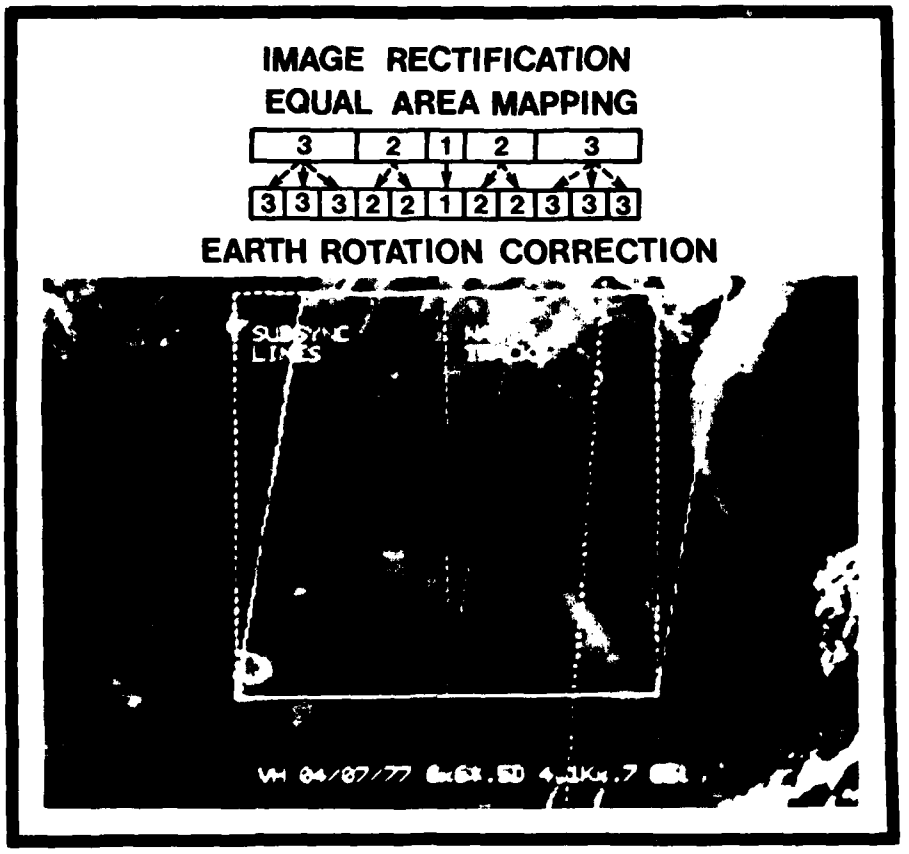

Figure 4. Pictorial representation of scan line and earth rotation remapping corrections.

constant-aspect-ratio data sets constructed from the polar orbiter raw data, are geometrically and radiometrically similar to geosynchronous spin-scan and other small acceptance angle scanners. All subsequent analyses utilize this data-base store for input which simplifies the succeeding levels of analysis algorithms.

High Precision Navigation

Orbiting vehicles can easily be engineered with accurate time bases, but it is more difficult to maintain precise vehicle position and attitude information. Older sensing systems, of which NOAA-5 is a prime example, have marginal attitude sensors (± .5 degree stabilization)[4]. Newer vehicles such as TIROS-N[5], DMSP-BLOCK 5 D,[19] have accurate attitude (± 1° stabilization) and temporal (± 50 msec.) determination systems. The TIROS-N time-keeping accuracy is primarily determined by ground-station operational constraints on spacecraft clock update frequency. Since a one-second error translates into an along-track position error of 6.6 km., this is a tight constraint on update accuracy. We observe (1979-1980) variations as large as two seconds (13 km along track error) in clock accuracy.

In all cases there has been little done to provide useable onboard navigation-linked sensor processing. An ephemeris-driven algorithm,[21] has been constructed to provide latitude, longitude and height information for low-precision mapping. A Keplerian model is utilized with second and fourth order gravity terms; second order secular perturbation corrections on the period, mean anomaly and ascending node are applied in addition. Functionally the position:

$$P_{\lambda' \phi h} = P_{\lambda' \phi h}\,(\text{Ephemeris}) \qquad (9)$$

is derived. The ephemeris consists of the orbital elements: longitude of ascending node, angle of orbital inclination, argument of perigee, semi-major axis, eccentricity, and universal time. λ' is the

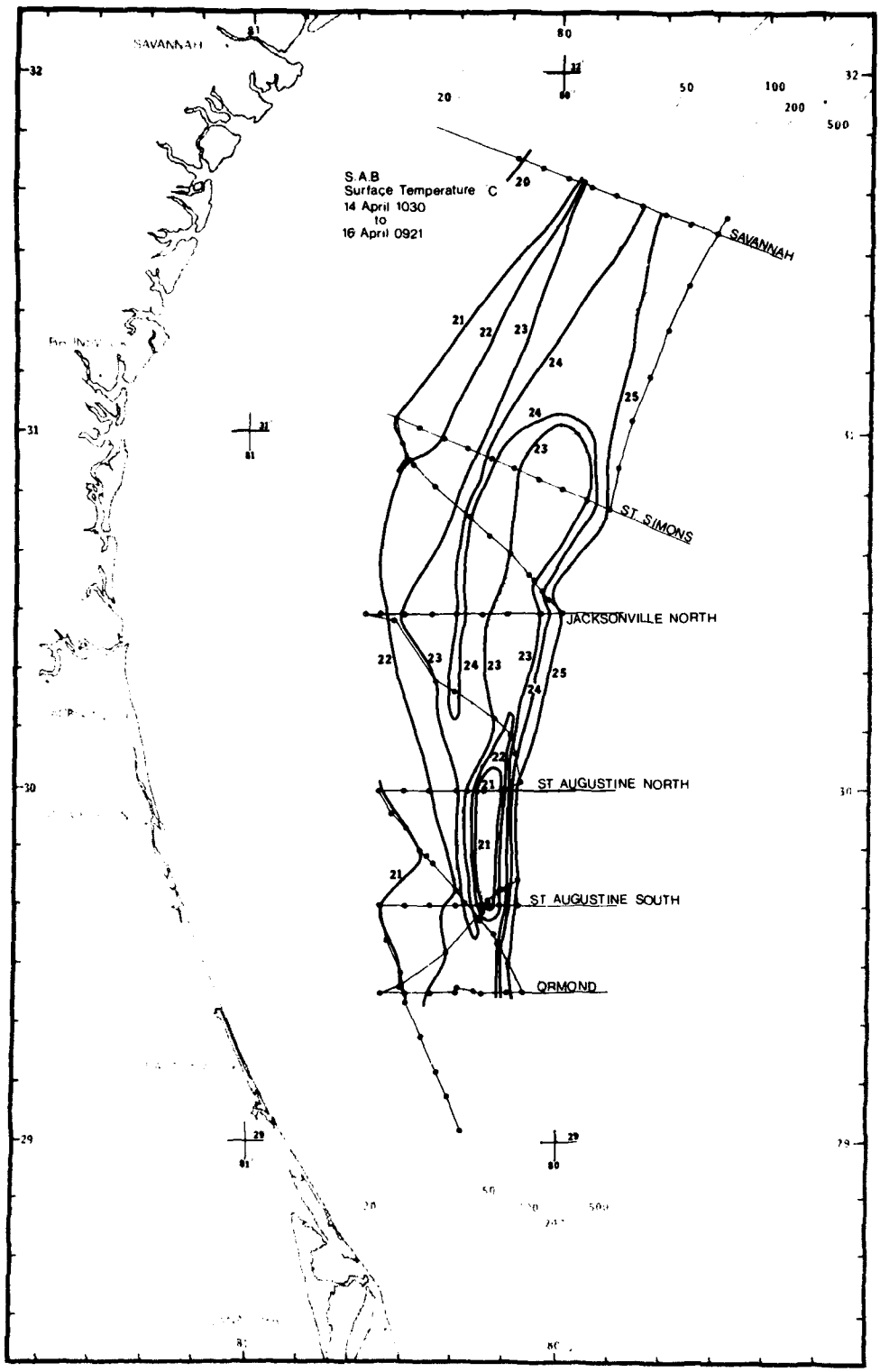

Figure 5. Cruise track and derived temperature field from R/V Columbus Iselin Cruise CI7704 for April 10-12, 1977 (Courtesy Dr. T. Lee).

longitude, ϕ latitude, h height. This procedure is well known and is lucidly documented[22]. Tests of this high-precision navigation algorithm, $P_{\lambda,\phi h}$, demonstrate that satellite position can be predicted on the basis of daily mean orbital elements (ephemerides) to $\pm$ 1 km.

Precision Navigation/Mapping

The high precision of the ephemeris-driven navigation cannot be fully utilized to establish precise scan, element location due to spacecraft clock drift (c-13 km induced error) and attitude control($\pm$ 4 km induced error in roll, pitch, and yaw). Quantification of these errors requires generation of a precision polar-orbit navigation model. Philips and Smith[23] describe a landmarking (control point) approach for navigation of geosynchronous satellites. Knowledge of the scanner geometry permits computation of corrections to the ephemerides by comparison of known earth location positions with model-predicted positions. Daily update of the model then allows "predictive" navigation of the spin-scan radiometer data. This approach is not directly applicable to the low altitude, several-pass-per-day polar-orbiter situation due to the presence of non-secular perturbations.

A navigation method for polar orbiters has been developed in our laboratory.[24] In this method, the nadir track and the scan lines are considered to define great circles on a spherical earth such that the any scan line great circle is always perpendicular to the nadir track great circle. (This is equivalent to the approach of Ruff and Gruber,[25] however, the transform analysis is performed quite differently.) The procedure to establish navigation parameters for a satellite pass consists of the following steps: First, from the universal time of the initial scan line, the high precision navigation model is used to calculate the earth location of the nadir pixel. Second, landmarks (or continental outlines) are selected with an emphasis on maximizing their spatial spread with respect to the nadir track. This is done to minimize the entry of systematic error in the transform equations. Third, corrections from the outlines can be computed for the coordinates of the initial scan line, the time correction and mean pitch, roll and yaw of the satellite.

Analytical transforms are generated by this technique which relate constant-aspect-ratio pixel scanline elements to latitude, longitude and vice-versa. These transforms form a basis for derivation of mapped projections of scanner data.

Performance of detailed analyses of satellite derived ocean skin temperature also requires a humanized interface for data extraction, enhancement and display. An intelligent extraction algorithm founded on the precision navigation transforms yields an easily useable method to display an image centered at some earth/scanner coordinates with a given resolution. This resultant data set (or the original) with an appropriate transform function can then be projected into various coordinate systems (transverse mercator, polar stereographic, etc.) which are stored on disks and are available for recall at the analyst's convenience.

Case Studies

In the first part of this report we summarized the radiative transfer, navigation and data bases needed for satellite remote sensing of visible and infrared radiance from the ocean. Now we will describe several case studies which illustrate that application of the above methodology yields quantitative and qualitative improvement of our understanding of the ocean.

NOAA-5 Gulf Stream Location Observation in the South Atlantic Bight

During early April, 1977, Dr. T. Lee (University of Miami/Rosenstiel School of Marine and Atmospheric Science) mapped the thermal structure of the Gulf Stream/shelf water interface in the Georgia Bight.[26] A surface thermal field derived from these measurements is shown in Figure 5. Simultaneously the ocean skin temperature was observed from space by the NOAA-5 Very High Resolution Infrared Radio-meter. These data were processed by the afore-mentioned procedure and a 3 km gridded equal-area product was generated for analysis purposes. This result is illustrated in Figure 6. All continental outlines and political boundaries have been inserted from a national data base in terms of earth location pairs via the earth-scanner mapping transform. Retrieval of the temperature values along the ship track is accomplished with the inverse mapping transform. The ship track location and corresponding temperatures were digitized as triplets of latitude, longitude and temperature from Figure 5 with a graphics tablet. Figure 7 shows the highlighted ship track off the Georgia coast. Magnifying the area of interest about the ship track (Figure 8), we notice the strong gradients in thermal field at the Gulf Stream/shelf water interface. Visual comparison of Figures 5 and 7 illustrates the fact that the satellite data with its inherently higher spatial definition can yield a good surface thermal map in situations with

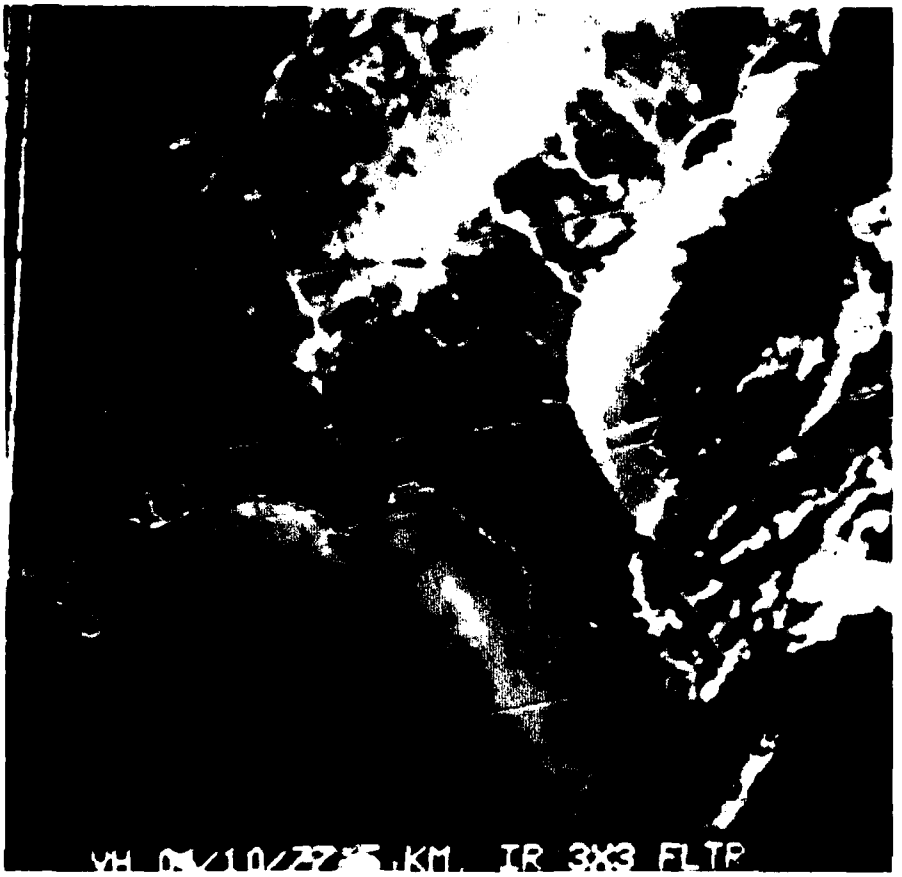

Figure 6. NOAA 5 VHRR equal-area processed thermal map for 10 April 1977.

low to moderate atmospheric water vapor (< 1 gm/cm²). [A mean airmass correction of 1.25 C is subtracted from the satellite observations.] The temperature along the ship track comprises a one dimensional series as a function of cumulative along-track distance. Frontal definition and temperature agreement between both methods is quite good. Quantitatively we find the standard deviations of the ship and satellite track-line series to be 2.1C and 2.2C, respectively, while the rms difference of the two series is 1.2C. These values are calculated for a set of several thousand observation pairs. The near equivalence of the ship and satellite standard deviations implies there is little second order-moment bias, or conversely the satellite shows the same biases as the ship. A mean square difference of 1.2C is the expected difference at ± 1 standard deviation. This is comparable to estimates NOAA/NESS has made for other temperature products.[27] We believe the main contributor to this difference is the inherently different sampling scales of the two methods. The mean square and mean differences are extraordinary in that the comparison values are representative of total error, that is errors arising from navigation inaccuracies, time and space sampling mismatch, water vapor contamination, radiometer calibration, etc. This verification area was chosen for two reasons: high quality ship and satellite data were available nearly concurrently and strong thermal features with small scales were present which would magnify navigation, mapping, and calibration errors. Thus we believe that this comparison is indicative of the procedure's utility in relatively clear, homogeneous atmospheric water vapor situations. A spatially inhomogeneous moisture field would render this analysis less valid.

Figure 7. Magnification of Figure 6 about the ship track.

NIMBUS-7 CZCS Observations of Color Variability in the Middle Atlantic Bight

A recent work by Gordon et al[28] utilizes CZCS (Coastal Zone Color Scanner) observations to map the surface chlorophyll structure of a warm-core ring off the Northeast coast of the United States. Warm-core rings occur when extended meanders of the Gulf Stream pinch off on the cold-wall (north side) and form a closed anticyclonic rotating vortex of Gulf Stream and Sargasso Sea waters. This vortex of Gulf Stream and Sargasso Sea waters is imbedded in the surrounding slope or shelf waters and is thought to isolate an ecosystem at some point in its life cycle. Rings have horizontal dimensions of 100-200km and vertical extents equal to or greater than 1000m.[29,30] We show in this study that mean chlorophyll concentration in surface waters can be observed to 35% utilizing satellite method alone.

Figure 9 is an overview of the shelf and slope water chlorophyll concentration off the northeast United States coast for 15 June 1981. The readers attention is directed to several prominent features: the low chlorophyll values (lighter grays) in a warm core ring located at 39° N, 69° W, (catalogued as 79-B by Fitzgerald and Chamberlin[31]) the low and high chlorophyll streamers wrapping into the ring, their length, and the overall decrease of chlorophyll as one travels north of the Gulf Stream and away from the coast.

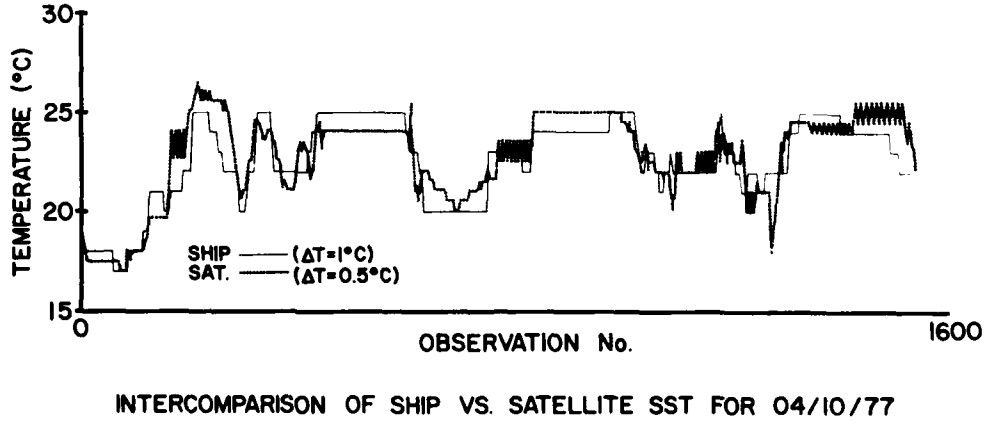

Figure 8. Satellite versus ship derived temperature intercomparison.

The fact that this warm core ring has such a strong chlorophyll signature implies that it can be tracked as either a color or an infrared anomaly. Qualitatively the color structure raises several interesting theoretical questions: How is it that the surface chlorophyll streamers cross the ring-front and spiral in the central regions of the ring? What is the mechanism underlying propagation of ring effects (through the streamers) to distances of one to two ring-diameters away? Are there differences in the thermal and color signatures of a warm-core ring? Does a regional water mass analysis support the large-scale chlorophyll surface pattern we observe? Comprehensive delineation of the first two effects awaits 1982 warm core ring cruise work, the latter question can be addressed qualitatively by looking at the slope water mass distributions in the area. McLellan's analysis[32] of the water mass areal distributions in this area agrees with the present observations in that he finds shelf-type waters in the Bight and up into the Gulf of Maine and cooler, lower oxygen waters of Labrador origin offshore. This juxtaposition of water masses yields the strong horizontal chlorophyll contrasts seen in the present imagery.

Figure 10 is an enlarged view of Figure 9 centered about the ring. Streamer delineation and local chlorophyll minimum in the ring interior are seen. Figure 11 is an enlarged view of the ring as seen several hours earlier in TIROS-N AVHRR infrared imagery. Ring frontal outlines are consistent between the different sensing methods, however delineation of cross boundary flows is quite a bit more difficult in the infrared. The local minimum in central waters seen in the chlorophyll is mirrored in the thermal imagery as a temperature maximum. One is left with the impression that although there is coherency between the two methods, color is a more sensitive indicator for study of cross-boundary surface flows.

Fine-scale features may be atmospheric artifacts. One must know which features are atmospheric and/or oceanic in origin. A cruise in support of the NIMBUS CZCS validation made a section through this ring at 0000 EDT, 10 June 1979. NIMBUS orbits 3157 and 3171 bracket this ship coverage occurring approximately 12 hours before and after, respectively, ship passage through ring center.

Pigment concentration was measured along the ship track by using a Turner Designs flow-through fluorometer (Model 10) to monitor the in-vivo fluorescence of water drawn continuously from about 1.5m below the surface. Periodically, discrete samples were drawn from the same source and extractions performed to determine fluorometrically the concentrations of chlorophyll and the associated phaeopigments, using the technique described by Yentsch and Menzel[33] with the modifications of Holm-Hansen et al[34]. These discrete determinations

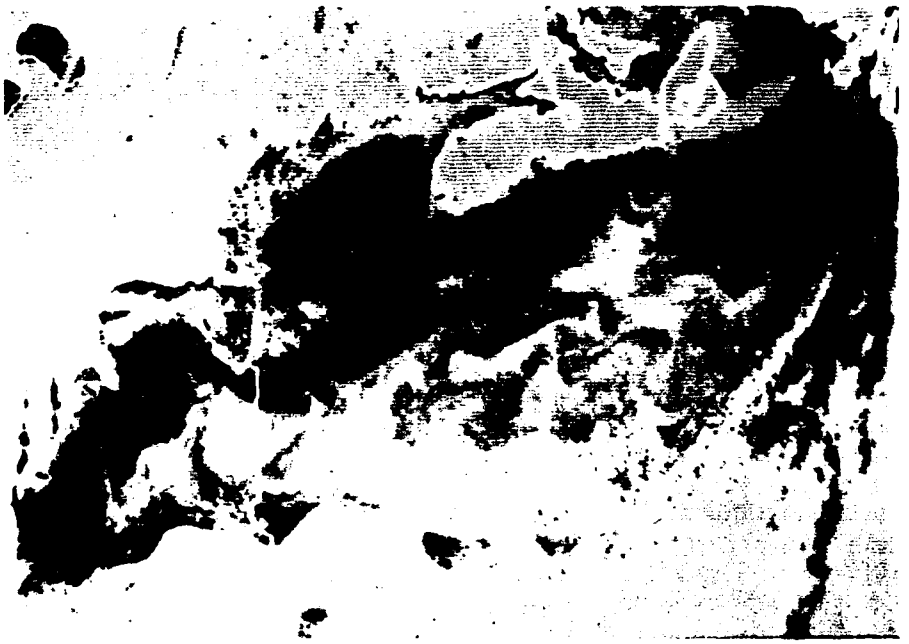

Figure 9. NIMBUS-7 CZCS derived chlorophyll image for 15 June 1979, orbit 3226. Lighter shades denote lower values, darker higher (from Gordon et al., 1982).

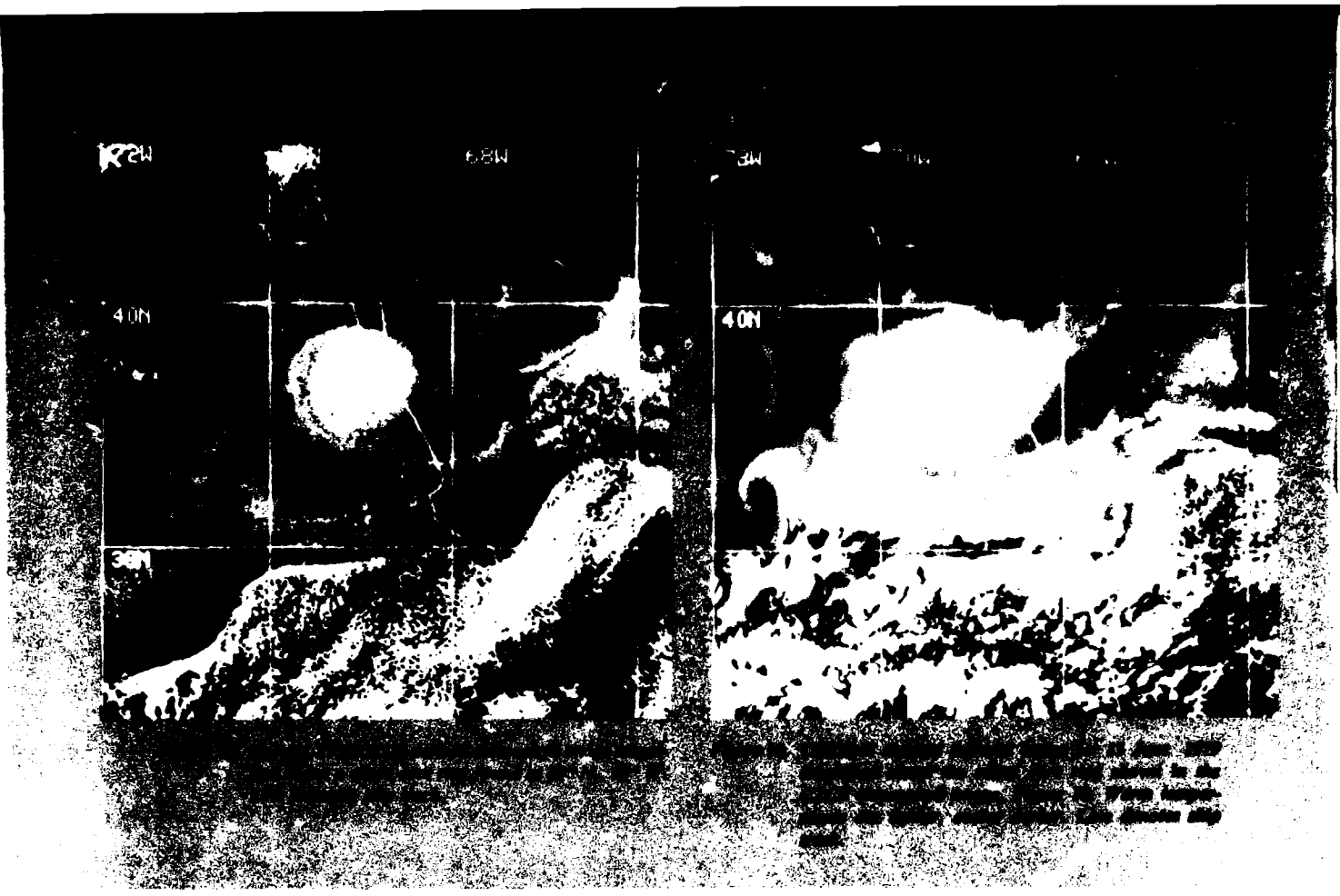

were then used to relate the continuous in-vivo fluorescence measurements to the pigment concentration. CZCS-derived pigment concentration (heavy line) is compared with these continuous determinations in Figure 12. This track is from south to north, starting in the Gulf Stream, passing through the slope water, the warm-core ring and finally ending on the shelf. These distinct water types are apparent in Figure 12. The cold wall of the Gulf Stream is at about 220km on the axis, and the ring extends from 300 to 350km. Satellite determined pigment concentration is split between orbit 3157 from 320 to 440km and orbit 3171 from 420 to 600km. Gaps in the satellite-derived values are due to clouds. Agreement between the two methods is apparent.

Examination of warm-core rings is an ideal application for remote sensing since they have signatures in the color and infrared. Technically they are easy to study as well since the Gulf Stream offers a clear-water area for CZCS calibration and slowly varying thermal signal for infrared observations.

TIROS-N/NOAA-6 Observations of Somali Current Response to the Summer Monsoon

Our purpose in this section is to give a summary of surface temperature variability near the East African Coast as observed by satellite and ship during the mature phase of the summer monsoons of 1976-1979. Sea surface temperature (SST) pattern changes have been shown to be strongly correlated with changes in the surface-current field[35,36]; as such they yield a sequence of observations of the East African current-system variability during the summer monsoon.

Monsoonal forcing has two major large-scale effects on the northwestern Indian Ocean: Somali Current spinup and maintenance, and cooling of the upper mixed layer. Delineation of these effects on the ocean is complicated by the presence of large scale eddies near the ocean boundary (which maybe the Somali Current) and in the ocean interior[37], intensive upwelling near the boundaries[38], and other large scale disturbances.

Historically physical oceanographers have con-

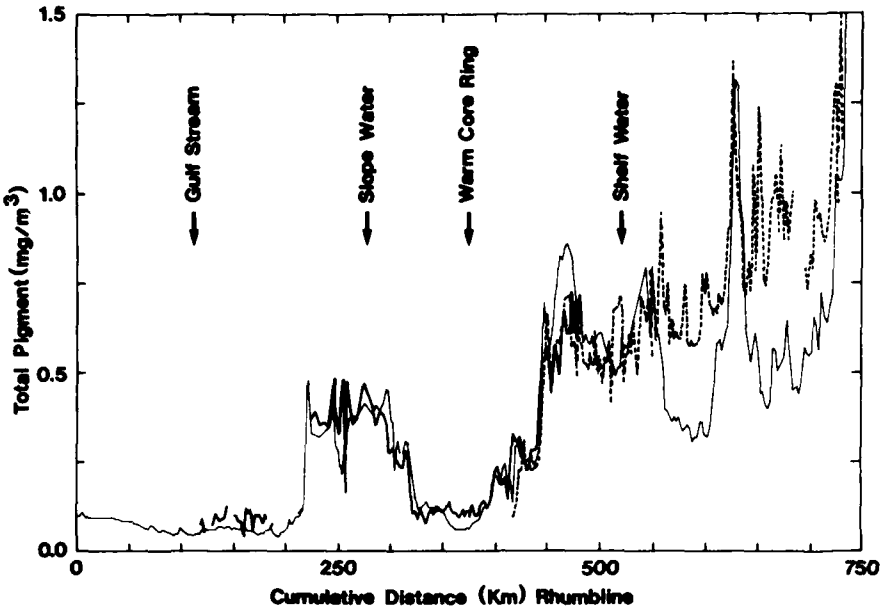

Figure 12. Comparison of ship and satellite derived surface pigment concentrations for NIMBUS-7 orbits 3157 and 3171, and R/V Athena II in-situ observations. Ship observations are denoted by the light line, satellite observations by the heavier solid and dashed lines, orbits 3157 and 3171 respectively (from Gordon et al., 1982).

sidered the Somali Current to be a seasonally reversing western boundary current. Source waters from south of the equator flow north along the East African Coast, separating and flowing into the interior as part of the "Great Whirl" between 10° and 12°N[39,40,41,42], the Great Whirl being a large anticyclonic eddy which is observed off the coast of Somalia during the summer monsoon. It has dimensions of 500 km (parallel to coast) by 400 km (perpendicular to the coast.[43] Bruce and Brown find several instances (1970, 1976, 1979) when the Somali Current is observed to separate from the coast south of the Great Whirl between latitudes 2° N-5° N.[44,35] It was assumed that there were "single gyre years" and "two gyre years." In 1979 Brown found both cases at different stages of the summer monsoon.[35]

Figure 13 illustrates the ship derived surface thermal fields as observed during the mature phase of the summer monsoon in 1979[35]. In the surface-current field at this time offshore flow was found at 2° N, together with an anti-cyclonic gyre between 5° N and 10° N with offshore flow from 10° N to 12° N.[36] Surface current and thermal fields are strongly coupled as might be expected from earlier observations[41]. Separation regions are expressed in the SST as cold wedge shaped areas.

Figure 14 presents a time series of frontal positions as observed during the period June to October, 1979, by satellite. The southern frontal region starts to move poleward, slows and then quickly translates to a position ~1° south of the original northerly separation location. During the same time interval the northerly region (dashed area) moves slowly poleward to the region of Socotra and thence more quickly southward, coalescing with the southern region south of its earlier position near Ras Hafun. Ship observations made during the latter phases of this process near Ras Hafun find fresher, cooler water in the upper ~100 m. overlaying warmer, more saline waters in the northwest quadrant of the Great Whirl. That is, surface waters are characteristic of Somali Current origin while deeper waters are compatible with Arabian Sea sources (John Bruce, private communication, Woods Hole Oceanographic Institution).

Analysis of the 1979 results stimulated interest in reprocessing of earlier satellite data archived during 1976-1978. Figure 15 illustrates observed frontal time series for 1976. Southern frontal translation occurs later and is much slower than the 1979 case. The

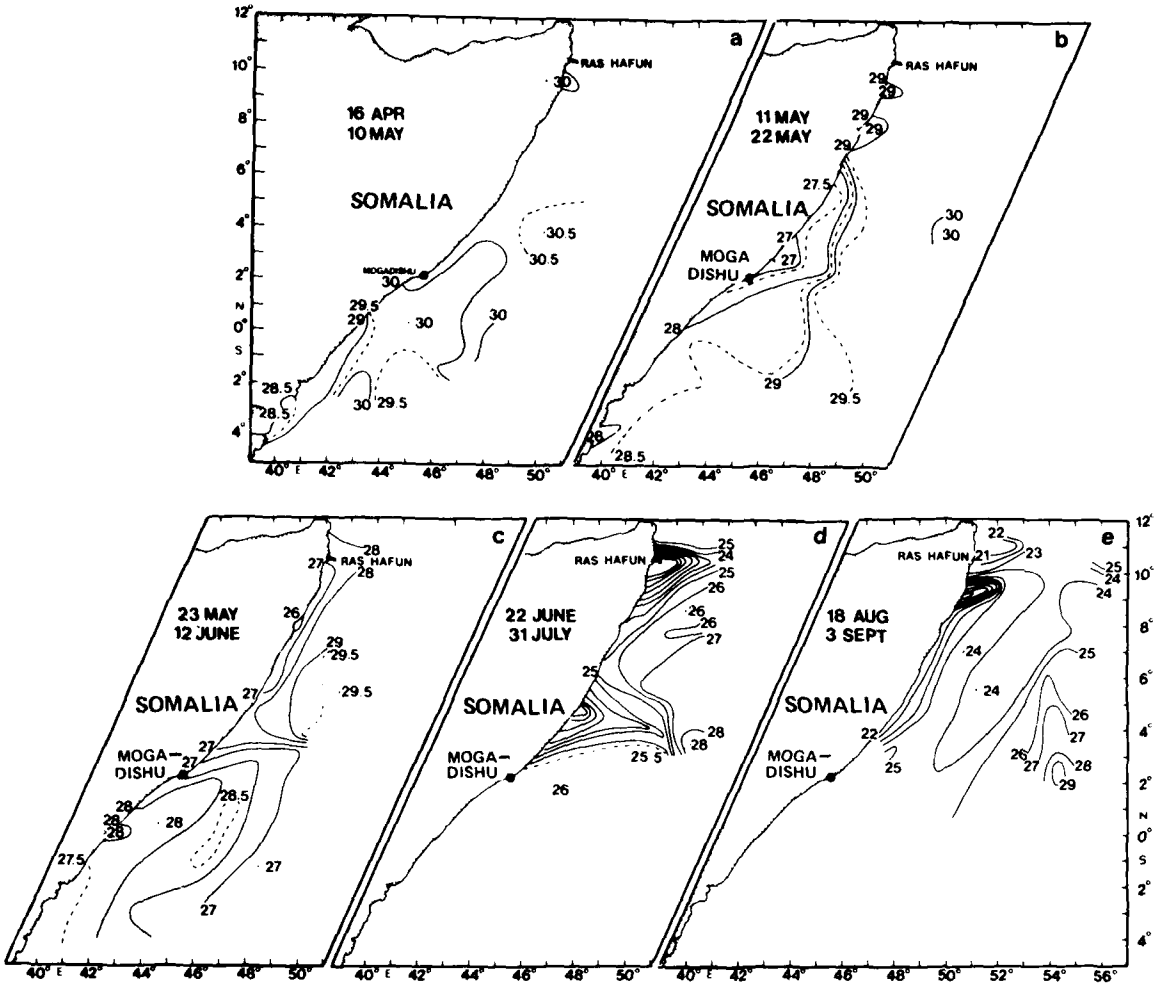

Figure 13. Time sequence of ship observed sea surface temperature fields for oceanic response to the southwest monsoon, 1979. 1a: 16 April-10 May, 1b: 11 May-22 May, 1c: 23 May-12 June, 1d: 22 June-31 July, 1e: 18 August-3 September. (from Brown et al, 1980).

multi-phase nature of the transition is evident, although the absolute changes in translation rate are much less.

Satellite imaging of the area in 1977 was inadequate for resolution of weaker thermal differences due to spacecraft malfunctions and related problems. Imagery on hand neither supports nor denies the presence of the dual separation region in this year. Research ship observations of surface temperature are available for 1977 from the *R/V Shokals'kii* which was deploying INDEX moorings off Somalia. A temperature map for early June is presented in Figure 16 (Donald Johnson, private communication, Old Dominion University, Norfolk). Temperatures are not as low as in the other three years, but a wedge is apparent at 6 N.

Satellite-derived frontal positions during summer 1978 are illustrated in Figure 17. Fronts occur at the same times as in 1979, however, the northern frontal region passes through the Socotra topographic arc and eventually dissipates in the western Arabian Sea. Southern wedge translation rates are intermediate between those observed in 1976 and 1979.

Satellite-derived frontal patterns suggest that dual separation regions (double gyre configuration) occur in three of the four years studied. This interpretation is at variance with classical views of Somali Current circulation.

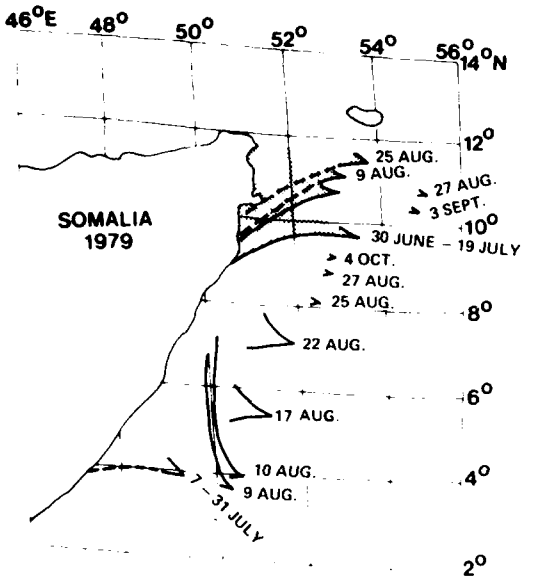

Figure 14. Time sequence of satellite observed frontal locations for northern and southern frontal wedges for year 1979. The northern wedge front is hatched (from Evans and Brown, 1981).[48]

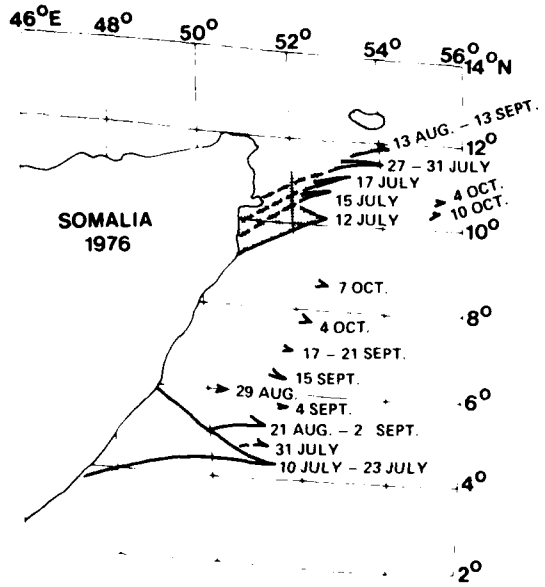

Figure 15. Time sequence of satellite observed frontal locations for northern and southern frontal wedges for year 1976. The northern wedge front is hatched (from Evans and Brown, 1981).

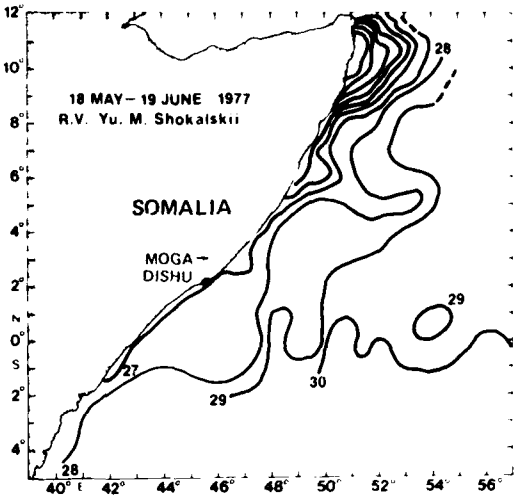

Figure 16. Surface temperature map derived from measurements made onboard the R/V Shokals'kii during May-June, 1977 off Somalia. (from Evans and Brown, 1981, courtesy Dr. D. Johnson).

These observations show coalescence of the Somali Current system is abrupt and can be thought to consist of four phases. During phase I the southern separation region moves north from its onset location during the mature phase of the summer monsoon to ~6° N. Simultaneously the northern frontal region translates poleward to the region of Socotra. In phase II the system is in quasi-steady state for a period of several days to a week. The third phase begins with reversal of northern frontal propagation in 1976 and 1979; in 1978 phase III is initiated when the northern frontal zone breaks through the topographic arc connecting Socotra and East Africa. The southern region moves more quickly poleward than in phase I, while the northern zone translates equatorward (1976, 1979); in 1978 the northern zone translates into the Gulf of Aden and dissipates. Finally coalescence occurs during phase IV in 1976 and 1979. This phase lasts for periods of days to weeks.

From the data presented for the period 1976-1979 we assert that this "anomalous" separation is confirmed in 3 of the 4 years. More interestingly these satellite data give us a first look at the temporal evolution of the Somali Current from the anomalous separation case to the more historically expected circulation. It may well be that the single or dual gyre nature historically observed is a function of the time when observations were made rather than being indicative of interannual differences in oceanic

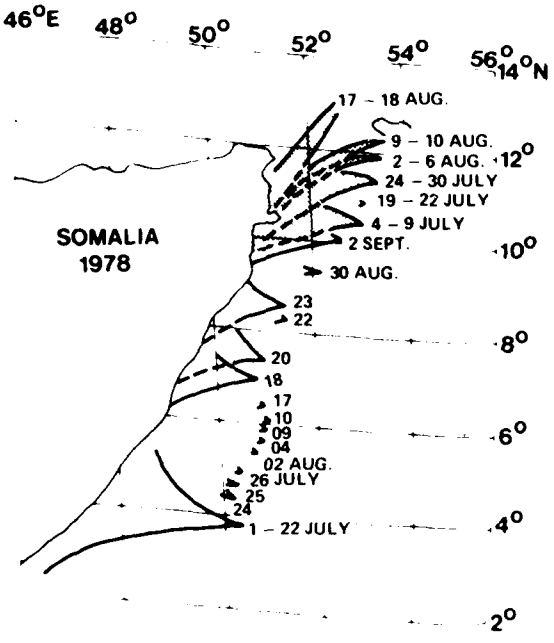

Figure 17. Time sequence of satellite observed frontal locations for northern and southern frontal wedges for year 1978. The northern wedge front is hatched (from Evans and Brown, 1981).

response.

Spinup model results suggest that, at least in some years, the Somali Current can separate from the coast south of the Great Whirl at 5° N. This variability may be due to the strength of the monsoon. Cox has shown the generation and stall characteristics of the eddy circulations are strongly dependent on the the wind stress.[46] If one assumes that there is a transition from a stalled-eddy state to a poleward-translating state with diminution of the wind stress, then the Cox (1979) model may also be relevant to the phase I observations.

Conclusions

In this report we give an overview of the sensing data flow problem, solutions and several applications. We have shown that it is possible to do quantitative visible and infrared remote sensing and apply it to an improved understanding of the ocean. However, an important facet of these applications is that it is the patterns of a given parameter which yield the most valuable information, not the quantitative results. For example, one asks: Where is the Gulf Stream? not, How warm is it? or, Where is a warm core ring? and, What is its size? Does the ring have high or low chlorophyll values? What is the pattern of SST response to the summer monsoon? This is not to say that quantitative results are unnecessary; they directly give us an appreciation for atmospheric contamination of retrieval and enable us to judge which signals are oceanic in origin. It is important to understand that these types of passive measurements permit generalization of accurate in-situ process observations to larger scales, but do not at this time have the accuracy of in-situ observations. Satellite oceanography currently is a highly descriptive endeavor, only in limited cases will it be possible to obtain very quantitative results. However even in its presently crude quantitative form it does and will enable workers to test hypotheses of ocean circulation and transient response to forcing.

Acknowledgements

The authors would like to acknowledge the work of Messrs. James Brown and Angel Li in the software and navigation generation. Dr. Howard Gordon played an instrumental role in the theoretical developement of the atmospheric correction algorithms used for the CZCS processing in our laboratory. Many discussions with him and Dr. Donald Olsen have helped elucidate the significance of the color signatures. We wish to thank Mr. Dennis Clark of NOAA/NESS who provided the ship trackline data used in the intercomparison with the satellite chlorophyll algorithms. This work could not have come to its present level without the early help of the late Dr. Walter Duing. Support of the Office of Naval Research is gratefully acknowledged. ■

References

1. Newell, H. E., Jr., 1953, *High Altitude Rocket Research,* Academic Press, New York, New York.

2. Newell, H. E., Jr., 1959, *Sounding Rockets,* McGraw-Hill Book Co., New York, New York.

3. Newell, H. E., 1980, *Beyond the Atmosphere, Early Years of Space Science.* The NASA History Series, NASA SP-4211. Superintendent of Ducuments No.: NAS 1.21:4211.

4. Schwalb, A., 1972, *Modified Version of the Improved TIROS Operational Satellite (ITOS D-G).* NOAA TM NESS 35. Available from NTIS as COM-72-10547. 48 pp.

5. Schwalb, A., 1978, *The TIROSN/NOAA A-G Satellite Series.* NOAA TM NESS 95. Available from NTIS. 75 pp.

6. Koffler, R., 1976, "Digital Processing of NOAA's Very High Resolution Radiometer (VHRR) Data." *Proceedings of AIAA- International Astronautical Federation, October 10-16, 1976,* Anaheim, California. 7 pp.

7. Anding, D. and R. Kauth, 1970, "Estimation of Sea Surface Temperature from Space." *Remote Sensing of the Environment,* 1:217-220.

8. Maul, G., M. Sidran, 1973, "Atmospheric Effects on Ocean Surface Temperature Sensing from NOAA Satellite Scanning Radiometer." *Journal of Geophysical Research,* 78:1909-1916.

9. Smith, W. L., P. K. Rao, R. Koffler and W. L. Curtis, 1970, "The Determination of Sea Surface Temperature from Satellite High Resolution Infrared Radiation Measurements." *Monthly Weather Review,* 98(8):604-611.

10. Deschamps, P. Y. and T. Phulpin, 1980, "Atmospheric Correction of Infrared Measurements of Sea Surface, Temperature Using Channels at 3, 7, 11, and 12. *Boundary Layer Meteorology,* 18(1), pp. 131-144.

11. McClain, E.P., 1981, "Multispectral Approaches to Satellite-derived Sea Surface Temperatures." *EOS,* AGU 62 (17) p, 294.

12. Gordon, H. R., D. K. Clark, 1980a, "Atmospheric Effects in the Remote Sensing of Phytoplankton Pigments." *Boundary Layer Meteorology,* 18, 299-313.

13. Morel, A. Y., 1980, "In-water and Remote Measurements of Ocean Color." *Boundary Layer Meteorology,* 18, 177-201.

14. Clark, D. K., 1980, "Phytoplankton Algorithms for the NIMBUS-7 CZCS." COSPAR/SCOR/IUCRM Symposium Oceanography from Space, Venice, Italy. May 26-30.

15. Smith, R. C., W. H. Wilson, 1980, "Ship and Satellite Bio-optical Research in the California Bight." COSPAR/SCOR/IUCRM Symposium on Oceanography from Space, Venice, Italy. May 26-30.

16. Gordon, H. R., D. K. Clark, 1980b, "Remote Sensing Optical Properties of a Stratified Ocean: An Improved Interpretation. *Applied Optics,* 19, 3428-3430.

17. Gordon, H. R., D. K. Clark, J. L. Mueller and W. A. Hovis, 1980, "Phytoplankton Pigments Derived from the NIMBUS-7 CZCS: Initial Comparisons with Surface Measurements." *Science,* 210, 63-66.

18. Morel, A. Y., and A. L. Prieur, 1977, "Ocean Color Analysis," *Limnology and Oceanography,* vol. 22, pp. 709-722.

19. Nichols, D., 1975, *Block 5D Compilation.* Headquarters, Space and Missile Systems Organization, Air Force Systems Command, United States Air Force. 600 pp.

20. Legeckis, R., J. Pritchard, 1976, *Algorithm for Correcting the VHRR Imagery for Geometric Distortions Due to Earth Curvature, Earth Rotation, and Spacecraft Roll Errors.* NOAA TM NESS 77. Available from NTIS as PB-258 027. 31 pp.

21. Brouwer, D., 1959, "Solution of the Problem of Artificial Satellite Theory Without Drag." *The Astronomical Journal,* 64(9):1274.

22. *Escobal, P., 1965, Methods of Orbit Determination,* John Wesley and Sons, Inc. New York, London, Sydney. 463 pages.

23. Philips, D., E. Smith, 1973, *Geosynchronous Satellite Navigation Model.* NASA-GSFC Contract Report, NAS5-21794.

24. Brown, J., R. Evans and O. Brown, 1978, A Precision Navigation Method for Polar Orbiting Satellites. In preparation.

25. Ruff, I., A Gruber, 1975, *Graphical Relations Between a Satellite and a Point Perpendicular to the Satellite Velocity Vector (Side Scan).* NOAA TM NESS 65. Available from NTIS as COM-75-10678. 20 pp.

26. Lee, T., 1978, *Measurement of Gulf Stream and Wind Induced Shelf Circulation in the South Atlantic Bight.* A progress report submitted to the Department of Energy, Contract EY-76-S-05-5163. University of Miami, RSMAS. 101 pp.

27. Brower, R. L., W. G. Pichel, C. C. Walton and T. L. Signore, 1966, *Current Status and Quality of Global Operational Sea Surface Temperatures from Satellite Infrared Data.* NESS Internal Memo.

28. Gordon, H. R., D. K. Clark, J. W. Brown, O. B. Brown and R. H. Evans, 1982, "Satellite Measurement of the Phytoplankton Pigment Concentration in the Surface Waters of a Warm Core Gulf Stream Ring." *Journal of Marine Research*, 40(2), in press.

29. Saunders, P. M., 1971, "Anticyclonic Eddies Formed from Shoreward Meanders of the Gulf Stream" *Deep Sea Research*, 18, 1207-1219.

30. Lai, D., P. Richardson, 1977, "Distribution and Movement of Gulf Stream Rings." *Journal of Physical Oceanography*, 7, 670-683.

31. Fitzgerald, J. and J. L. Chamberlin, 1981, "Anticyclonic Warm Core Gulf Stream Eddies off the Northeastern United States during 1979." *Annales, Biologues*, 36, in press.

32. McLellan, H. J., 1975, "On the Distinctness and Origin of the Slope Water off the Scotian Shelf and Easterly Flow South of the Grand Banks." *Journal of Fishery Board CANADA*, 14(2), 213-239.

33. Yentsch, Thomas C., and D. W. Menzel, 1963, "A Method for the Determination of Phytoplankton Chlorophyll and Phaeothytin by Fluorescence." *Deep Sea Research*, vol. 10, pp. 221-231.

34. Holm-Hansen, O. G., C. J. Lorenzen, R. W. Holmes and J. D. H. Strickland, 1965, "Fluorometric Department of Chlorophyll." *Journal de la Counseil de l'Exploration de la Mer*, 30, 3-15.

35. Brown, O. B., J. G. Bruce and R. H. Evans, 1980, "Sea Surface Temperature Evolution in the Somali Basin During the Southwest Monsoon, 1979." *Science*, 209, 595-597.

36. Duing, W., R. Molinari and J. C. Swallow, 1980, "Somali Current: Evolution of Surface Current." *Science*, 209, 588-590.

37. Duing, W., 1970, *The Monsoon Regime of the Currents in the Indian Ocean.* East-West Center Press, University of Hawaii, Honolulu. 68 pp.

38. Bruce, J.G., 1974, "Some Details of Upwelling off the Somali and Arabian Coasts." *Journal of Marine Research*, 32, 419-423.

39. Defant, A., 1961, *Physical Oceanography.* Vol 1. Pergamon Press, New York, N.Y., 567-568.

40. Stommel, H. and W. S. Wooster, 1965, "Reconnaissance of the Somali Current During the Southwest Monsoon." *Proceedings of the National Academy of Science U.S.A.*, 54, 8-13.

41. Swallow, J. C., J. G. Bruce, 1966, "Current Measurements off the Somali Coast during the Southwest Monsoon of 1964." *Deep-Sea Research*, 13, 861-888.

42. Warren, B., H. Stommel and J. C. Swallow, 1966, "Water Masses and Patterns of Flow in the Somali Basin During the southwest Monsoon of 1964." *Deep-Sea Research*, 13, 825-860.

43. Duing, W., 1978. The Somali Current, "Past and Recent Observations." In *Review Papers on Equatorial Oceanography. FINE Workshop Proceedings.* NOVA/MIT University Press, June, 1978.

44. Bruce, J. G., 1979, "Eddies off the Somali Coast During the Southwest Monsoon." *Journal of Geophysical Research*, 84, 7742-7748.

45. Duing, W. and K.-H. Szekielda, 1971, "Monsoonal Response in the Western Indian Ocean." *Journal of Geophysical Research*, 76, 4181-4187.

46. Cox, M. J., 1979, "A Numerical Study of Somali Current Eddies." *Journal of Physical Oceanography*, 9, 311-326.

47. Selby, J. E. A., F. X. Kenizys, J. H. Chetwynd Jr., R. A. McClatchey, 1978, *Atmospheric Transmittance/Radiance: Computer Code LOWTRAN 4.* AFGL-TR-78-0053, Environmental Research Papers, No. 626. Available from NTIS.

48. Evans, R. H., O. B. Brown, 1981, "Propagation of Thermal Fronts in the Somali Current System." *Deep-Sea Research*, 28A:521-427.

As a past doctoral student in physical oceanography at the University of Miami, Dr. Otis B. Brown participated in the GATE Program as associate chief scientist on board the Alexander von Humboldt studying the South Equatorial Current. These initial studies have expanded to include Gulf Stream and Antilles Current work as well as an extensive satellite observation/field program in the Somali Current. Presently he is a research associate professor of physical oceanography at the Rosenstiel School of Marine and Atmospheric Science, University of Miami.

Dr. Robert Evans joined the Division of Meterology and Physical Oceanography at the Rosenstiel School of Marine and Atmospheric Science, University of Miami in 1974. His research activities with NASA and NOAA, included development of large computer codes and work with prototype multi-spectrum scanners. His experience was important in establishing a satellite remote sensing program at the University of Miami. This program has since progressed to include both color and infrared observation of the Atlantic and Indian Oceans.

Scripps Institution of Oceanography's remote sensing facility. This facility is typical of man-interactive, display system

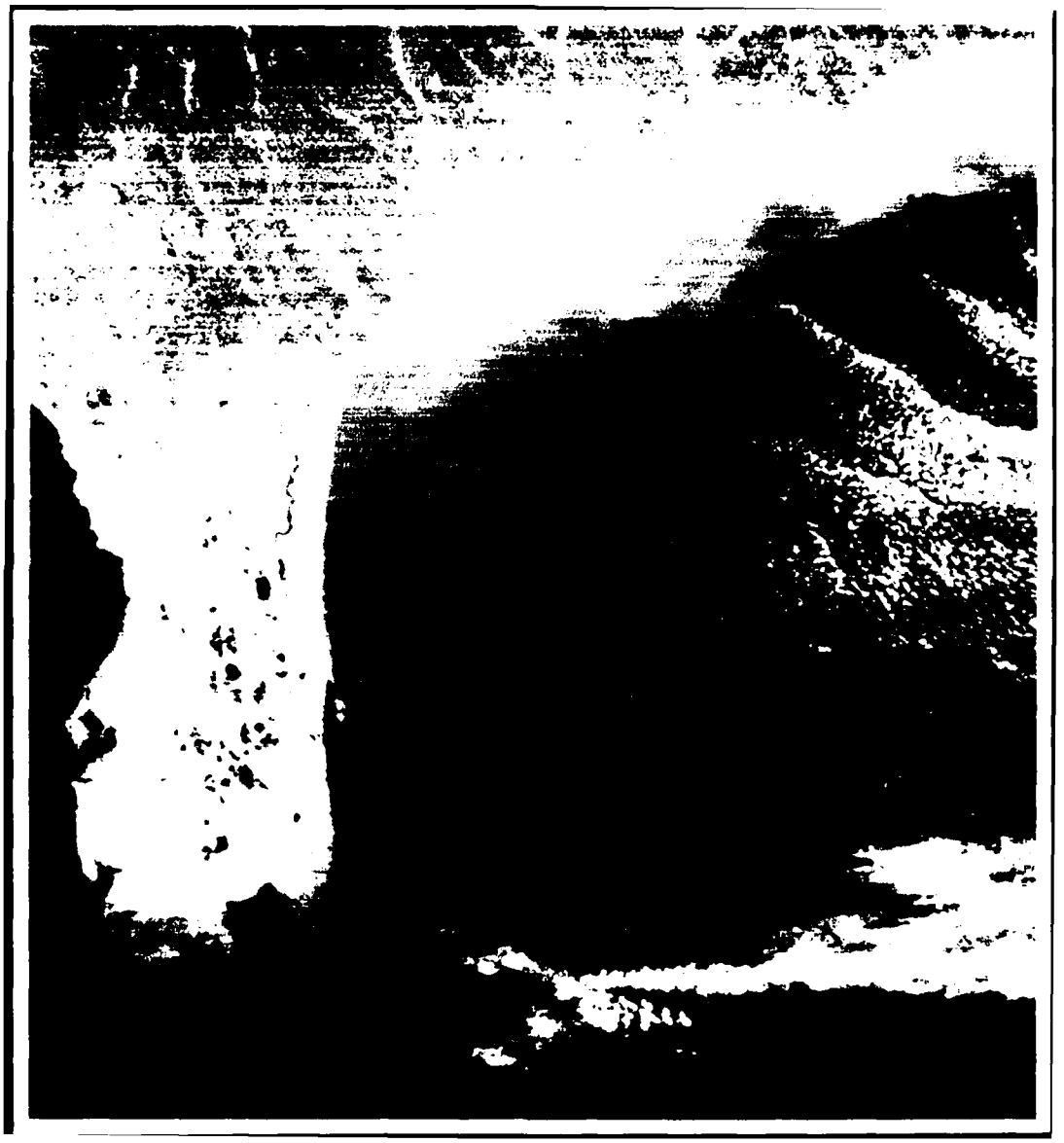

by

Oscar K. Huh

Lawrence J. Rouse, Jr.

Coastal Studies Institute, Louisiana State University

and

Paul F. Twitchell

Office of Naval Research, Boston

Introduction

The great difficulty of acquiring requisite observational data plagues all efforts at ocean analysis and forecasting. In recent decades oceanographers and acousticians have acquired measurements that indicate kinetic energy at mesoscales (≤ 24 hours and tens to hundreds of kilometers) often exceeds that of the synoptic mean motion by as much as two orders of magnitude.[1] The importance of mesoscale processes and the means to observe and model them now commands the attention of much modern ocean research. Our understanding of mesoscale processes in coastal or oceanic boundary regions has at present inadequate observational and theoretical bases. Oceanic processes at those scales generally defy prediction or even detection. Satellite scanning radiometers have the potential to supply the needed synoptic data but for two serious problems. First, the atmosphere, even without clouds, can obliterate the desired oceanographic information. Secondly, the radiometric temperatures may represent only the skin temperature of the sea. We have found, and describe here, those times and places where these problems are minimized and a "window" on the mesoscale structure of the upper ocean occurs.

Over the continents in winter, the vast high-pressure systems of cold, dry, and dense polar air are generated largely by radiative cooling. The mobility of weather systems in mid-latitudes results in periodic outbreaks of this air across coastal regions into the adjacent ocean basins. The "window" results from two aspects of this process. First is the development of clear, dry, relatively uniform air over the sea, through which best quality radiometric measurements can be made. Second is the deeply mixed conditions caused by strong winds and negative oceanic heat fluxes, which make surface measurements representative of much of the upper water column. Under these conditions infrared and visible sensors of satellites can detect the mesoscale patterns of surface temperature and turbidity particularly well. These outbreaks occur in 3-6-day cycles, bringing one or more days of ideal imaging conditions at a time and yielding imagery of excellent quality.

Atmospheric Effects

Implicit in the above discussion is the fact that polar continental air is superior to maritime air for satellite observations and measurements. Satellite scanning radiometers collect the planetary radiances that reach altitudes of "inner space" (850 km for NOAA satellites). The radiances in the thermal infrared part of the spectrum are a combination of radiant energy emitted from the earth, cloud, or sea surface that has been altered more or less by the intervening atmosphere. This alteration by a cloud-free atmosphere is a complex function of molecular absorption and reemission processes. In the simplest terms, a variable fraction of the surface-emitted infrared radiation is absorbed and the energy is reemitted at a different temperature, mainly by the triatomic molecules of the atmosphere (H_2O, O_3, and CO_2). Of these, water vapor is the most effective and variable in distribution. Its effect varies along the radiation path as a function of its concentration and temperature. Under warm and moist conditions the sea-surface temperature patterns may be completely obliterated even without condensation and cloud formation. The entire absorption and reemission effect is, however, minimal in winter when cold, dry air overlies the lands and seas of mid- and high-latitude regions.

The whole problem of attenuation of infrared measurements has been approached by most investi-

gators from the standpoint of correcting satellite-derived effective radiation temperatures to closely approach true surface temperatures measured directly by ships. Through all types of atmospheres, investigators have found satellite temperatures lower by 1-10 °C. A uniform cooling of the field of sea-surface temperatures is not so serious a problem for sea-going users.[2] The satellite data can be calibrated with surface measurements transmitted from ships or buoys to make full use of the finely resolved horizontal patterns of temperature. Cooling of radiation temperatures is, however, not the whole attenuation problem. Our studies of the satellite- and aircraft-based surface temperature measurements over coastal regions indicate that the atmospheric effects can be usefully separated into two problems:

(1) Atmospheric attenuation—the lowering of radiation temperatures from the surface-measured values due to the imperfect transparency of the atmosphere.
(2) Suppression of temperature differences—the reduction of measured surface temperature differences between warm and colder parts of the scene caused by the wavelength variation of radiative transfer through the atmosphere.

This second problem, from a practical standpoint, is more serious, since it means that atmospheric effects could obliterate oceanic fronts and mesoscale features of tactical interest, to mislead the user.

A number of studies of atmospheric effects on infrared radiation measurements of sea-surface temperature have been conducted at aircraft altitudes. In June 1971 off the Massachusetts coast an aircraft radiometer was unable to detect temperature changes of 2 °C in the sea surface with a moist layer of about 300 m depth present over the sea.[3] Another well-documented case was reported by scientists of the Research Division, Japan Research Committee of Environmental Remote Sensing from aircraft multispectral scanner flights over Ofunato Bay, Honshu, Japan. In the morning on 25 July 1978 the infrared channel showed excellent-quality imagery, with absolute temperatures slightly cooler than ground truth, as expected. That afternoon, thermal contrast was almost nil, and aircraft measurements of surface temperatures were warmer than surface truth measurements. A review of the experimental results revealed that the morning flights had been conducted after the nighttime land breezes had brought drier, cooler air out over the coastal bay. In the afternoon the sea breeze had brought warm, moist air in from the Pacific, which obliterated the gradients in the same manner as we have seen in satellite data. Radio-sonde measurements available simultaneously with the flights show that the 2 km-thick atmospheric column beneath the aircraft of the morning flight was an average of 2 °C cooler and had 1 g cm^{-2} less precipitable water than the afternoon air mass.

Atmospheric suppression of surface temperature differences is well illustrated with the NOAA-4 infrared image (10.5-12.5 μm band) acquired at 0100Z on 4 April 1976 over the Florida Peninsula (Figure 1). The temperature gradients associated with the Gulf Stream are seen to disappear near the bottom of the image. The Florida Peninsula at this time was partly overrun by an atmospheric cold front moving rapidly south. The air mass boundary between the continental air and the tropical maritime air, visible just south of Lake Okeechobee, was unusually cloud free. Surface observations indicate zero cloud cover for all stations, except for two-tenths registered at West Palm Beach on the east coast, which was directly in line with the clouds seen seaward on the image. This cloud mass is the landward extension of the cloud shield of the cold front visible over the Atlantic. Air temperatures are 20-21 °C with dew point readings of 2-4 °C just north of the front, and 26 °C with dew point readings of 18-20 °C to the south. There is a 35% humidity drop and a 10 g m^{-3} moisture content difference in the air between the surface stations across the front (Vero and West Palm Beach stations). Analysis of the Miami radiosonde data before and after the frontal passages indicates that the warm, moist atmospheric conditions, with 2.6-3 g cm^{-2} of total precipitable water (TPW), were replaced by colder, dry air with 1.1-1.5 g cm^{-2} TPW. Nearly all surface temperature differences at the edge of the Gulf Stream and Florida Peninsula have been suppressed in the radiation temperature field by these atmospheric conditions.

Maul and Sidran[4] calculated that an 8 °C temperature difference at the sea surface, when viewed vertically through the 30 °N July Standard Atmosphere, would be recorded as less than 3 °C by satellite and further reduced to 1 °C when viewed through the atmosphere at an angle of 60° off the vertical. Using the Maul and Sidran model, the radiative transfer process through the two air masses over Florida at the time of the image (Figure 1) has been simulated, and the results are shown in Figure 2. The solid line is the distribution of atmospheric water vapor in terms of absolute humidity versus altitude. The dashed lines are plots of the calculated radiation temperatures, as they would be measured by a downward-looking radiometer, rising through the atmo-

sphere for surface radiation temperatures of 20 and 22 °C. Starting with the 2° temperature difference at the sea surface (20 and 22 °C), both atmospheres reduced the temperatures and the temperature differences calculated for the top of the atmosphere. The warm, humid air reduced the temperature difference from 2 to 0.8 °C, whereas the cooler, dry air reduced the temperature difference from 2 to 1.4 °C. Examination of the moist air plot shows that the suppression of the temperature difference has occurred in the lower moist boundary layer of the atmosphere (lower 3 km). The calculated radiation temperature has been increased in the lower 3 km prior to the decrease in the upper atmosphere. This is a result of the infrared radiance contribution made to the overall upward radiation by the warm, humid maritime air. The suppression of temperature differences is the cumulative effect of two processes. The Lambert-Beer Law states that the decrease in spectral intensity of radiation by absorption with distance is a function of the intensity of the initial radiation as well as of the concentration of the absorbers. The second process is the emission of infrared energy by the atmosphere itself. The result of both processes is to reduce the effective brightness temperature of a warmer body more than that of a cooler body.

Our field data suggest that atmospheric attenuation occurs under all conditions but that the suppression of temperature differences is an air-mass-dependent phenomenon. We have attempted to quantify this effect by obtaining surface temperature measurements of two distinct bodies of water simultaneously with an offshore atmospheric sounding and a satellite overpass. We accomplished this five times with the NOAA-5 satellite in February 1977 in the coastal waters of the north-eastern Gulf of Mexico.[5] In the cases of higher levels of TPW, the thermal contrast between the warm and cold waters was suppressed, and the suppression appears to increase with increasing TPW. In the cases of cold, dry air over the sea, the atmospheric effect appears to be primarily one of uniform lowering of surface temperatures, without loss of gradients in the data field. The few observations available with the older lower resolution satellite radiometer provide only a preliminary look at the "water-vapor versus infrared-imagery contrast" relationship which requires further study. A number of atmospheric radiative transfer models are available[4,6], but we have found that they seriously overestimate the at-

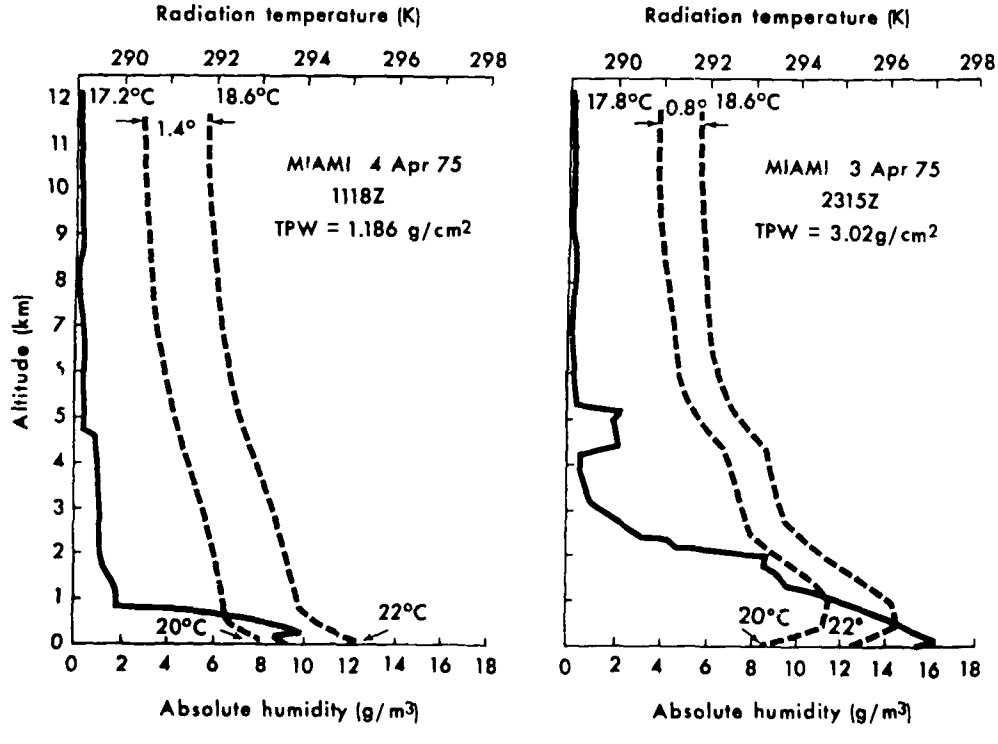

Figure 2. Atmospheric humidity profiles and simulated radiative transfer of infrared energy for 20 and 22 °C water surface through the two air masses, 3 and 4 April 1975.

mospheric attenuation. They do somewhat better in estimating temperature difference suppression.

Some Mesoscale Structures of the Upper Ocean

Examples of the best quality infrared imagery available from the new generation of NOAA satellites are drawn from the study of the Korea Strait and adjacent seas sponsored by the ONR Coastal Sciences Program. Perhaps the most severe outbreaks of polar continental air in the world occur over this oceanic region off northeast Asia. A great variety of marine environments occur here, ranging from the Kuroshio-dominated edge of the Pacific Basin to the shallow, runoff-freshened reaches of the Yellow Sea and East China Sea. The Kuroshio-Tsushima Current System complexly branches and distributes warm, saline waters to the North Pacific, Sea of Japan, and Yellow Sea after transport through and mixing within the East China Sea. The latter two basins have vast areas of shallow water of < 100m depth, strong tidal activity, severe atmospheric forcing events, and among the largest freshwater and fine-grained-sediment fluxes on the globe. In these shallow-water regions and adjacent shelf edges, horizontal mixing is extremely important as runoff from coastal regions encounters and is mixed with the equatorial waters of the Kuroshio-Tsushima system. The vigorous winter-season cooling processes destratify the water column, forming oceanic fronts between shallow and deep waters and waters of northern versus southern origin. These effects facilitate detection and tracking of various water types by surface temperature using satellite infrared scanners and by turbidity (color) using satellite visual-range sensors.

Geographic orientation is provided by Figure 3, illustrating ocean basins, land masses, and national boundaries. Figure 4 is a daytime infrared image of the region from the older NOAA-5 satellite of 8 April 1978. It shows the patterns of earth-emitted radiation, with highest intensities (dark) over the Kuroshio and sun-warmed land masses, lowest intensities (white) over the cold cloud masses, and various gray tones showing sea-surface temperatures with well-developed mesoscale convolutions. The data from this older satellite system had a spatial resolution of 0.9 km (at nadir), a 0.5 °C quantization interval, and an analog data link with a resulting noise level of 1-2 ° RMS. The current generation of NOAA satellites (TIROS-N series) has a spatial resolution of 1.1 km, a relatively noise-free digital link, and a 0.125 °C quantization interval. The data are processed here to a 0.25 °C resolution. Both systems have sun-synchronous orbits with a 12-hour repeat period.

Data we have processed from one of the new generation of satellites (NOAA-6) over the Korea Strait are shown in Figures 5-9. These are parts of two overpasses from 8 and 17 November 1980 acquired in computer-compatible tape format from National Climatic Center and analyzed at the Remote Sensing and Image Processing Laboratory of Louisiana State University. Data from the arrays of measured temperatures acquired by the satellite are presented in three formats: imagery, temperature-distance transects, and spot samples. Spot samples are the mean values of temperature within the triangular areas labeled on the imagery. The images were individually enhanced to maximize the gray-shade contrast between the oceanic features. Imagery in Figures 5, 7, and 8 were specially processed with very cold land and cloud areas electronically blackened to improve photographic reproduction. Aside from these artificially blackened areas, the darker tones represent warmer temperatures. The white lines in Figures 5 and 6 replicate ship track lines from the Korea Strait-East China Sea-Yellow Sea Remote Sensing Experiment (KEYRSEX 80), which was conducted in November and December 1980. During this oceanographic experiment soundings of the ocean and the atmosphere were obtained for correlation with satellite imagery. The numbered transects in Figure 8 do not indicate ship tracks, but are presented to show surface temperatures and the strength of the gradients observed in the image.

Overviews of both scenes in Figures 5 and 6 show the warm waters of the Tsushima Current extending from the south to a strong front between Cheju and Tsushima Islands. During this experiment and throughout the year this front is convoluted into a series of mesoscale loops and meanders. Near Tsushima Islands the warm waters split into two branches. The main branch, the Tsushima Current proper, flows eastward along the coast of Honshu, Japan, toward the Tsugaru Strait. The smaller northward branch is the East Korean Warm Current, following a broadly meandering path parallel to the peninsula. Radiation temperature differences across the front on both days are shown in the transects of line E for each. Sea-surface measurements and STD stations acquired along line E on 17 November verified the presence and strength of the front. Table I summarizes a comparison of ship and satellite measurements. 17 November was a relatively warm and humid day for this region at this time of year, with surface air temperatures of around 16 °C and total

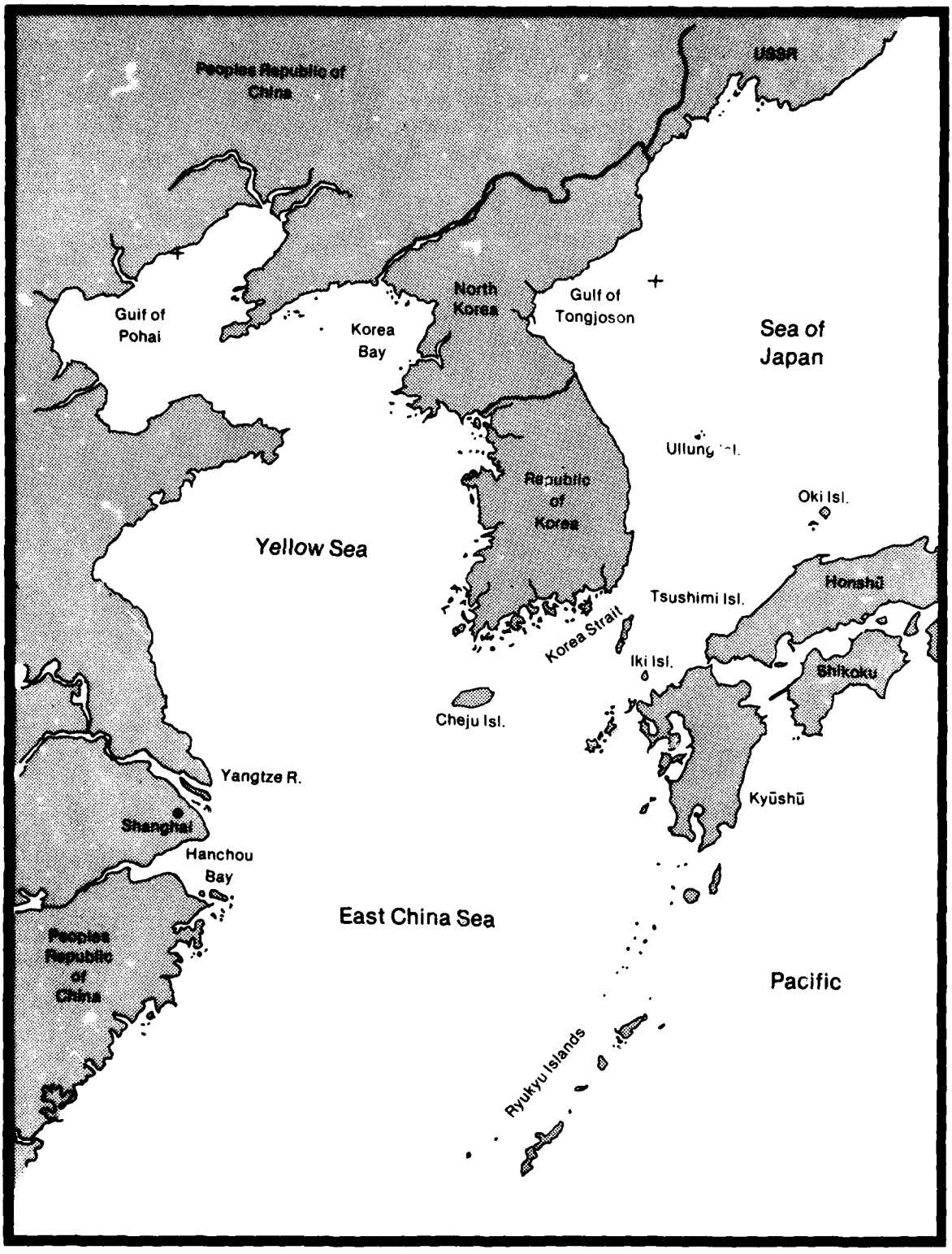

Figure 3. Geography of lands and seas near Korea Strait.

Figure 4. NOAA-5 satellite thermal infrared image (10.5-12.5 mm) covering the Sea of Japan, Yellow Sea, East China Sea, and a small part of the North Pacific, 8 April 1978. A surge in the winter monsoon has brought cloud-free polar continental air out over the entire region. Clouds (white) occur in a broken mass over southern Japan and in a broad band to the southeast.

precipitable water levels of 1.5 g cm $^{-2}$. As noted in Table I, radiation temperatures of both water masses are lowered by several degrees from actual surface values, but the temperature of the warmest waters was affected the most. The lowest temperatures and salinities were found by surface measurements to oc-

Table I

	Coastal Region Waters	Tsushima Current Waters	Cross Front T°C
Ship	14°C (32.8 °/$_{oo}$)	22° (34.3 °/$_{oo}$)	8°C
Satellite	11.5°C	18.25°C	6.75°C
Ship minus Satellite	2.5°C	3.75°C	1.25°C (The T suppression)

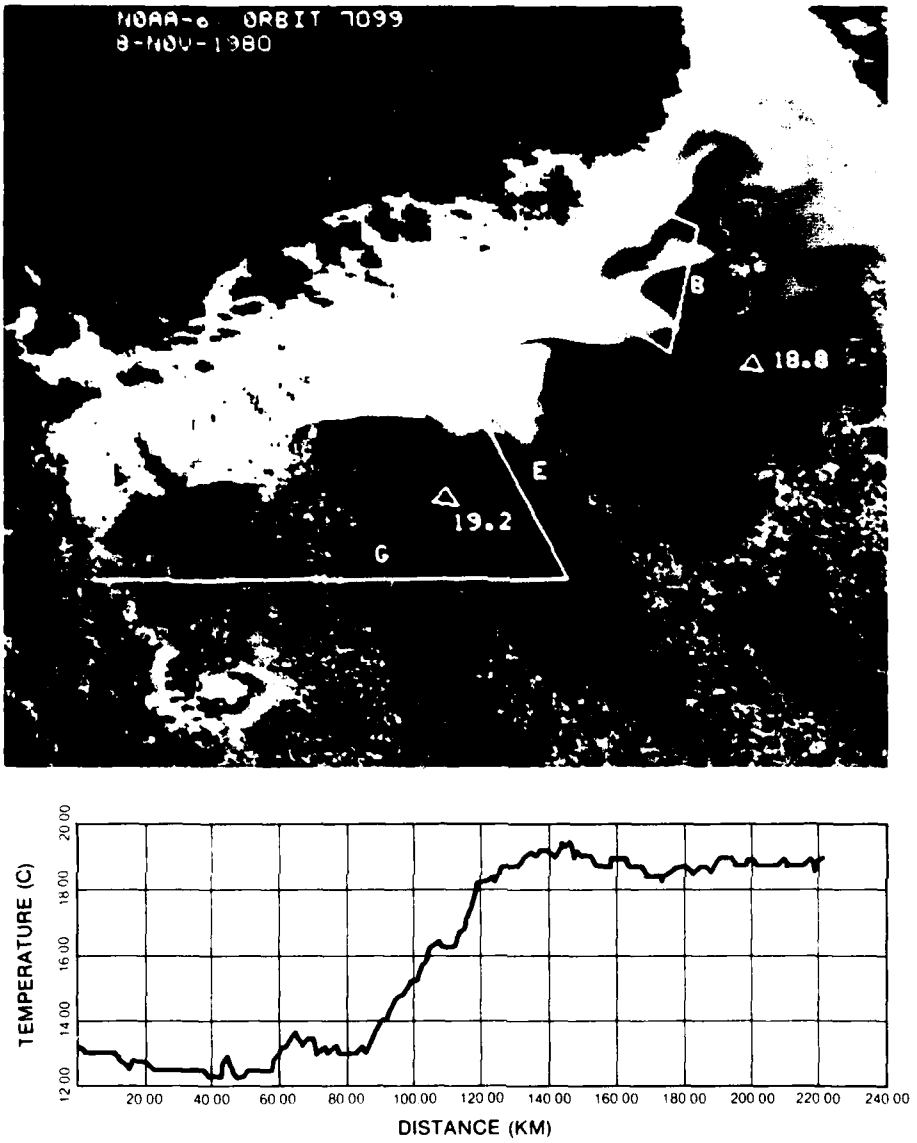

Figure 5. NOAA-6 satellite thermal infrared image (channel 4, 10.5-11.5mm) of the south coast of Korea and Korea Strait, 2325Z, 8 November 1980. Mean temperature of the contained picture elements is labeled next to the triangular sample areas. Lettered lines are locations of ship tracks of cruise that commenced on 14 November. Line E of satellite temperatures versus distance is plotted below. Cold land and cloud tops have been electronically blackened to optimize the display.

cur just north of the front rather than in the coastal regions. This narrow belt of cool, low-salinity water extends from the East China Sea-Yellow Sea region west of Cheju eastward through the strait. It is shelf water known to discharge eastward between the north wall of the Tsushima Current and the local coastal water from late summer to early winter.

Electronically expanded sections of these images are presented in Figures 7 and 8. The narrows of the strait by the Tsushima Islands from 8 November are enlarged to show mesoscale details with greater clarity. The radiation temperature patterns and values from the southern Sea of Japan, just east of Korea, from 17 November are shown in Figures 8 and 9. The extreme enhancement of the image provides water mass outlines and temperature stream line patterns.

The land masses are extremely cold at this hour (7:30 a.m. local sun time) and so produce an abrupt temperature drop at the land-water boundary. Low cumulus clouds to the right of the imagery near Japan generate the distinct sawtoothed pattern seen in transect 1 of Figure 9. From this perspective, Tsushima Island mass acts as a fixed water vane, deflecting parcels of Tsushima Warm Current waters from the northward meanders of the frontal boundary along the path of the East Korean Warm Current. As a result, alternating warm and cold water parcels flow north along the east coast of Korea.

Conclusions

A practical consequence of these studies is the knowledge that usable information on the horizontal temperature structure of the upper ocean may be reasonably expected behind outbreaks of polar continental air. Under other conditions, however, such as

Figure 6. An electronic expansion of the vicinity of Korea Strait from the previous 8 November overpass. This subscene includes Korean coast to teh northwest, Tsushima Islands in the center, and clouds plus other Japanese islands to the southeast. Sea-surface temperature patterns show Tsushima Warm Current waters interleaved with the cold waters of the coastal region.

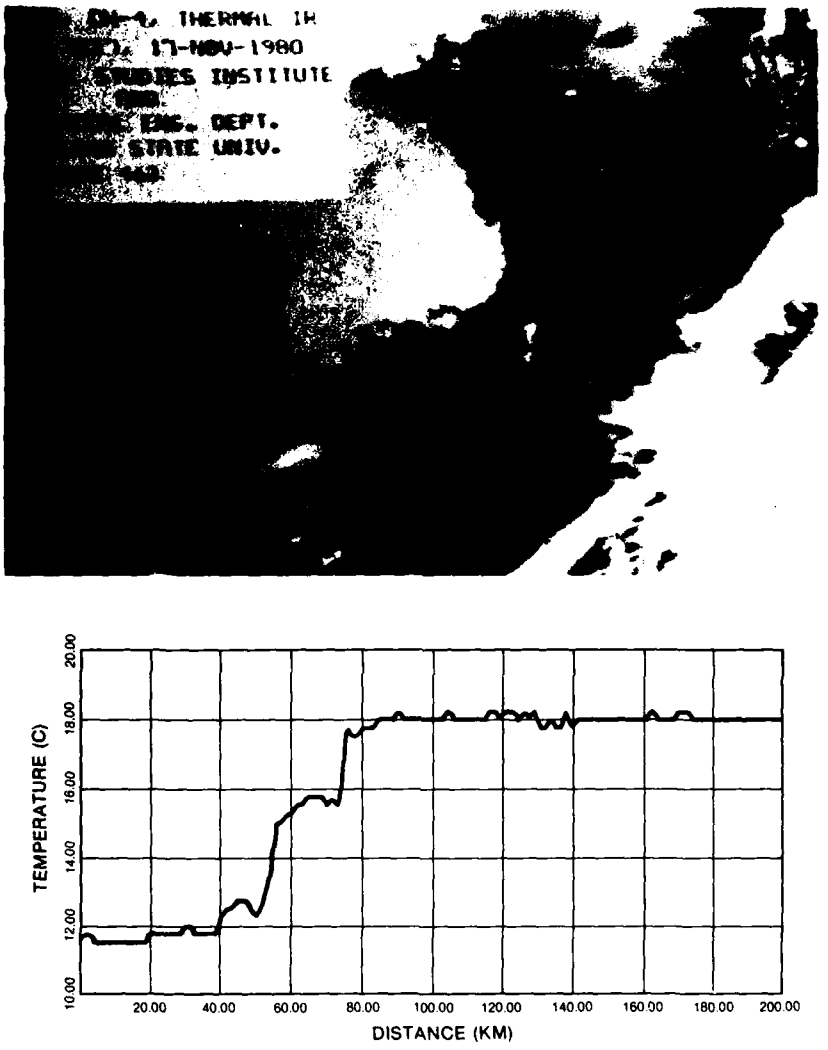

Figure 7. NOAA-6 satellite thermal infrared image (channel 4, 10.5-11.5 mm) of the Korea Strait and parts of adjacent seas, 2326Z, 17 November 1980. The temperature-distance plot corresponds to a line of oceanographic measurements made by a ship on the same date.

in humid tropic regions or deep ocean areas where maritime air masses predominate, the single-channel data from a satellite infrared radiometer (8-13 μm band of the spectrum) has little chance to faithfully record surface temperature patterns. On longer time and space scales, the atmospheric marine boundary layer (MBL) is strongly influenced by the sea surface, its major source of heat and water vapor. Satellite observations of radiation temperature patterns may follow oceanic fronts in humid regions by virtue of the strong influence that surface conditions have on the MBL. As sea-surface features move or change, its thermal counterpart in the MBL may lag behind, or vice versa. We would judge that cloud-free temperature patterns in warm, humid oceanic regions would not serve as an operationally reliable link to the upper ocean because of the strong surface atmospheric absorption and emission effects noted above.

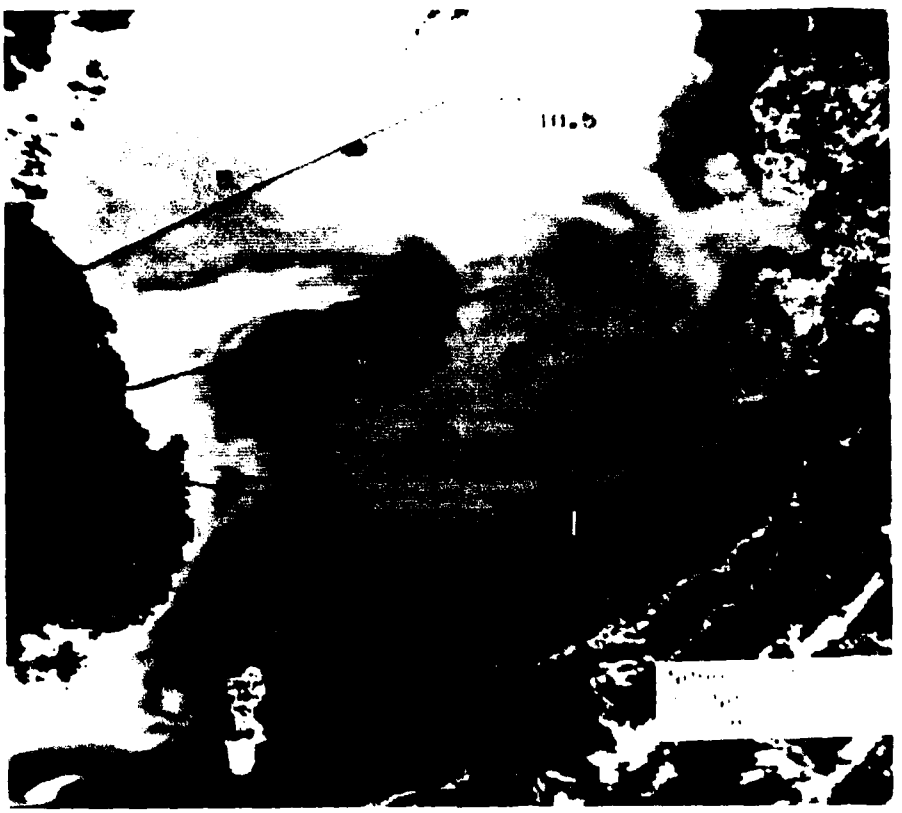

Figure 8. NOAA-6 satellite infrared image of the Korea Strait and southern Sea of Japan electronically expanded from the 17 November 1980 overpass. Flow paths of the Tsushima and East Korean Warm Currents are shown in the sea-surface temperature patterns of the southern Sea of Japan. Temperature transects 1 and 2 are presented in Figure 9.

However, analogous to cold-air outbreaks are localized mesoscale winds such as the mistral and land breezes. Although they are smaller in spatial and temporal scales, they too blow from land to sea. The drier and cooler air characteristic of such offshore winds may also provide "windows" for remote sensing of coastal and continental shelf waters. Certainly more meteorological/oceanographic/remote sensing team studies are needed to explore and make practical the use of atmospheric "windows" on the sea.

Avoidance of the atmospheric limiting effects is perhaps possible using other parts of the spectrum or using a multispectral approach, with calculations from spectral attenuation differences to correct each image element. The mid-infrared data from channel 3 (3.5-3.9 μm) of the NOAA satellites is much less susceptible to atmospheric effects, and preliminary studies indicate promise for this sensor.[6,7] It is usable at night only, because of the strong solar component in this part of the spectrum. At this time it appears that true all-weather day-night sea-surface temperature data must await development of high-resolution multispectral passive microwave radiometers. In the meantime there is much oceanography to be learned, models to be tested, and operational support possible under the outbreaks of polar continental air around the globe.

Acknowledgments

This research is sponsored by the Coastal Sciences Program, Office of Naval Research, Code 422CS, with support for meteorological studies by the Navy Environmental Prediction Research Facility, Monterey, California. Ship and technical staff support for cruises off the Korean coast was provided by the Republic of Korea through the Chinhae Research Laboratory, Chinhae, Korea. ■

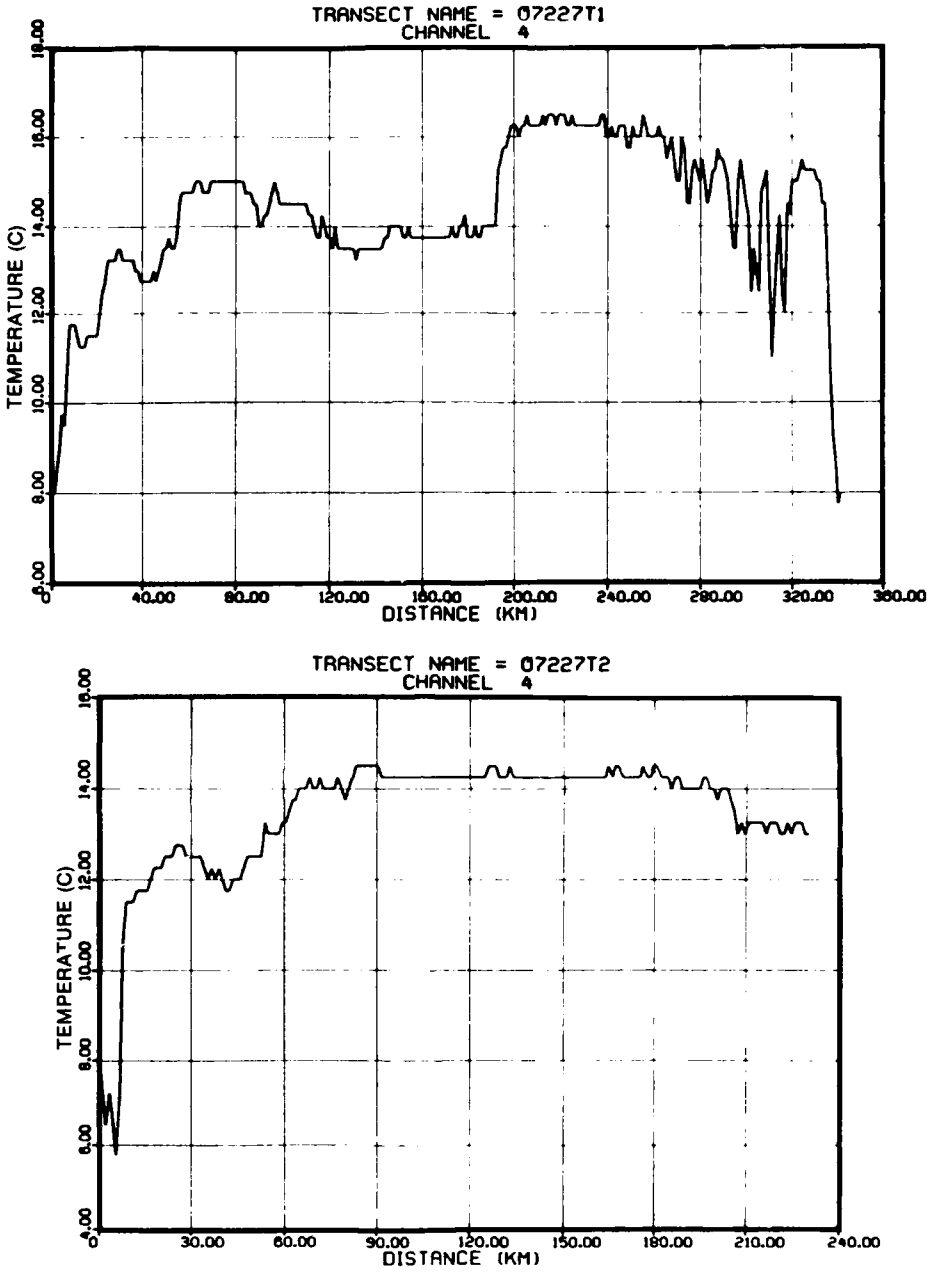

Figure 9. NOAA-6 temperature-distance transects 1 and 2 from Figure 8, 1 November 1980. The north wall of the Tsushima Current near Japan (upper) and the west wall of the East Korean Warm Current (lower) are 2.5°C radiation temperature steps. Intersection with land and cloud tops produces the lowest temperature values.

References

1. Munk, H.W., and P.Worcester, 1976, "Monitoring the Ocean Acoustically." *Science, Technology, and the Modern Navy, Thirtieth Anniversary 1946-1976,* ONR-37, ed. E. I. Salkovitz, ONR, Arlington, VA, 569 p.

2. Huh, O. K., 1976, "Detection of Oceanic Thermal Fronts off Korea with the Defense Meteorological Satellites." *Remote Sensing of Environment,* Vol. 5, pp. 191-213.

3. Church, J. F., and P. F. Twitchell, 1972, *Atmospheric Corrections for Airborne Radiation Thermometers.* Air Force Cambridge Research Laboratory, Environmental Research Paper No. 399, Bedford, MA, [illegible] pp.

4. Maul, G. and M. Sidran, 1973, "Atmospheric Effects on Ocean Surface Temperature Sensing from the NOAA Satellite Scanning Radiometer." *Journal of Geophysical Research,* Vol. 78, pp. 1909-1916.

5. Hsu, S. A., L. J. Rouse, Jr., and O. K. Huh, 1978, "Comparison of Onshore and Offshore Radiosoundings and the Correction of Sea-Surface Temperature from Satellite Infrared Measurements." *Proceedings, 4th Symposium on Meteorological Observations and Instrumentation.*

6. Selby, J. E. A., and R. A. McClatchey, 1975, *Atmospheric Transmittance from 0.25 to 28.5 μm:* Computer Code LOWTRAN III. AFCRL TR-75-0255, Environmental Research Paper 513, Air Force Cambridge Research Laboratory, Bedford, MA. 109 pp.

7. Cagle, B. J., and Robert Writner, 1981, *Arabian Sea Project of 1980—The Development of Infrared Imagery Technique.* ONR WEST 81-3, 13 illus., 12 p., Pasadena, CA.

Dr. Oscar Karl Huh is an associate professor and senior researcher in remote sensing of coastal and continental shelf processes at Coastal Studies Institute, Louisiana State University. In 1972 he designed and directed the first experiment using a combination of ship, aircraft, and Defense Meteorological Satellites in a study of oceanic fronts in the Sea of Japan. He has since directed four more major multiplatform experiments off northwest Florida and northeast Asia in studies of shallow-water air-sea interactions induced by cold-air outbreaks.

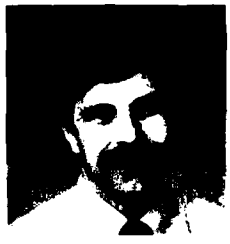

Dr. Lawrence Rouse, Jr., is an associate professor and senior researcher at the Coastal Studies Institute, Louisiana State University. His interests are in remote sensing of coastal circulation and sedimentary processes and the atmospheric effects on radiation. He has directed and participated in research programs in the Gulf of Mexico, Spitsbergen, and the Korea Strait.

Dr. Paul F. Twitchell is a meteorologist and physical science administrator at the Office of Naval Research Detachment, Boston, Massachusetts. This year he is a Visiting Professor at the Oceanography Department, United States Naval Academy, Annapolis, Maryland. He received his doctorate from the University of Wisconsin, Madison where his research focused on the interface between natural water surfaces and the atmosphere.

Field Study of "Anomalous Gray-Shades"

Satellites have been used for many years to observe clouds and cloud systems to better understand atmospheric processes. Clouds are rather easy to "see" with a satellite due to their high reflectance or albedo. Recently introduced satellite sensors are capable of detecting variations of very low albedo in the atmosphere. These variations of brightness away from bright cloudy regions are called "anomalous gray-shades" and are frequently observed in visible and near-infrared images from other satellite systems.

A team of investigators under the direction of Professor Thomas Vonder Haar at Colorado State University, funded by the Office of Naval Research's Selected Research Opportunity Program has been studying these anomalous gray-shades.

To investigate these features, a coordinated research effort was conducted between 19 September and 2 October 1980, off shore of Southern California. Airborne state-variable, air motion, particulate and radiometric measurements were obtained to determine the structure of gray-shade regions identified in satellite images. Preliminary results indicate that certain of these features are associated with the marine boundary layer. They seem to be related to variations in size and concentrations of large particles primarily within the boundary layer. (Figure 1 shows a set of features observed with the NOAA-6 Advanced Very High Resolution Radiometer (AVHRR). They were observed on the 28th of September in the wake of

Figure 1. Anomalous Gray-Shade Features in the Wake of Santa Rosa and Santa Cruz Islands off of Santa Barbara, California as Observed by the NOAA-6 Advanced Very High Resolution Radiometer (AVHRR) on 28 September 1980.

Santa Rosa and Santa Cruz Islands just off of Santa Barbara, California. The features are aligned with the boundary layer wind and although some of the brightness variations can be attributed to surface roughness variations, most of the signal is due to atmospheric reflection.) Anomalous gray-shade regions, when fully understood, may provide great observational insight into stratocumulus formation and dissipation, humidity variations, visibility determination and forecasting as well as boundary layer dynamics and air-sea interactions. ■

Surface Wave Modulation Patterns in Radar Images

by

Erik Mollo-Christensen
Massachusetts Institute of Technology

Images formed from radar sea surface scatter return to aircraft and satellite platforms show coherent patterns that can be associated with current shear, eddies, internal waves, and patterns on the sea surface and bottom topography. Seasat SAR (*S*ynthetic *A*perture *R*adar) data show a wealth of detailed patterns. An example of this in Figure 1, shows a digitally-processed image of Nantucket Island, Massachusetts and its surroundings. The magnified part in Figure 2 indicates a velocity shear at the edge of a current of less than one knot running to the WNW, south of the Shoals. One cannot explain these changes in the wave packet structure of sea surface waves in terms of the results of the customary approximation in terms of waves of infinitesimal amplitude or linear theory. The patterns in wave amplitude and wavelength are due to effects of finite wave amplitude, where nonlinear phenomena become important. The tendency for waves to undulate in amplitude and frequency is typical of finite amplitude waves. We refer to these as amplitude (AM) and frequency (FM) modulations, and, since they are due to nonlinear dynamics, we call them nonlinear wave modulations.

I shall attempt to describe in this article some features of modulational dynamics for surface waves, and how the detection process used for SAR and Side Looking Airborne Radar data rely on intermodulations of the scattering wavelets and the underlying dominant wave field. Then I will go on to suggest that the same kind of forced modulation and intermodulation changes the patterns in the dominant wavefield to make eddies, shear layers and other coherent motions visible. First consider modulations of the surface wavefield.

Surface Wave Modulations

Both surfers and boatmen know that swell and wind waves vary in amplitude and arrive in packets or groups. A wavefield tends to develop variations in wave amplitude, a, because, at a given wave steepness, a dip in amplitude ($a_{xx} > 0$) tends to move faster than a positive bump in wave amplitude ($a_{xx} < 0$). So, dips and bumps will tend to separate rather than merge and cancel. This instability process makes disturbances in wave amplitude grow initially, when a uniform amplitude wavefield is disturbed. But near the bumps, there tends to be larger wave steepness $ak = 2\pi a/\lambda$, defined in terms of amplitude, a, and wavelength, λ. Steeper waves tend to propagate faster, so there will be a tendency for the front of wave groups to steepen further.

These effects of amplitude variation and steepness on the phase speed of finite amplitude periodic waves (Stokes waves) are contained in the dispersion relation, relating phase speed c, wave number $k = 2\pi/\lambda$, and wave steepness $ak = \epsilon$

$$c^2 = gk(1 + a^2k^2 + \frac{a_{xx}}{8k^2a}) \qquad (1)$$
$$= gk[1 + \epsilon^2 + a_{xx}/(8\epsilon k)].$$

Eventually, in the interplay between steepness and bumpiness effects, an equilibrium situation is established, so the mature wave field consists of constantly changing groups of waves, maintaining an average steepness and wave amplitude. This is the typical sea surface wave field under weakly generating wind wave conditions, with nearly constant average properties, but always changing locally in terms of group lengths and amplitude. Now and then accidents happen, in the sense that a further instability occurs where subharmonic transitions take place, and a crest is lost. Due to such accidents, the average wavelength of a wavefield will tend to increase and the wave steepness decrease until there is an open ocean swell wavefield of modest steepness. The description I have given is based on analytical results for nonlinear waves, but not all the detailed steps have been verified as occurring in the order described, so, in that sense, my description is somewhat speculative.

Linear and Nonlinear Wave Dynamics

Linear theory is excellent for describing wave development over limited distances and times; for surface waves, linear approximations are good for propagation distances, L, of much less than λ/ϵ^2, for larger distances nonlinear effects become more important. For 100 m wavelength swell of amplitude 1.5 m or nearly 5 ft. crest to trough height, $\epsilon = 0.1$ and the propagation distance is 10 km. For small wavelets of 10 cm wavelength and 0.5 cm amplitude $\epsilon = 0.3$, the propagation distance is only one meter.

For propagation over longer distances, the cumulative effects of nonlinear terms in the equations of motion become important, and one has to develop the dynamics to third order in wave steepness and obtain the Davey-Stewartson equation[1] in wave-complex amplitude A(x,y,t),

$$i(A_t + c_gA_x) - \frac{\omega^2}{4k^2}(A_{xx} - 2A_{yy}) - \frac{\omega k^2}{2}|A|^2 A = 0. \qquad (2)$$

Figure 1. Digitally processed image of Nantucket Island and the surrounding waters obtained from SEASAT SAR data.

Figure 2. Magnified portion of Figure 1., showing the shear instability of a current edge shear layer.

The water surface deflection is

$$z = \zeta(x,y,t) = \mathrm{Re}\{A(x,y,t)\, e^{i(kx - \omega t)}\}. \quad (3)$$

Here, k and ω are the average wavenumber $k = 2\pi/\lambda$ and average frequency $\omega = 2\pi/T$, T is the wave period.

The Davey-Stewartson equation gives a valid approximation over distances of propagation much smaller than $L_3 = \lambda/\epsilon^3$. (L_3 is not the same as the L for linear approximation. It gives a "good" description for propagation time scales of order T/ϵ^2 and for group lengths of order λ/ϵ. For the swell example, $\lambda = 100$ m, $\epsilon = 0.1$, $L_3 \approx 100$ km. For the wavelets of $\lambda = 10$ cm and $\epsilon = 0.3$, $L_3 = 30$ m.

The Davey-Stewartson equation (2) has exact solutions[2] in the form of periodic and solitary disturbances. In two dimensions, this equation reduces to the cubic Schrodinger equation[3,4], first used in wave mechanics to solve for the electron as a wave packet. Also when applied to sea-surface wave modulations, the solutions to the cubic Schrodinger equation have quantum properties, limiting the energy content of a single wave packet for a given wavelength. The solutions also possess certain conservation properties, so that wavepackets that collide will survive collisions. This suggests that wave packets can have long half life, and that wavepacket descriptions of a sea-surface wave field may be useful for some purposes.[5] But, as will be argued further along, the modulation field is also very sensitive to disturbances, which can alter the wave-packet structure of a wave field encountering current, wind or topography.

Forced Modulation

The modulation field, as described by equation (2), will, when otherwise undisturbed, reach an equilibrium state where the linear and nonlinear terms balance. A current shear $dv/dx = vk$, where the mean velocity changes by an amount v in a wavelength λ, will introduce additional terms in the Davey-Stewartson equation. One term comes from the energy-flux divergence term in the energy equation[6], and introduces a term $(vA)_x \approx (vAk)$ in equation (2). There are additional terms due to radiation stresses[7], but they are of the same order-of-magnitude.

Velocity shear will be as important as the nonlinear term in equation (2) when

$$Avk \approx \frac{\omega k^2}{2} |A|^2 A,$$

setting

$$c_g \approx \frac{\omega}{2k} \quad \text{and} \quad k^2 |A|^2 \approx \epsilon^2,$$

one finds that

$$\frac{v}{c_g} = \epsilon^2,$$

is the criterion for current shear to affect modulations. This shows that small current shear can be important.

For an example of a 100 m wavelength swell of steepness $\epsilon \approx 0.1$, the group velocity is $c_g \simeq 6$ m/s and the current variation required to disturb the modulation field is $v = \epsilon^2 c_g \cong 6$ cm/sec $\simeq .12$ knots. For the 6 cm waves of steepness $\epsilon \cong 0.3$, the current-change needed is of order $v \approx 1.5$ cm/sec. For less steepness, with $\epsilon = 0.1$ and $\lambda = 6$ cm, we find the current-variation needed to upset the modulation field to be of order $v \cong 1.5$ mm/s.

This demonstrates how very small coherent disturbances in the current field can cause disturbances in wave modulation patterns in wavefields of moderate steepness, and if the disturbances are coherent, the modulational disturbances will also be coherent. The steeper the waves, the larger the disturbance needed to affect the modulation field. But ship wakes and weak eddies will show up in the modulation field of short wavelets of $\lambda \approx 6$ cm under a wide range of velocity disturbances down to a few cm/s.

Disturbances in wave propagation speed due to bottom topography will affect the modulation field the same way; for shoaling from very deep to a depth of 20 m will change the group velocity of 100 m waves from 6.25 m/sec to 5.32, so that the change is $v = 0.93$ m/sec, sufficient to change the modulation field. This suggests the reason why one can see the location of the continental shelf edge in some SAR images, and why topography shows up so very clearly.

So far, we have discussed how waves, as they propagate, eventually accumulate effects of nonlinearity until they add up enough to change the wavefield by introducing modulation in phase and amplitude. The steeper the waves are, the quicker they show the effects of nonlinear processes. But through all this, the linear approximation is a good one for small time and distance of propagation. So observations of wavefields over short distances and times will tend to be dominated by linear effects and reveal little of the nonlinear dynamics. But for the much larger scales of observation made possible by remote sensing, the nonlinearities have room to show up,

and give disturbances their chance to modify wave modulation fields.

Intermodulation

The current that disturbs the wave modulation field may be a fluctuating current due to other waves. A field of λ = 10 cm waves riding on waves of 100 m wavelength of 3 m amplitude (ϵ = 0.10) will be subject to current fluctuations of ± 1.2 m/sec. According to our calculations, this current is sufficient to dominate the modulation field of the 10 cm waves. The orbital velocity field is convergent-divergent, so that it plays accordion with the wavelet field, inducing large steepness and leading to fourth-order effects becoming important, the wavelet field may undergo subharmonic transitions and even wave-breaking at certain phases of the underlying dominant sea.

The mechanism of forced modulation of the wavelets by the dominant sea is the basis for the SAR detection of sea surface waves[8,9,10]. The SAR signal is scattered from wavelets and the intensity and Doppler shift of the reflected wave is interpreted as a modulation signal due to the dominant wave and, through a suitable algorithm, translated as sea surface shape due to the underlying waves. This interpretation algorithm for SAR and other radar scattering imagery is, of course, a crucial element in data interpretation. Because of the complexity of the intermodulation processes, one has to develop better algorithms by simultaneous observation of both wavelets and underlying waves over a range of wind and wave conditions. This should preferably be done without the need for flying radars on aircraft or satellites, since the cost of sufficiently extensive overflights would be prohibitive. I have therefore designed a scattering-wave gauge which simulates radar backscatter.

The "Harp" Wave Gauge

A student, J. Menoher, and I have built and tested a simple wave gauge whose output simulates radar scatter return. The wave gauge consists of a single capacitance wire, strung on a frame with parallel vertical segments a distance ℓ apart, as shown in Figure 3. The capacitance of the wire varies proportionally to the sum of the water level displacements at all the wires. A capacitance detector circuit will then provide a wave gauge output proportional to the sum of displacements. For very long wavelengths, compared to the length of the array, the gauge will work like a single point wave gauge. For

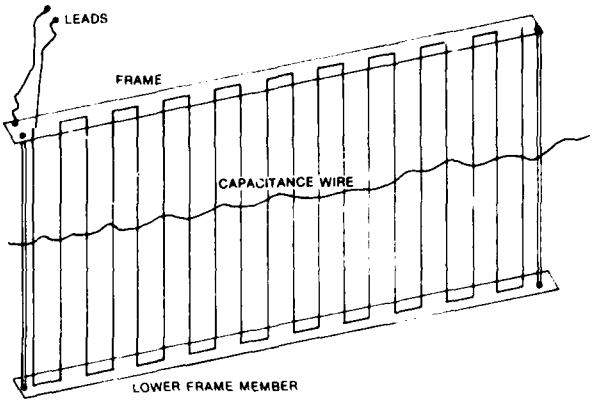

Figure 3. "Harp" wave gauge, with a wire strung in parallel runs. Resonant wave contour shown.

waves of wavelength equal to the wire spacing, the capacitance variation of all the wires will be in phase, and the output will be a maximum. For wavelengths twice the wire spacing, the output will be zero. The output amplitude will vary with wavelength as shown in Figure 4. The wave gauge functions as a resonant scattering detector. It can also be built for less than the cost of a satellite; its capital cost will be comparable to an aircraft flight hour.

A first test of a ten-wire wave "harp" gave the results shown in Figure 5. The upper trace is the "harp" output and the lower one is the output of a single-wire capacitance wave gauge placed next to it in a wave tank. The frequency of the wave-generating paddle increases slowly, and the resonance peak is evident. But it is also interesting to note that there are bursts of high-frequency output for incoming waves of frequencies of 1/2 and 1/3 of the frequency of the resonant wave.

This means that a scattering detector also detects higher harmonics of Stokes waves. The same must be the case for a Bragg scatter-return of radar signals. This result illustrates the complexity of interpretation of scatter returns, and indicates the need for careful observations to establish relationships between scattering waves, wind and dominant sea. Data processing of data from such an experiment or from SAR data, for that matter, requires the use of processing methods that produce information about modulations in phase and amplitude and intermodulations.

Eduction of Modulations from Signals

What we need is information about the complex modulation variable A in equation (3). One method, taken from communications engineering, uses Hilbert Transforms[11] and has been used for surface

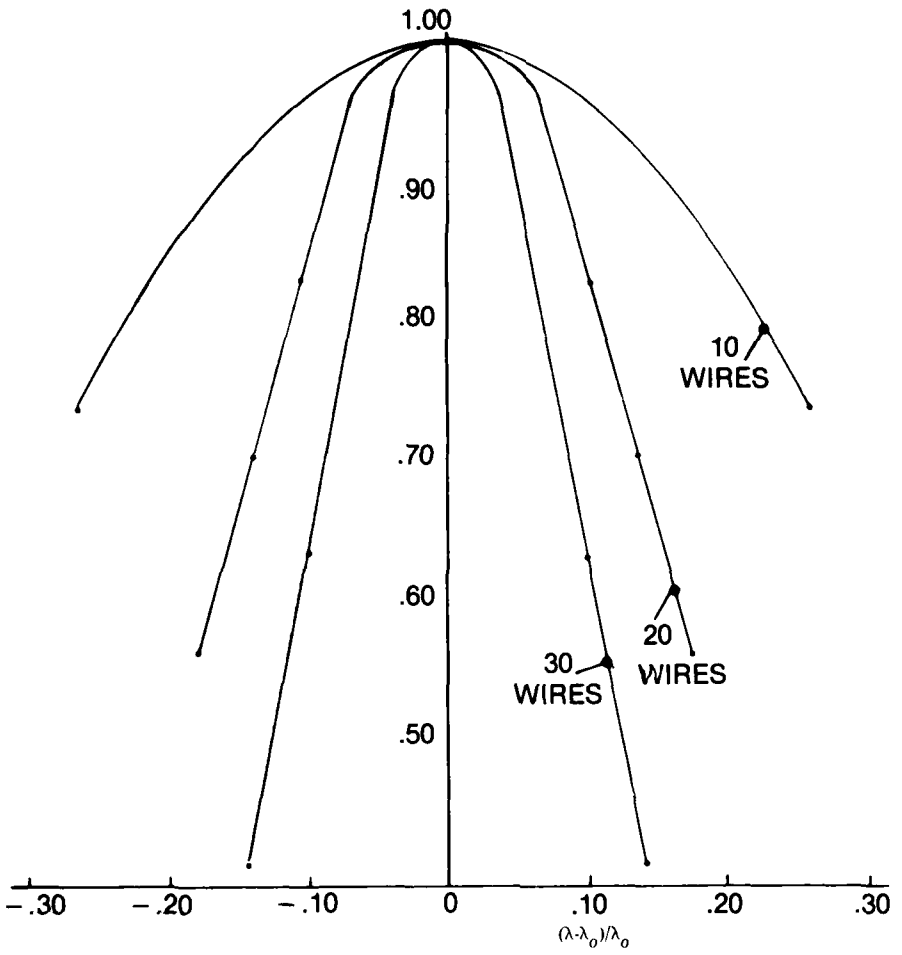

Figure 4. Calculated output of "harp" scattering wave gauge a function of wave length.

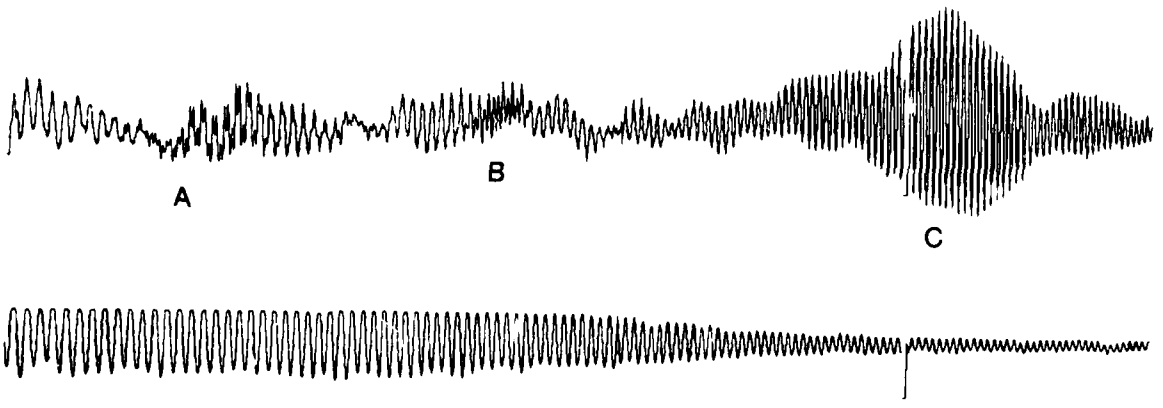

Figure 5. Output of "harp" wave gauge (upper trace) compared to signal from a single wave gauge (lower trace) as wave frequency is slowly increased showing higher harmonic resonance (A&B) and main resonance peak (C). (Result obtained by J. Menoher).

wave processing by my colleague W. K. Melville. One of our students, G. Sahar,[12] has used the method to process laboratory wind wave data.

Figure 6 shows a wave gauge output, with the amplitude $|A|$ superimposed, and, in the lower trace, the phase Θ of $A = Re^{i\Theta}$; the linear trend due to the carrier wave $\exp[i(kw-\omega t)]$ has been taken out. Once one obtains A, one can relate it to the other scale processes that drive or interact with the modulations. The interpretation of SAR return by scattering wavelets and relating it to the dominant sea is a difficult problem and is similar to the challenges of relating wave modulation to internal waves and other large scale processes. They present similar data processing problems.

In learning to interpret data in terms of such intermodulational relationships, we need to do some controlled experiments, guided by existing work on nonlinear waves and intermodulation and with an awareness of the limitations of simple and convenient approximations.

Applications to Oceanography

The real advantage of active electromagnetic sensors in oceanography is their insensitivity to clouds and fog. One does not realize the prevalence of cloud and fog patches before one starts looking for visible and infrared satellite data for the sea surface. For some locations, such as the Drake Passage, for example, one may find one day a year with a good view. Other areas are nearly as frustrating; climatological records of sunshine, cloud-cover and fog are readily available to demonstrate this. Also, interesting events, such as hurricanes, gales and intense air-sea interaction do not occur on sunny days. So, without sensors that see through clouds, we cannot obtain the synoptic view of patterns that are uniquely available from remote sensing devices.

Good distance-resolution, another crucial feature of SAR and SLAR data, derives from the fact that distance is measured in terms of time for a signal to return rather than through optical resolution of geometry. A spatial resolution better than fifty meters makes it possible to see the dominant surface waves and swell, internal waves and current shear. Because the dominant waves can be resolved, it is also possible to educe from the data the amplitude and modulation field of those waves, and to interpret the modulation patterns in terms of larger scale phenomena. It is worth emphasizing that, because the modulation field is governed by nonlinear processes, one cannot use linear filtering theory to calculate resolution. The resolution of an image needed to discover a 100 km eddy from the surface wave modulation field must be sufficient to resolve individual waves.

As an alternative, one can build a modulation eduction operator into the processing scheme. One reason for the clear view of amplitude modulations afforded by existing SAR imagery is that somehow such an eduction operator is present in the data processing chain, possibly by inadvertence or because of the skewness of modulations of scatterers on surface waves.

I will next give a few examples of data use in oceanography.

Density Structure from Internal Wave Patterns

When and if SAR and similar active sensor sea surface data become available, it will be possible to put into routine use a method for estimating vertical density structure that a student, A. da. S. Mascarenhas, Jr., and I developed a few years ago. We used Landsat images that showed patterns that could be identified with internal waves propagating on the seasonal thermocline. These internal wave packets occur in the New England continental shelf region. The waves are generated by tidal flow over topography, and the packets are generated once per M_2 tidal period, which is approximately 12.4 hours. One sees packets generated several tidal periods apart in many Landsat images. The spacing between packets is the distance travelled in 12.4 hours. This gives the propagation speed, c, of the wave packets.

The linear approximation for internal waves on a density jump $\Delta\varrho/\varrho$ at a depth h from the surface in otherwise deep water gives

$$c^2 \cong g\,h\,\frac{\Delta\varrho}{\varrho}.$$

Since we have found c from the satellite image, one can calculate $h\,\frac{\Delta\varrho}{\varrho}$. If one knows $\Delta\varrho/\varrho$ from other sources, one can find h. We argued that the density jump on the seasonal thermocline was due to the temperature difference, so that $\Delta\varrho/\varrho = -\alpha\Delta T$. We then said that $h\Delta T$ was a measure of heat storage in the upper layer, and calculated its distribution for the months of July and August[14]. (Figure 7).

We were constrained by limited data availability, caused by fog and the Landsat data acquisition schedule. This method may well prove applicable to internal waves on the main thermocline, since one should expect such waves to be generated all along the continental edges by the tides. We may need bet-

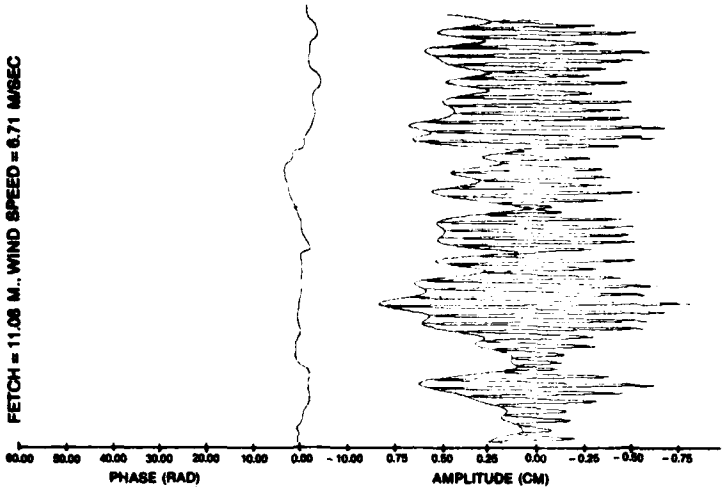

Figure 6. Wave gauge output from laboratory wind wave experiment, with amplitude modulation superimposed and phase modulation shown in lower trace. (Results obtained by G. Sahar).

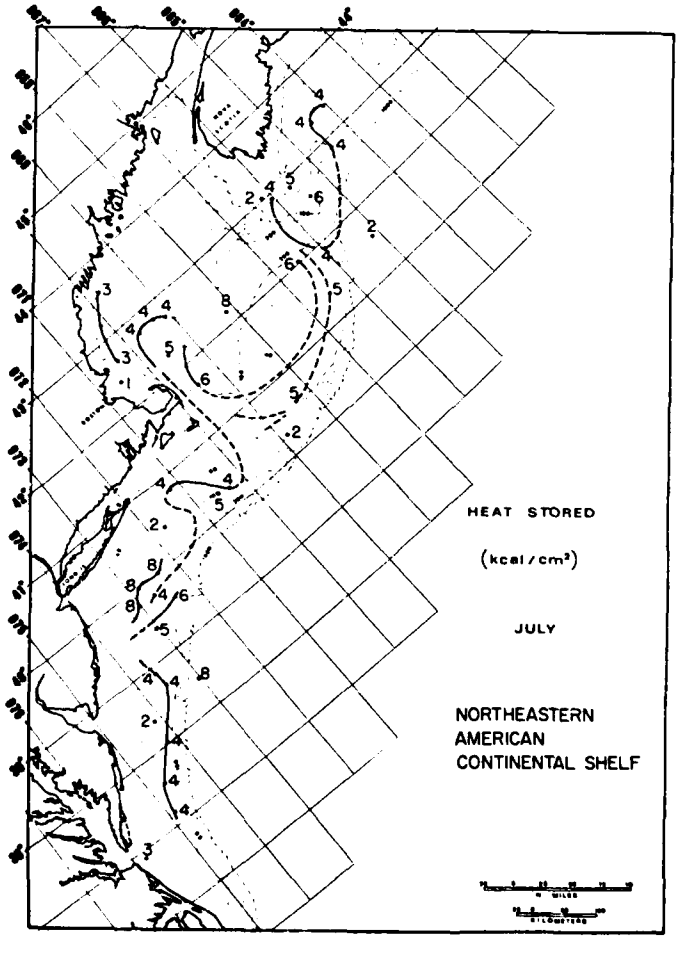

Figure 7.

Heat storage in upper ocean derived from internal wave packet spacings. Mollo-Christensen (1980).

ter methods of processing radar data to see the surface modulation patterns generated by these internal waves. The distance between wave packets will give the speed, and one can again observe h $_{\varrho}^{\varrho}$. Another phenomena that can be excited by the tides is shear-layer instability.

Estimating Current Speed from Satellite Data

Another example of interpretation of patterns visible in radar images is given by regarding the undulations of a current edge shear layer as a tidally forced hydrodynamic instability.[15]

Where a current passes a prominent topography feature and speeds up locally, oscillations and turbulence tend to decrease in comparison to the organized motion; in part, this is due to the increase in mean velocity, without a corresponding increase in oscillations and turbulence. Also, since the current touches a boundary, there will be little oscillation normal to the boundary. Further downstream, where the current loses the support of the boundary and the current edge becomes a free shear layer, the flow becomes unstable. An unstable flow tends to amplify fluctuations due to external disturbances, so that the shear layer develops lateral fluctuations in the form of travelling waves of increasing amplitude. This is clearly visible in TIROS-N infrared images of the Gulf Stream near Cape Hatteras, North Carolina, shown in Figure 8. Another current edge can be seen in the Seasat SAR image of the Nantucket Shoals, where the edge of the WNW current south of the Shoals, reported in the U.S. Coastal Pilot, forms an undulating shear layer edge, shown in Figure 2.

The excitation for shear flow instability will be velocity fluctuations caused by incoming internal waves, storms and tides. The most reliable excitation is the tide, and, in the examples shown, the M_2 tide.

We can calculate the speed of the shear layer waves by measuring the wave length in the satellite image and dividing by the period of the M_2 tide. For the Gulf Stream just beyond Cape Hatteras we find $c \approx 1$ m/sec. Next, we use the fact that shear layer waves tend to move at a speed $c = (U_1 + U_2)/2$, the average of the current velocity on the two sides. We now assume that the current velocity on one side of the shear layer is zero: $U_2 = 0$; one then finds

$$U_1 = 2C = \frac{2\,(\text{wavelength})}{(\text{M-period})}.$$

For the Gulf Stream, we found $U_1 \approx 2$ m/sec, very close to the reported value.

In order to verify such methods of current estimation, one needs a series of sea-surface images spaced a day apart or so, so that one can follow a shear layer wave. But regions where a cold or warm current passes a headland tend to be active meteorologically, breeders of storms, regions of cumulus convection or just foggy. It is hard to find infrared radiometer images of Hatteras or the Nantucket Shoals free of clouds. The same goes for most other major currents like the Kuroshio, the Antarctic Circumpolar, the East Greenland, and the Somali Current as well as the many minor currents we could analyze this way.

Again, active sensor data, such as SAR or SLAR data, would be very important for estimating currents, analyzing the growth of fluctuations and meanders as the first stage in formulating predictive models of such undulations.

Ship Wakes as Diagnostic Tools

Ship wakes show up in high resolution images such as those produced by SAR. The deformation of a ship wake by current shear can be used to deduce the shear, provided the ship keeps steady course and speed, and one knows the speed. One can find the speed from the wavelength of the stern wave. As anybody who has spent time leaning on the stern rail of a ship knows, the stern wave moves at the speed of the ship; this means that the stern wave propagates at the speed of the ship, v. If λ is the wavelength of the stern wave, one has the relation

$$V \cong \sqrt{(g\lambda/2\pi)}.$$

Combining the analysis of shear instability with use of ship wakes as a diagnostic can aid one in mapping out current fields and fluctuations in a region. This requires high-resolution sea-surface data without cloud or fog clutter.

The Data Volume Problem

High resolution data represent high data density per unit area of the sea surface. SAR data with a resolution of 15 x 15 m^2 contains approximately 30 megabytes for a 100 km^2 data field. Transmission, storage and processing of such large data volumes are just now becoming routinely possible at manageable cost. The technologies of multiprocessors and mass storage devices are advancing so rapidly that within a

decade, data handling problems and costs will have changed for the better, and we must try to anticipate technological advance as best we can, and guess at where future bottlenecks will occur.

Data archives and data distribution to research workers may end up on high-density disk media, while operational users will get their data via communications satellite.

Improvement in Quantitative Interpretation of Data

A crucial element in interpretation of sea-surface radar-scatter data are nonlinear wave processes. We need to know such processes better, and we need to be able to analyze the data field to take apart the results of nonlinear interactions. We can learn much about nonlinear waves from laboratory and field experiments and much of the knowledge we need can be obtained without having to fly satellites or aircraft.

The analysis methods we now have work with time series and joint time series, that is for functions of a single independent variable. We need to extend such methods to two-dimensional and three-dimensional data fields, such as those we obtain by remote sensing.

The nonlinear methods for time series are not always easy to generalize. One need only realize that while the order in which one applies linear processors to a signal may not affect the result, the order of application of nonlinear processors can make a large difference. For example

$$\sin\sqrt{u(t)} \neq \sqrt{\sin u(t)} \text{ and } \log u^2(t) \neq (\log u(t))^2.$$

Conclusion

Radar scatter data are now useful in operations and research. Improvement in quantitative interpretation of the data requires research on wave dynamics and data processing. Technology of data transmission and storage will keep improving and will be available to handle remote-sensing data when needed.

Patterns in remote-sensing images can be interpreted quantitatively to produce information on current speed and density structure. For such use, the all-weather capability and the good spatial resolution of active sensor data will be especially valuable. ■

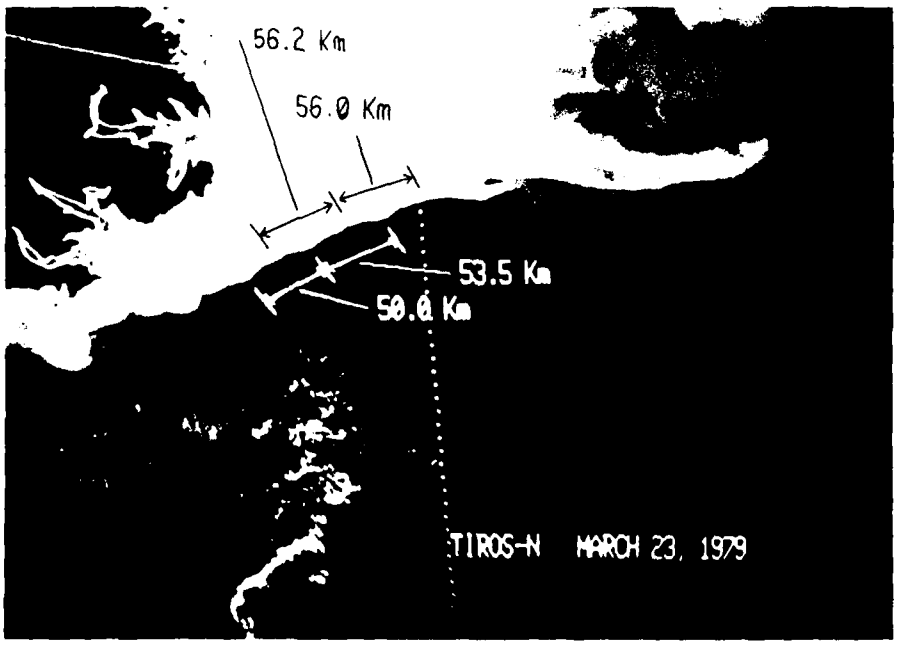

Figure 8. The edge of the Gulf Stream beyond Cape Hatteras, showing shear waves (from TIROS-N, AVHRR Data).

References

1. Davey A. and Stewartson, K. 1974, *Proc. Roy. Soc. A 338*, 101.
2. Hui, W. H. and Hamilton, J. 1979, "Exact Solutions of a Three-dimensional Nonlinear Schroedinger Equation Applied to Gravity Waves," *J. Fluid Mech. 93*, 117-133.
3. Yuen, H. C. and Lake, B. M. 1975, "Nonlinear Deep Water Waves, Theory and Experiment," *Phys. Fluids 18*, 956-960.
4. Zakharov, V. E. and Shabat, A. B. 1972, "Exact Theory of Two-dimensional Self-focusing and One-dimensional Self-modulation of Waves in Nonlinear Media," *Sov. Phys. J. Exp. Theor. Phys. 34*, 62-69.
5. Mollo-Christensen, E. and Ramamonjiarsoa, A. 1979, "Modeling the Presence of Wave Groups in a Random Wave Field," *J. Geophys. Res. 83*, 4117-4122.
6. Whitham, G. B. 1974, *Linear and Nonlinear Waves*, Wiley-Interscience.
7. Longuet-Higgins, M. S. and Steward, R. W. 1960, "Changes in the Form of Short Gravity Waves on Long Waves and in Tidal Currents," *J. Fluid Mech. 8*, 565-583.
8. Valenzuela, G. 1978, "Theories for the Interaction of Electromagnetic and Oceanic Waves—A Review," *Boundary-Layer Meteorology, Vol. 13*, p. 61-85.
9. Alpers, W. and Hasselman, K. 1978, "The Two-frequency Microwave Technique for Measuring Ocean-Wave Spectra from an Airplane or Satellite," *Boundary-Layer Meteorology, Vol. 13*, p. 215-230.
10. Shuchman, R. A. and Zelenka, J. S. 1978, "Processing of Ocean Wave Data from a Synthetic Aperture Radar," *Boundary-Layer Meteorology, Vol. 13*, p. 181-191.
11. Oppenheim, A. V. and Schafer, R. W. 1975, *Digital Signal Processing*, Prentice-Hall.
12. Sahar, G. 1981, "Modulation of Sea Surface Waves, Observations and Processing Methods, M.I.T. S. M. Thesis, August.
13. Mollo-Christensen, E. and Mascarenhas, A. Da. S., Jr. 1979, "Heat Storage in the Oceanic Upper Mixed Layer Inferred from Landsat Data," *Science, Vol. 203*, p. 653-654.
14. Mollo-Christensen, E. 1980, "Surface Signs of Internal Oceanic Motions," talk given at the SEASAT-SAR Symposium at Applied Physics Lab., Johns Hopkins U., Laurel, Maryland.
15. Mollo-Christensen, E., Cornillon, P. and Mascarenhas, A. Da. S, Jr. 1981, "Method for Estimation of Ocean Current Velocity from Satellite Images," *Science, Vol. 212*, p. 661-662.

Dr. Erik Mollo-Christensen was educated in Norway and obtained his Sc.D. in Aeronautical Engineering from M.I.T. in 1954 and has been at M.I.T. ever since, holding faculty appointments, first in the Department of Aeronautics and the Department of Meteorology and Physical Oceanography, where he now is Professor of Physical Oceanography. He has worked in fluid mechanics, and his research has involved aeroelasticity, transonic flow, jet noise, blood flow, boundary layers in supersonic flows and over the sea surface, wind waves, internal waves and turbulent processes.

profiles in science

Dr. Verner E. Suomi is Professor of Meteorology and Director of the multidisciplinary Space Science and Engineering Center, which he organized at the University of Wisconsin at Madison. Dr. Suomi is a contractor of the Office of Naval Research and a renowned environmental scientist. His unique combination of talents allows him to translate natural occurrences into quantitative measurements with which men can comprehend their environment. Professor Suomi's research includes: moisture measurements in the stratosphere, sonic anemometry and thermometry for studies of atmospheric turbulence near the ground, and energy budgets of the earth's surface. He has invented radiant temperature sensing devices and a light weight radio altimeter for balloon programs.

Dr. Suomi's best known device is the "spin—scan camera" which has revolutionized satellite meteorology. The spin-scan camera has made it possible to look at the same weather system repeatedly at intervals of a few minutes; data from this camera describe weather accurately.

He is a member of the Mariner/Jupiter Saturn Imaging Team and a member of the Pioneer Venus Science Steering Group. The holder of many national and international awards, Professor Suomi is a member of the American Philosophical Society, a Fellow of the American Arts and Science Society, and a member of the National Academy of Engineering. ■

Three Dimensional Representation Of Clouds From Satellite Images

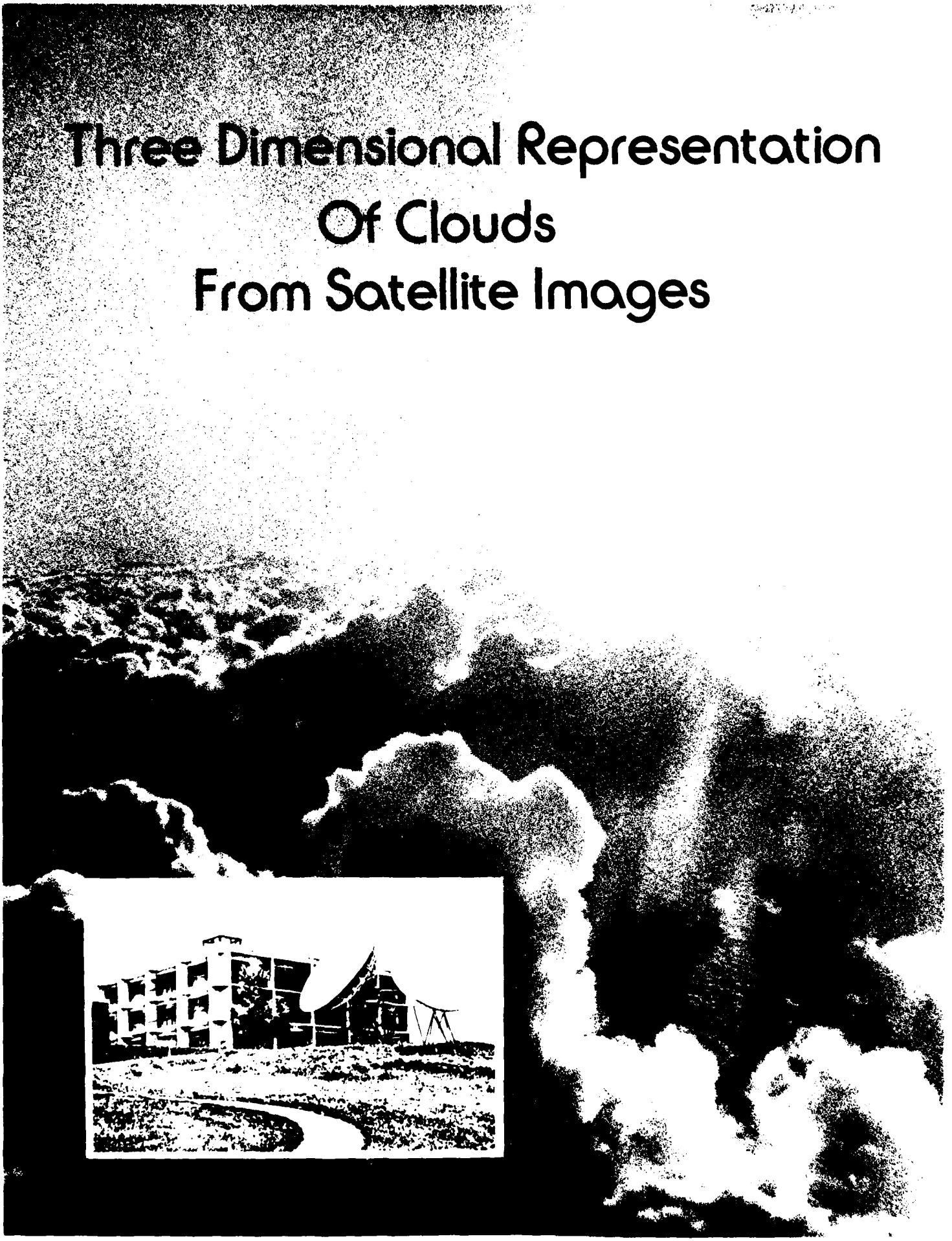

by

Thomas A. Brubaker
Colorado State University

Introduction

The evolution of computer technology has provided scientists and engineers with the capability to process information efficiently in the form of images or pictures. This has resulted in a great deal of research interest in image processing as exemplified by the May, 1981 special issue of the Proceedings of the IEEE[1] devoted to papers on image processing. The collection of papers emphasized two aspects of image processing: (1) the processing of image data to achieve desired improvements, and (2) image understanding which is concerned with the way humans visualize and utilize image information.

In the meteorological satellite community, scientists now routinely use computers to process image data to improve image quality and image understanding. For example, an algorithm to remove white background due to snow provides a better quality picture for cloud studies. Another example is the assignment of separate colors to cloud heights which allows the user to differentiate clouds quickly at different levels and thus provides improved image understanding. The two examples deal with flat images as viewed from the satellite. Currently, the majority of satellite imagery is viewed in this context and the user must visualize the three-dimensional structure of the atmosphere in his mind.

Given a flat satellite image, contouring algorithms can be employed to operate on the visual or infrared data to generate three-dimensional cloud images. Another alternative is to use polygons to approximate a three-dimensional cloud surface. These methods result in three-dimensional surfaces that more realistically depict what a pilot will see from an airplane or what an observer will see from the ground. The result is improved image utilization. We will define image utilization as a transformation that results in a product that directly depicts a desired phenomenon.

This paper describes the use of satellite pictures and computer-driven imagery to represent clouds as three-dimensional objects in a viewer's frame of reference. Given a flat satellite picture, the procedure for generating the cloud pictures is described. The use of shading to provide a more effective three-dimensional picture is illustrated. Then dimensioning of the images is described, again from the viewer's frame of reference.

The visual and infrared image data were collected by the ground station at the Atmospheric Science Department at Colorado State University. The computing and display equipment consisted of a Digital Equipment Corporation PDP-11/60 minicomputer and a RAMTEC 9050 Color Image System. The RAMTEC has a display of 512-by-512 pixels with each pixel storing an 8-bit value. A video lookup table is used in the RAMTEC to define the color associated with each possible pixel value. A 13-bit word stores each color definition. The lower 12 bits are divided into 3 groups of 4 bits each. Each group controls the intensity of one of the three standard color guns in the monitor. This provides a possibility of 16 intensity levels for each color gun and a total of 4096 colors and intensities. Only 256 colors and intensities may be defined at one time, however, and only 16 intensities can be generated for a single color. A more detailed description of the work is given by Johnson.[2]

Two Dimensional Representations

The data that were received from the satellite consisted of visible and infrared data. In the visual data, the pixel values are related to brightness which does not directly relate to altitude. This limits the usefulness of visible data for representing clouds in three dimensions. The infrared temperature data can

Figure 1. Original infrared image.

be correlated to altitude via data collected from balloons so that reasonably accurate altitude representations can be achieved.

Thus, the first task is to use balloon data to relate each infrared pixel value to altitude. After this is done, a new image is generated to scale the altitude values between the values of 0 and 255 which represent the lowest and highest altitudes respectively. The resulting new image can then be displayed again as a flat image.

An example of the results is shown in Figures 1, 2 and 3. Given the original image as shown in Figure 1; a histogram plot of the data after conversion is shown in Figure 2. The relationship between pixel values and altitude is given by

$$A = (64.5)I \qquad (1)$$

where I is the pixel value and A is the altitude in meters. The resulting reconstructed flat image is shown in Figure 3 with a gray scale from 0 to 200. Two hundred was used as the upper bound since values above 200 are constant. A pseudocolored representation of Figure 3 is shown in Figure 4. This dramatically brings out the two clouds in the center of the picture and these are the two clouds we will place into a three-dimensional image in the next section.

To summarize, given a flat infrared image from the satellite, a conversion to altitude is made using the best available information to convert temperature values to altitude. Histogram values are then adjusted between 0 and 255. This may cause distortion, but the impact of this is still not known. Then a new image is constructed and pseudo-colored if it is to show relevant features.

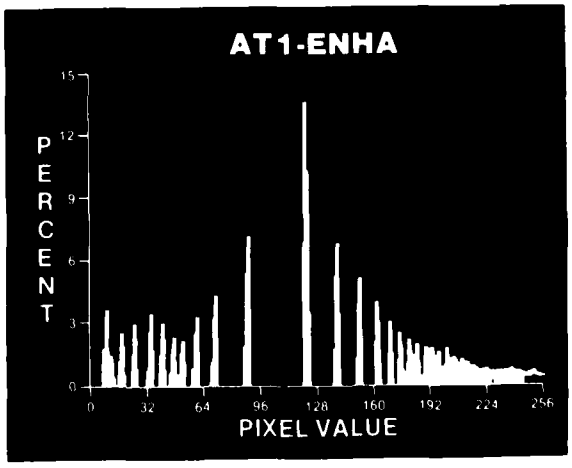

Figure 2. Pixel histogram plot; pixels converted to altitude.

Figure 3. The image of Figure 1 adjusted for altitude.

Three-Dimensional Representations

Given the infrared images, clouds in a desired sector can be converted to three-dimensional objects that can be viewed from any angle. The resulting images can be shaded and dimensioned to provide the viewer with a realistic view of a cloud or group of clouds from any desired viewing angle.

A surface can be created from the reconstructed data by means of a collection of surface drawing subroutines that are available from National Center for Atmospheric Research (NCAR)[3] in Boulder, Colorado and were modified at CSU for use with our computer equipment. With the PDP-11/60 and RAMTEC system we are limited to an array of 32-by-32 points. Since the number of pixels in the portion of the image used to create the surface is much greater, a method to utilize the data was needed. The method which we chose was to select pixels at regular intervals so that they form 32 rows of 32 columns within a selected portion of the image. The resulting surface can be generated as a true contour map or using an X, Y, Z coordinate system. Modification of the programs resulted in surfaces with dimensions. Here, labeled axes are used to give the dimensions of the X and Y axes and a color bar provides the altitude or Z axis dimensions. The software operates as follows.

The program is initiated by having the user specify the file name of the desired image. This image is then transferred to the RAMTEC, and the lookup table is defined for a gray scale from 8 to 255. The user interactively indicates what portion of this image is to be used to create a surface. As before, software is used to reduce this portion to an array of 32-by-32 points. There are a number of ways to do this. Averaging is used in this case. The portion of this image specified by the user is selected so that the number of pixels in both directions is a multiple of 32. This new portion of the image is then divided into 32-by-32 sections. The pixel values in each section are totaled, and these totals are divided by the number of pixels per section. A potentially undesirable effect of this method of reduction is low-pass filtering. High-frequency features in the image will be attenuated. It should be noted, however, that some information will be lost in any type of reduction.

The program next converts the array of infrared data to altitude as discussed previously. The conversion table is created sometime before running this program and is stored in a data file which is accessed to make the conversion to altitude. The user specifies a maximum altitude that will control the size of the cloud surface in the vertical direction. The distance

from the zero elevation to the maximum altitude will always be the same for a given orientation.

Since ground features are not necessarily of any interest and tend to create a more confusing surface, the program now removes all features below an altitude specified by the user by setting these array elements to zero. The procedure up to this point will produce a ragged edge on the bottom of the surface. To make the lower edge of the surface smooth, the program changes the values of the points around the edge of the nonzero surface to the lower altitude that was specified by the user.

The program then creates the surface on the RAMTEC screen through the use of display subroutines. The surface draws the X, Y, and Z directions. User interaction specifies how shape-defining sets of contours are to be drawn. Each set of contours is chosen to be close together and cover a narrow band of altitudes. The surface is drawn over and over again each time with a different set of contours. Each set of contours is drawn with a different pixel value which is defined as a different color. The result in this program is a surface on which the color changes from blue at low altitudes to white at high altitudes. This produces a known relationship between color and altitude within the program. The entire surface, including points that are zero, is drawn one last time without any contours. The pixel value used is defined as black. The corners are made equal to zero to provide screen coordinates that will be used to draw the axes. The angle of view for the surface is specified by the user.

Last of all, this program adds dimensions to the surface if so desired. The horizontal directions will be described with labeled axes. Vertical size will be indicated by a color bar with altitudes marked on it. The corners of the surface that were set to zero provide the screen coordinates for the ends of the axes. The user must then interactively choose three of the four corners to define the end-points of the horizontal axes. The first corner chosen is the one with a screen coordinate that is lowest on the screen. The other two corners are those adjacent to the first. These are identified as right and left by comparing the X screen coordinates. Two lines are drawn on the screen for the axes using these screen coordinates. In order to find the scaling for each axis it must be determined whether the axis represents north-south or east-west. In this case, if the subscripts of the first corner are equal, then the axis on the right represents an east-west direction.

The distance represented by an axis can be found by multiplying the distance per pixel by the number of pixels used to create the surface in that direction. The distance per pixel must be entered by the user and is dependent on the creation of the original image data file. Once the length represented by an axis is known, the interval between tick marks can be

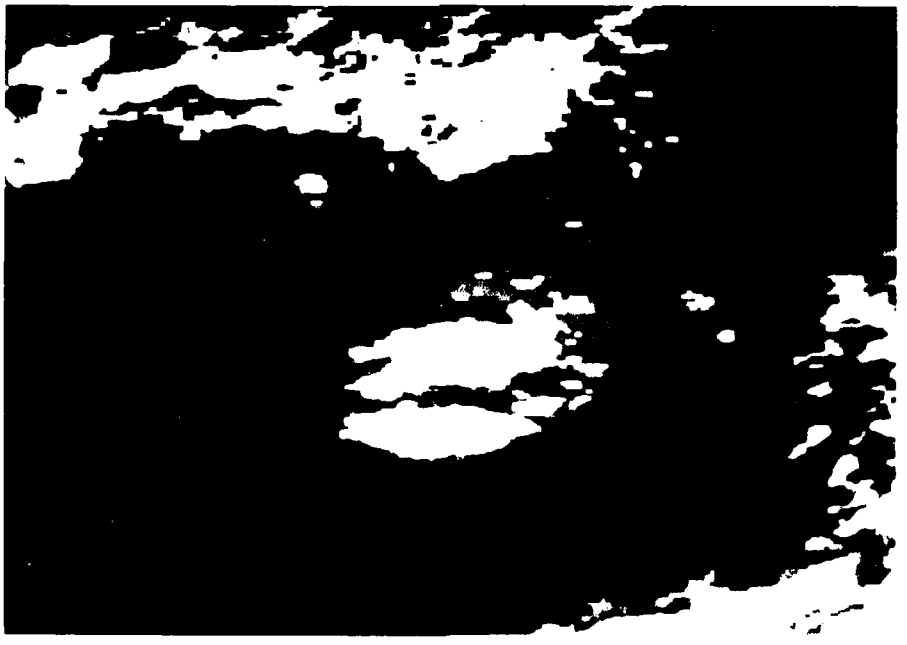

Figure 4. Pseudo-color representation of image in Figure 3.

chosen. This program chooses the interval to be some power of ten. This power is found by

$$p = \text{int}(\log_{10}(L)) \qquad (2)$$

where 10^p is the interval represented between tick marks and L is the total length represented by the axis. The distance between tick marks in terms of screen coordinates is found by

$$s = \frac{A \times T}{L} \qquad (3)$$

where s is the distance between tick marks in screen coordinates in the X or Y direction, A is the total length of the axis in screen coordinates in the X or Y direction, T is the distance represented by the tick mark interval and L is the total distance represented by the axis. By knowing the tick mark interval in screen coordinates, one can use a loop to draw tick marks at these intervals until a location is found for a tick mark that is not on the axis. The values written on the screen next to these tick marks are multiples of the interval. The value at the first corner is zero. This procedure is done for each axis.

To indicate vertical dimensions, a vertical color bar is drawn in the upper-right corner. The color on this bar changes from bottom to top in the same way that the surface does. The relationship between the pixel value used to create a color on the color bar and its representative altitude was stored when the surface itself was drawn. The altitudes at the color boundaries are written on the screen. The program then writes the units of measurement on the screen.

Examples of the results are shown in Figures 5 and 6 which are three dimensional views of the two clouds shown in the center of Figure 4. Figure 5 is an intermediate result with the flat base still attached. Figure 6 is the finished product with some shading employed and dimensions included. Note that the image in Figure 6 is viewed from a different position than the image in Figure 5, demonstrating the option of different viewing angles.

A second method for viewing clouds as three-dimensional objects utilizes a set of polygons to approximate the three-dimensional surface. A software package called MOVIE, developed at Brigham Young University, is available as a starter for doing this.[4] The MOVIE package contains the initial subroutines needed for polygon approximation of a surface, arbitrary coloring and shading of the resulting surface, and the use of transparency to allow the viewer to see objects in back of other objects. At present, MOVIE does not run well on the 16 bit

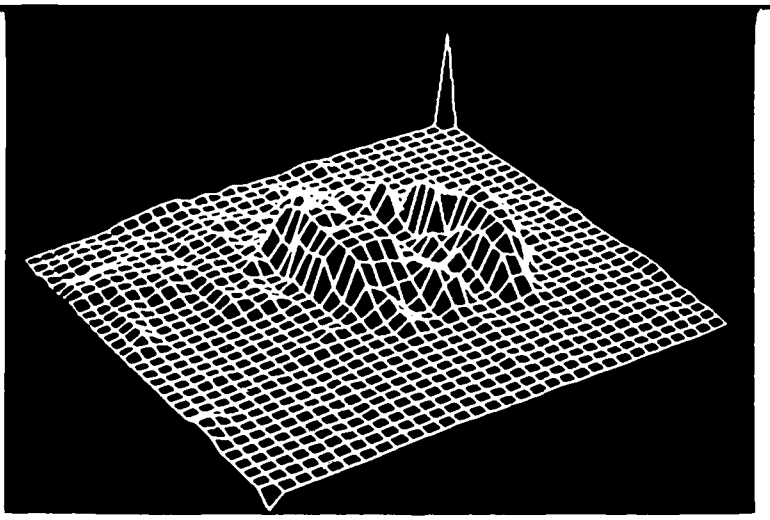

Figure 5. Intermediate three-dimensional represenation of the two clouds in center of figure 4.

PDP-11/60 computer because of the lack of dynamic memory. However, we have been able to obtain simplified approximations to demonstrate the use of the software for cloud representations. The dimensioning software was programmed for inclusion in MOVIE.

As before, the initial image must be sectored and operated on to obtain altitude information. Because of the lack of memory only crude polygon approximations can be generated, but these are often sufficient for cloud representations. An example of the results is shown for the previous two clouds in Figure 7. We call these slab cloud representations.

While the polygon approximations appear to give a much coarser representation, the use of a larger computer will allow a much better polygon approximation to be obtained. We anticipate the results will be more cloud-like although this hypothesis must be proven.

As a final example, we have recently used our software to depict the output of computer models for modeling cloud growth. Three of the results are shown in Figures 8, 9 and 10 which show the beginning, an intermediate stage and the final stage of a simulation.

Figure 6. Three-dimensional cloud picture with dimensions.

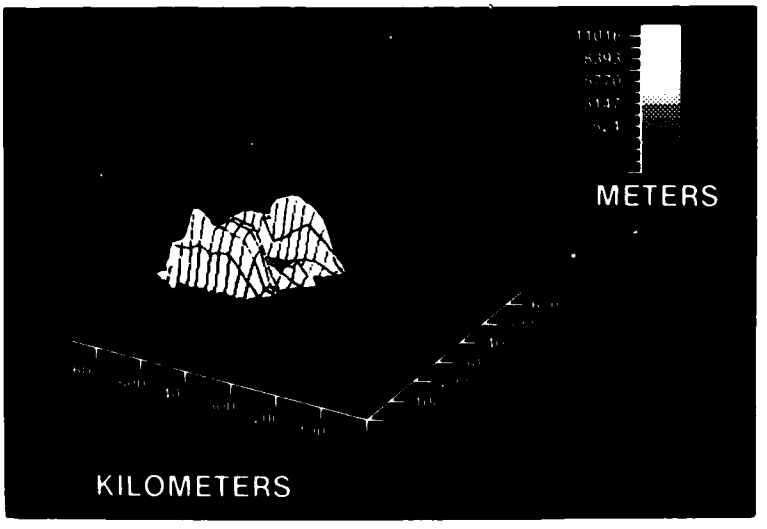

Conclusions and Future Work

This paper describes the methods for generating three-dimensional cloud images from data generated by geosynchronous weather satellites. The resulting images are reasonable representations of clouds from an observer's point of view. The use of X, Y, and Z dimensions provides the viewer with accurate information concerning cloud size from the observer viewing position. The cloud images can be easily manipulated to permit observation from any desired viewing angle and from any distance. The use of imaging to represent model output is also described.

The work was done using a small computer system. The next phase will utilize a DEC VAX-11/780 computer and this will greatly enhance our ability to investigate more sophisticated ways of utilizing and presenting three-dimensional data. By utilizing the full version of MOVIE, we will be able to more effectively represent clouds using better polygon approximations to solids and improved shading algorithms. The use of a transparency algorithm will allow us to "see through" clouds and to study cloud-cloud interactions. The transparency capability will allow the modeling personnel to see the inside of their model generated clouds, for example, stream lines can be displayed.

Work will also be started to relate cloud data to model output. This will be done by first displaying real clouds and model clouds in three dimensions. From this we hope to learn how to use satellite data better for model initialization. We will also begin to use temporal three-dimensional cloud images to study methods for estimating both horizontal and vertical wind fields. These studies will utilize our present man-interactive computing facilities to allow our scientists to evaluate quickly algorithmic approaches to the problems. ■

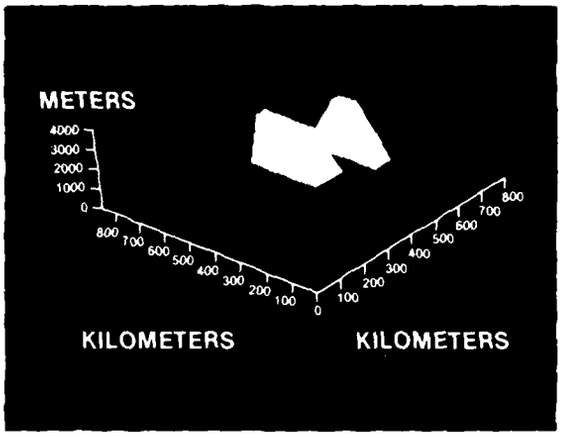

Figure 7. Cloud representation using a crude polygon approximation.

References

1. Proceedings of the Institute of Electrical and Electronics Engineers (IEEE)—Special Issue on Image Processing, May, 1981.

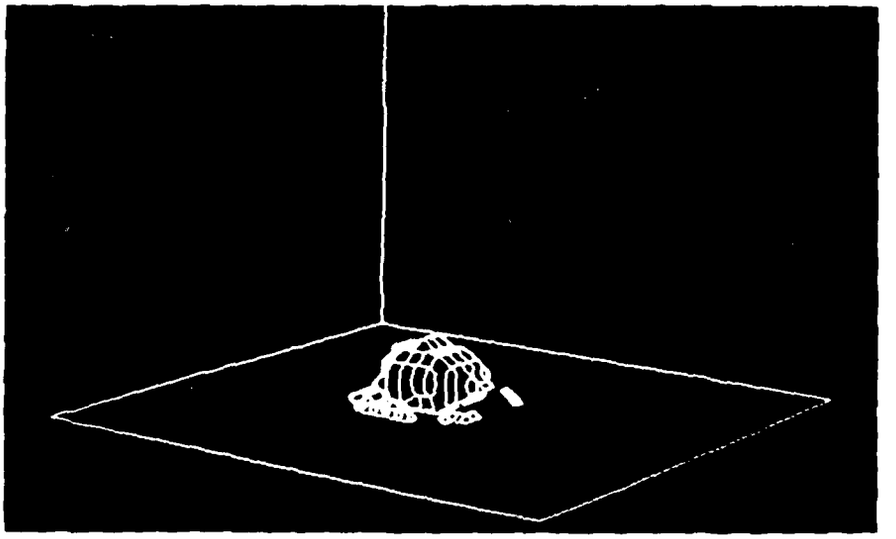

Figure 8. The first cloud from the model.

2. Johnson, Douglas E., *Computer Graphic Cloud Representations*, M. S. Thesis, Colorado State University, June, 1981.

3. Wright, Thomas, *NCAR Graphics Software*, National Center for Atmospheric Research, Boulder, CO, 1977.

4. Stephenson, Mike and Hank Christiansen, *MOVIE. ARIZONA*, Southwest Computer Graphics, Tucson, AZ, Brigham Young University, Provo, UT, 1979.

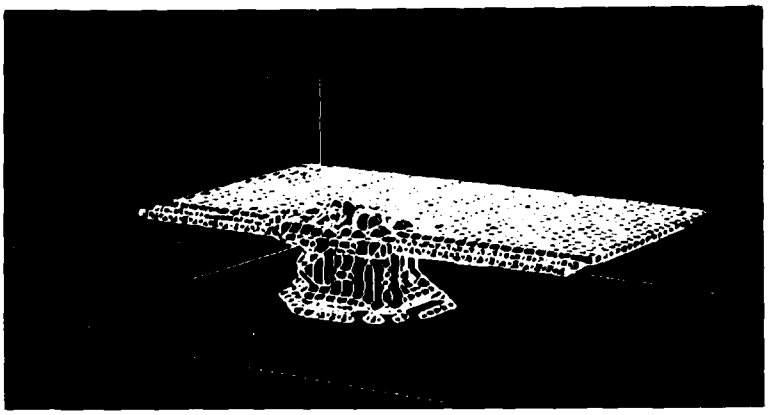

Figure 9. The model cloud at intermediate time.

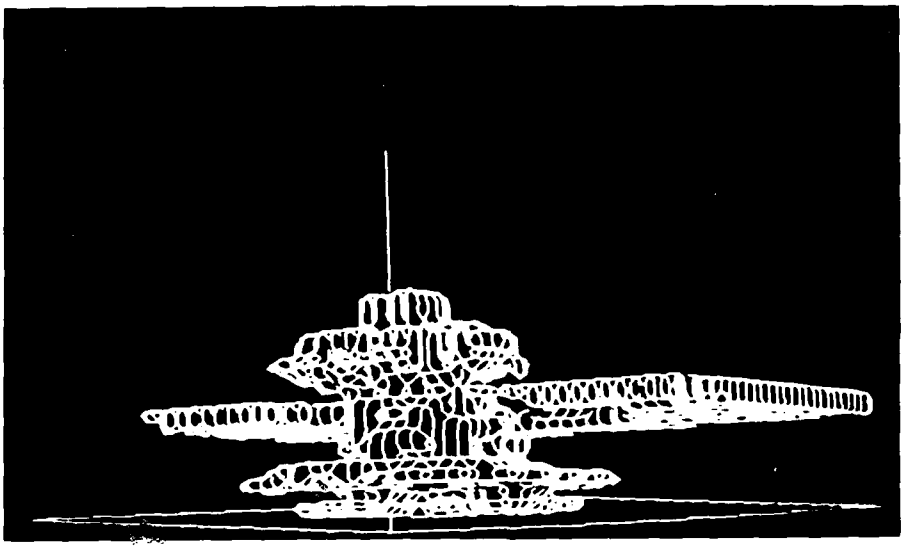

Figure 10. The model cloud at the final stage of simulation.

Dr. Tom Brubaker received his Ph.D. in Electrical Engineering from the University of Arizona in 1963. Since then, he has taught at the University of Wyoming, the University of Missouri-Columbia and at Colorado State University where he is currently a professor. Research interests include digital system design, image processing research oriented toward meteorological applications, digital signal processing and computer resource management.

research notes

Atmospheric Boundary-Layer Processes Over Coastal Waters and Across Oceanic Fronts

Supported mainly by the Coastal Sciences Program of ONR and Naval Environmental Prediction Research Facility, Dr. S. A. Hsu and his colleagues at the Coastal Studies Institute of Louisiana State University are studying the atmospheric changes across oceanic fronts as well as mesoscale processes associated with airflow adjustment over coastal waters. When cold air is situated over warm water the convective velocity scale and the height of the mixing layer can be estimated by the surface heat flux. On the other hand, when warm air flows over a cooler sea, the height of the modified layer is proportional to the square root of the fetch downwind from the coast. It can be shown that this equation is superior to that based on dimensional analysis. All of the above concepts have been verified by field experiments. At times, branches of warm oceanic currents such as the Gulf Stream and the Kuroshio Current, as well as cold oceanic eddies associated with upwelling such as the Somali Current, are very near the coast. Their impact on the atmospheric boundary layer is studied. It has been demonstrated that there is approximately a 30% increase in relative humidity and mixing ratio from the cold side to the warm side about 15km downwind from the oceanic front in the Korea Strait. Also, a 140m increase in the mixing height from the cold to the warm side has been observed. An example is an inversion layer that existed between approximately 200m and 600m over a cool pool because of the presence of a cold eddy offshore of the Somalia coast in summer; no inversion layer was observed on the warm side of the upwelling zone. ■

(Dennis Conlon, ONR)

Development of Techniques for the Remote Sensing of Surface Currents and Current Shear using Microwave Radar

Surface currents are defined as the mean horizontal flow of water within a layer which extends downward from the surface to a depth of several meters. The accuracy of conventional moored current meter measurements suffers in this layer because of competing wave amplitude and velocity effects. Lagrangian drifter measurements of spar buoys present difficult tracking and deployment problems and dye studies of surface flow are difficult to interpret quantitatively. Still the need persists to accurately map surface currents, because anything that floats on the surface (ships, pollutants, icebergs, nutrients and even waves) is transported by these currents.

Recently, a dual-frequency microwave radar technique has been developed at the Naval Research Laboratory which is capable of remotely sensing both ocean surface currents and vertical profiles of current strength to a depth of several meters. The radar measures currents by monitoring the perturbations in ocean wave propagation velocity caused by the presence of the current. This sensitive measurement is made possible by the dual-frequency radar's unique ability to "resonate" with one ocean wave at a time. The particular wave that is being used as a current measurement-tool can be changed at will be changing the separation between the pair of radar frequencies which are scattered from the ocean's surface. Temporal and spatial (mapping) studies of surface currents have been carried out using this basic mode of operation. Modern microwave technology facilitates an expansion of the radar's capability. In particular, signal multiplexing techniques using PROMS (programmable read-only-memories) have been developed which enable the radar to examine simultaneously the effect of currents on a set of up to one-hundred independent ocean waves. Because long wavelength waves are affected by much deeper currents than shorter wavelength waves, the multiplexed data can be analyzed to obtain information on the vertical distribution of currents beneath the ocean's surface. Information about currents near the surface

IF YOU WANT TO CONTINUE RECEIVING ***NAVAL RESEARCH REVIEWS,*** PLEASE FILL OUT THE SELF-ADDRESSED REPLY CARD AT THE BACK OF THIS ISSUE. BE SURE TO INDICATE YOUR CORRECTED OR NEW ADDRESS.

THANK YOU

☐ Yes. Please continue sending me the *Naval Research Reviews.*

☐ Please make the address change as indicated.

☐ Any comments you wish to make will be appreciated.

Old Address _____

_____

_____

New Address _____

_____

_____

Comments _____

_____

_____

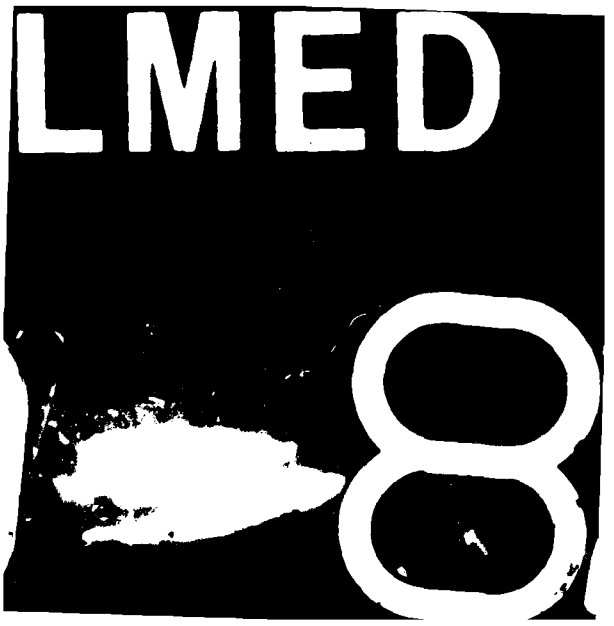
LMED
8